



Manual Assembly Modelling and Simulation for Ergonomics Analysis

Thesis submitted in accordance with the requirements of
the University of Liverpool for the degree of Doctor in Philosophy
by

Ziyun Ding

November 2013

Abstract

In manufacturing industry, although automation techniques have been employed widely, many tasks still require the flexibility and intelligence of human operators, especially in the product assembly process. Insufficient industrial ergonomics in the assembly process will cause the health problems and quality and productivity losses, ultimately increase costs of the final product. The purpose of this thesis is to integrate ergonomic considerations into the manual assembly process modelling and simulation in order to provide product/process design changes before their physical prototyping.

In this research, a state-of-the-art commercial software tool - DELMIA - is adopted for the ergonomics simulation and analysis. Associated with its capabilities for the ergonomics solution, a series of human related issues in the manual assembly process is simulated and studied in order to demonstrate the benefits of a virtual assembly approach to the product design, workplace design, time and energy saving.

Due to the poor repeatability and reproducibility of digital human postures in DELMIA manipulation, a posture prediction method is developed aiming at a practical and precise ergonomics analysis. A 10-degrees-of-freedom, 4-control-points digital human model concerned with assembly features and human diversity is established. The multi-objective optimisation method is applied to assembly posture prediction in which optimisation objectives (i.e. joint discomfort and metabolic energy expenditure) and constraints corresponding to manual assembly tasks are proposed and formulated. Following the verification of the posture prediction method, a series of posture strategies under different assembly conditions are investigated towards more comfortable and energy-efficient assembly postures.

Thus far, the consideration on assembly operators in assembly sequencing is insufficient though it plays a key role in the integrative product and process design. In this research, the use of new ergonomic constraints into assembly sequencing optimisation is proposed. Feasible assembly sequences are generated and evaluated based on the product geometry, assembly workstation layout, operator characteristics and working posture. A new Liverpool Assembly Sequence Planning System (LASP) is developed to achieve the integration by applying two evaluation criteria, i.e. visibility criterion, accessibility criterion or both. With LASP, possible design faults with respect to restricted visibility and obstructed accessibility is obtainable during the early design stage. Meanwhile,

the optimum sequences are provided to operators automatically for ease of manual assembly, facilitating higher assembly quality and efficiency.

Acknowledgements

First, I would like to express my deepest gratitude and admiration to my supervisor, Professor Bernard Hon for giving me the opportunity to undertake my PhD in the University of Liverpool and allowing me the space and freedom to explore new knowledge. I am grateful for his substantial amount of effort and guidance over the past four years. I would also like to express my sincere gratitude to Dr. Tim Short for his continuous encouragements and invaluable feedbacks.

I feel honoured to have had a learning and working experience in the Virtual Engineering Centre in the Daresbury Laboratory, Warrington. Many thanks to Dr. Antony Robotham for his support, allowing me to utilise a series of VR facilities in the VEC to accomplish my research. I am especially grateful to Dr. Fei Shao, for his generous sharing of knowledge and experience, assisting me to carry out experiments and realising my initial idea.

I would like to acknowledge the Chinese scholarship Council (CSC) of China, for the financial support that made this thesis possible.

Finally, a special thanks to my parents who have been an incredible source of support. I can never express how lucky I feel to be their daughter so I can pursue my dream so determinedly. Also, many thanks to my husband Dr. Zhangming Wu for his understanding and support mentally and academically.

Contents

Abstract	i
Acknowledgements	iii
List of Figures	vii
List of Tables	xi
Abbreviations	xiii
Notations	xiv
1 Introduction	1
1.1 Aim and Objectives	4
1.2 Research Overview	5
1.3 Structure of Thesis	6
2 Literature Review	8
2.1 Introduction	8
2.2 Ergonomic Simulation of Assembly Process	10
2.2.1 Manual Assembly	10
2.2.2 Ergonomic Consideration	11
2.2.3 Ergonomics Simulation in the Virtual Environment	12
2.3 Human Posture Modelling in Manual Tasks	16
2.3.1 Digital Human Modelling	16
2.3.2 Human Posture Prediction	18
2.3.3 Human Performance Measures	20
2.3.4 Human Task Evaluation	25
2.4 Virtual Assembly Process Planning	27
2.4.1 Assembly Sequence Planning	27
2.4.2 Assembly Sequence Planning System	27
2.4.3 Assembly Sequence Planning Criteria	31
3 Manual Assembly Process Simulation	33
3.1 Introduction	33

3.2	Simulation Tool: DELMIA	33
3.3	Virtual Ergonomics Solution	34
3.4	Virtual Assembly Environment	37
3.5	Ergonomics Analysis	40
3.5.1	Posture Analysis	40
3.5.2	Cycle Time Analysis	40
3.5.3	Energy Expenditure Analysis	42
3.5.4	Reach Analysis	42
3.5.5	Vision Analysis	43
3.5.6	Clearance Analysis	44
3.6	Case Study: A Comparison Study of Product Assemblability	45
3.6.1	Method and Materials	46
3.6.2	Development of Virtual Assembly Environment	46
3.6.3	Results	48
3.6.4	Discussion	53
3.7	Case Study: Ergonomic Design of Manual Assembly Workplace . .	56
3.7.1	General Workplace Design Procedure	57
3.7.2	Method and Materials	57
3.7.3	Results	62
3.7.4	Discussions	65
3.8	Conclusions	69
4	Posture Analysis of Manual Assembly	71
4.1	Introduction	71
4.2	Digital Human Modelling	72
4.2.1	Model Simplifications	72
4.2.2	A 10-DOF, 4-Control-Points Human Model	73
4.2.3	Human Diversity	81
4.3	Multi-Objective Optimisation Method for Posture Prediction	83
4.3.1	Overview of Multi-Objective Optimisation	83
4.3.2	Optimisation Objectives	85
4.3.3	Optimisation Algorithm	93
4.3.4	Model Verification	96
4.4	Task-Based Posture Analysis	105
4.5	Results	107
4.5.1	Optimum Posture Analysis	107
4.5.2	Effect of Object Height	108
4.5.3	Effect of Distance to Object	108
4.5.4	Effect of Object Weight	109
4.6	Conclusions	111
5	Ergonomic Evaluation of Assembly Sequence	113
5.1	Introduction	113
5.2	Type of Assembly Sequences	114

5.2.1	Number of Hands	114
5.2.2	Monotonicity	115
5.2.3	Linearity	115
5.3	Assembly Planning Description	116
5.3.1	Local Motion	116
5.3.2	Global Motion	116
5.3.3	Sweeping	117
5.4	Representations of Assembly Sequences	117
5.4.1	State Graphs	118
5.4.2	AND/OR Graphs	119
5.5	Assumptions	120
5.6	Generation of all Feasible Assembly Sequences	121
5.7	Criteria of Manual Assembly Sequence Evaluation	123
5.7.1	Visibility	123
5.7.2	Accessibility	135
5.7.3	Combination of Visibility and Accessibility	142
5.8	A Manual Assembly Sequence Planning System	142
5.8.1	System Description	142
5.8.2	System Input	144
5.8.3	Case Study	145
5.8.4	Discussion	151
5.9	Conclusions	152
6	Conclusions and Future Research	154
6.1	Conclusions	154
6.2	Future Research	157
Appendix A	Anatomical and Anthropometric Terminology	160
A.1	Anatomical Position	160
A.2	Reference Planes	161
A.3	Anatomical Relationship	161
A.4	Joint Movements	163
Appendix B	MATLAB Optimization Routines	166
B.1	Constraints	166
B.2	Multi-Objective	169
B.3	SQP Algorithm	172
Appendix C	Optimum Assembly Postures	174

List of Figures

1.1	Market values of enterprises [2].	1
1.2	Consequences of the poor product/process design from the ergonomic viewpoint.	3
1.3	Description of ergonomic influence during the product development process [8].	3
1.4	The thesis structure.	6
2.1	The literature review structure.	9
2.2	Reasons for reduction of automation [1].	11
2.3	Examples of commercial digital human models.	17
2.4	The lower arm posture score calculation [59].	23
2.5	Constraints for lifting tasks [78].	26
2.6	An example of the liaison graph [10]. (Part A is a screw that fastens part B to part C)	28
3.1	The interface for creating standard manikins.	35
3.2	Anthropometry tools in MHM.	36
3.3	An example of the Gantt chart in the human task simulation.	37
3.4	The angles editing panel [99].	38
3.5	A PPR environment in DELMIA.	39
3.6	Steps of the assembly process simulation.	39
3.7	Colours representing intermediate scores [99].	41
3.8	An example of RULA analysis.	41
3.9	An ideal reach envelope [99].	43
3.10	A 90% reach envelope [99].	44
3.11	A binocular vision window of a manikin [102].	44
3.12	A head clearance analysis [102].	45
3.13	Formula student car – ULM005.	46
3.14	The simulation flow chart of the FS car assembly process.	47
3.15	The virtual assembly environment of the FS car.	48
3.16	Operations in the engine assembly process.	49
3.17	RULA scores of operations in the engine assembly process.	50
3.18	Operations in the firewall assembly process.	52
3.19	RULA scores of operations in the firewall assembly process.	53
3.20	Task of the plenum assembly.	54
3.21	Task of the bodywork assembly.	55
3.22	The blower model for manual assembly [114].	58

3.23	The alternative work bench height designs.	60
3.24	The determination of level 2 of work bench height.	60
3.25	The alternative workplace layout designs.	61
3.26	The alternative part location designs.	62
3.27	The simulation flow chart of workplace design.	63
3.28	Simulation results.	64
3.29	ANOM diagram of process cycle time.	64
3.30	ANOM diagram of energy expenditure.	64
3.31	The optimum workplace design.	66
3.32	Reach analysis in the assembly process simulation.	66
3.33	Unacceptable postures in level 1 of work bench height.	67
3.34	Unacceptable postures in level 3 of work bench height.	68
4.1	A 10-DOF human model.	73
4.2	Parameters for the D-H method.	75
4.3	4 control points in the human model.	77
4.4	The position of assembly object.	77
4.5	The locations of centres of mass in the body segments in the sagittal plane [128].	82
4.6	The neutral position of the digital human.	87
4.7	Hip discomfort measure.	87
4.8	Knee discomfort measure.	88
4.9	Static force modelling on the sagittal plane.	90
4.10	The procedure for posture prediction via the SQP method.	95
4.11	Illustration of locations of subjects and objects in the experiment. . . .	97
4.12	The stereo vision system.	98
4.13	A suit configuration tool.	98
4.14	10 props for tracking objects.	99
4.15	The location of ten props.	99
4.16	A schematic plot of the experiment procedure.	100
4.17	Qualitative comparative results for target 1.	101
4.18	Qualitative comparative results for target 2.	101
4.19	Qualitative comparative results for target 3.	102
4.20	Qualitative comparative results for target 4.	102
4.21	Regression plot of joint rotation variables	103
4.22	The range of mean differences from q_5 to q_{10}	105
4.23	Illustration of the visual demands.	106
4.24	Optimum hip displacement for different operators.	108

4.25	The effect of object height.	109
4.26	The effect of distance to the operator.	110
4.27	The effect of object weight.	110
5.1	An example of no monotone binary assembly sequence [148].	115
5.2	An example of no linear assembly sequence [148].	116
5.3	An example of sweeping [88].	117
5.4	A simple product and its liaison diagram [10].	119
5.5	The liaison sequence diagram for the example product [10].	119
5.6	An example of the AND/OR graph [10].	120
5.7	The procedure for generating feasible assembly/disassembly sequences.	121
5.8	Properties of digital operator for the visibility evaluation.	124
5.9	Minimum entities required in a viewing system.	125
5.10	The determination of a view coordinate system in the assembly process.	126
5.11	A comparison between the parallel projection and the perspective projection.	127
5.12	Deriving a perspective transformation.	127
5.13	A product for the visibility evaluation.	129
5.14	Weiler-Atherton clipping.	133
5.15	Back-face elimination.	134
5.16	The flowchart for the visible area determination.	135
5.17	The procedure of assembly sequence selection based on the visibility criterion.	136
5.18	An example of hand manipulation space.	136
5.19	The flowchart to calculate the amount of approach directions.	138
5.20	An illustration of the approach direction.	140
5.21	Three types of hand grasp.	141
5.22	An example of the accessibility criterion application.	141
5.23	The framework of LASP system.	142
5.24	A typical interface of LASP.	143
5.25	The CAD model of air conditioner [158].	145
5.26	The disassembly environment of the air conditioner.	146
5.27	AND/OR graph of air conditioner assembly.	147
5.28	AND/OR graph of air condition assembly with the visibility criterion.	148
5.29	AND/OR graph of air condition assembly with the accessibility criterion.	149
5.30	AND/OR graph of air condition assembly with the visibility and accessibility criteria.	150

A.1	The human body in the anatomical position.	160
A.2	Reference planes.	161
A.3	Terms of relationship.	162
A.4	Extension and flexion of (a) the wrist; (b) the elbow; (c) the shoulder.	163
A.5	Abduction and adduction of (a) the wrist; (b) the shoulder.	164
A.6	The elbow rotation.	164
A.7	(a) Pronation and (b) supination of the shoulder.	165
C.1	Optimum assembly postures for 5th percentile operators.	174
C.2	Optimum assembly postures for 25th percentile operators.	175
C.3	Optimum assembly postures for 50th percentile operators.	175
C.4	Optimum assembly postures for 75th percentile operators.	176
C.5	Optimum assembly postures for 95th percentile operators.	176

List of Tables

2.1	A brief history of ergonomics [15]	12
2.2	DELMIA vs. Jack.	13
2.3	OWAS coding system [19]	21
2.4	PLIBEL questions relating to the low extremity [60]	22
2.5	Stress rating response and their explanations in postural checklist [61]	23
2.6	A summary of literature on the development of assembly planning systems	30
3.1	GARG equations	42
3.2	Common ergonomic requirements in automatic industry [103]	47
3.3	Weights of the assembly part or component	58
3.4	The assembly process of the blower	59
3.5	Design factors and their levels	60
3.6	Factor levels for each simulation	63
3.7	Range analysis of process cycle time (s)	65
3.8	Range analysis of energy expenditure (kcal)	65
3.9	Optimum factor values	65
3.10	Walking distance of workplace layout	69
4.1	List of body dimensions and their definitions	74
4.2	10 degrees of freedom and their descriptions	74
4.3	D-H parameters table between the foot and the hip	78
4.4	D-H parameters table between the shoulder and the hand	79
4.5	Anthropometric data for British male, aged 19 to 65 years. (all dimensions in millimetres, except for body weight, given in kilograms)	81
4.6	Masses of body segments as a percentage of the whole body mass [130]	82
4.7	Parameters in the joint discomfort model	86
4.8	Joint weights for discomfort	86
4.9	Joint neutral position and movement ranges (degree)	86
4.10	Joint torque limit [137]	89
4.11	Calculating formulae of $\theta_j (j = 1, 2, \dots, 6)$	91
4.12	Subject summary statistics	96
4.13	Target Objects in the experiment	97
4.14	Wilcoxon Signed-Rank tests of joint variables	104
5.1	Anthropometric variables	123
5.2	Optimum assembly sequences of air conditioner	151

A.1	Terms of relationship.	162
-----	--------------------------------	-----

Abbreviations

ANOM	Analysis of Means
BMR	Basal Metabolic Rate
DFA	Design for Assembly
DHM	Digital Human Modelling
DOF	Degree of Freedom
FS	Formula Student
LASP	Liverpool Assembly Sequence Planning
MAA	Human Activity Analysis
MHB	Human Builder
MHM	Human Measurements Editor
MHP	Human Posture Analysis
MHT	Human Task Simulation
MOO	Multi-Objective Optimisation
MTM	Methods Time Measurement
NIOSH	National Institute for Occupational Safety and Health
OSHA	Occupational Safety and Health Administration
OWAS	Ovako Working Posture Analysis System
PLM	Product Lifecycle Management
PPR	Product, Process and Resource
RTI	Real-Time Interaction
RULA	Rapid Upper Limb Assessment
SQP	Sequential Quadratic Programming
WMSD	Work-related Musculoskeletal Disorder
VR	Virtual Reality

Notations

t	Cycle time
t_h	Handling time
t_i	Insertion time
E	Energy expenditure
BW	Body weight
S	Gender
F	Lifting frequency
L	Load weight
s	Sample standard deviation
x_p	pth percentile value of the variable x
z_p	Standard normal vale correspoing to the pth percetile value of x
q_i	Current position of joint i
q_i^U	Upper limit of joint i
q_i^L	Lower limit of joint i
q_i^N	Neutral position of joint i
QU_i	Penalty term of upper limits
QL_i	Penalty term of lower limits
γ_i	Weighting value of joint i
\dot{E}	Muscle energy expenditure rate
\dot{E}_W	Muscle mechanical power
\dot{E}_M	Muscle maintenance heat rate
\dot{E}_S	Muscle shortening heat rate
\dot{E}_B	Basal metabolic rate
τ_i	Joint torque
\dot{q}_i	Joint velocity
ξ_i	Coefficient of the maintenance heat rate
\mathbf{L}_H	Magnitude of the workload held on the hands
$\mathbf{f}(\mathbf{q})$	A vector of objective functions
$f_i(\mathbf{q})$	The i th objective function

$f_i^N(\mathbf{q})$	The i th normalized objective function
$g(\mathbf{q})$	Inequality constraints
$h(\mathbf{q})$	Equality constraints
w_i	Weight of the i th objective function

Chapter 1

Introduction

The human element is the most valuable resource a company has in building up core competence and business excellence [1]. Skilled operators are essential for efficient innovative technological and logistical processes. As a so-called process owner, operators take responsibilities to optimise productivity and quality and minimise production costs. The fact is described by the changing value components to a company as shown in Figure 1.1 [2]. Nowadays, 70% of a company's market value is made up of the value of intellectual property (IP), which is represented by its employees. Despite the significance of the human element, countless organisations in a variety of industries are facing the same problem: the human element is not being considered early or thoroughly enough in the design, assembly and maintenance stage of products. More importantly, this is having a devastating impact on cost, time to market, quality and safety.

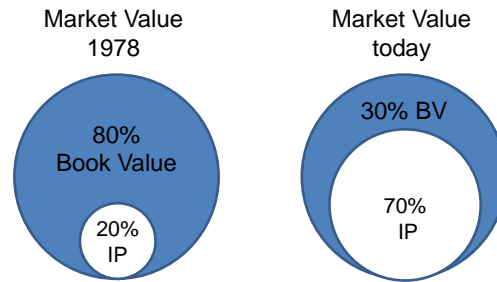


FIGURE 1.1: Market values of enterprises [2].

In manufacturing industry, although automation techniques have been employed widely, many tasks are still accomplished manually especially in the product assembly process. Assembly is the most relevant area of human involvements for several major reasons. For instance, market factor and

competition increase the number of product variants and lead to a decrease in batch size. Human operators are capable of mastering different variants in assembly to save expensive investments in automation and to increase the flexibility and reconfigurability of production systems. Deficient industrial ergonomics is a major reason for sick leave and work injuries in manufacturing industry [3–5]. Replacement of staff and rehabilitation consume considerable resources in manufacturing companies and cost a huge amount of money for companies and societies. According to the US Occupational Safety and Health Administration (OSHA), work-related musculoskeletal disorders (WMSDs) account for more than US\$15-\$20 billion in workers' compensation costs; the total costs, direct and indirect, may be close to US\$60 billion each year. High staff turnover and sick leave cause production disturbances and inefficiencies and result in productivity losses. Moreover, several studies have identified a relationship between ergonomically problematic tasks and quality deficiencies to the extent that around 30-50% of all quality flaws are related to or directly due to ergonomics problems [6]. Investigations from manufacturing companies further reveal a correlation that 60-70% of WMSDs are caused by the product design and 30-40% by the assembly process [7]. Product design-related issues could be, for example, hand access problems due to bad clearances, or high assembly force due to poor fittings. Assembly process-related issues include poor workplace design (e.g., bad visibility, awkward workplace layouts and unsuitable working heights); poor work method design (e.g., ineffective motions and hazardous working postures); and poor assembly process planning. The relationship between the poor product/process design and its negative effect on health, productivity, quality and cost is summarised in Figure 1.2.

As shown in Figure 1.3, it is extremely important to establish ergonomic requirements and to apply a holistic view at product level as early as possible because, in the early design phase of the new product and in the production planning phase, changes are less costly and easier to make than are late changes to the product, the work method, and the workplace design [8]. For these reasons, ergonomics simulation has been frequently used to predict ergonomic issues before the product and process exist physically.

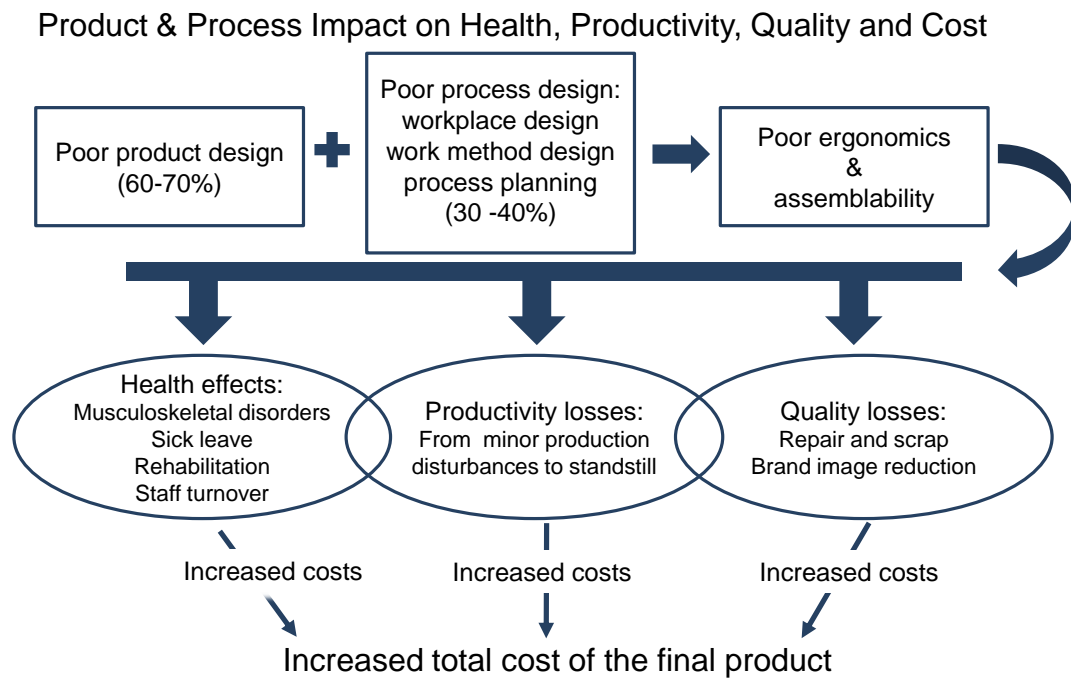


FIGURE 1.2: Consequences of the poor product/process design from the ergonomic viewpoint.

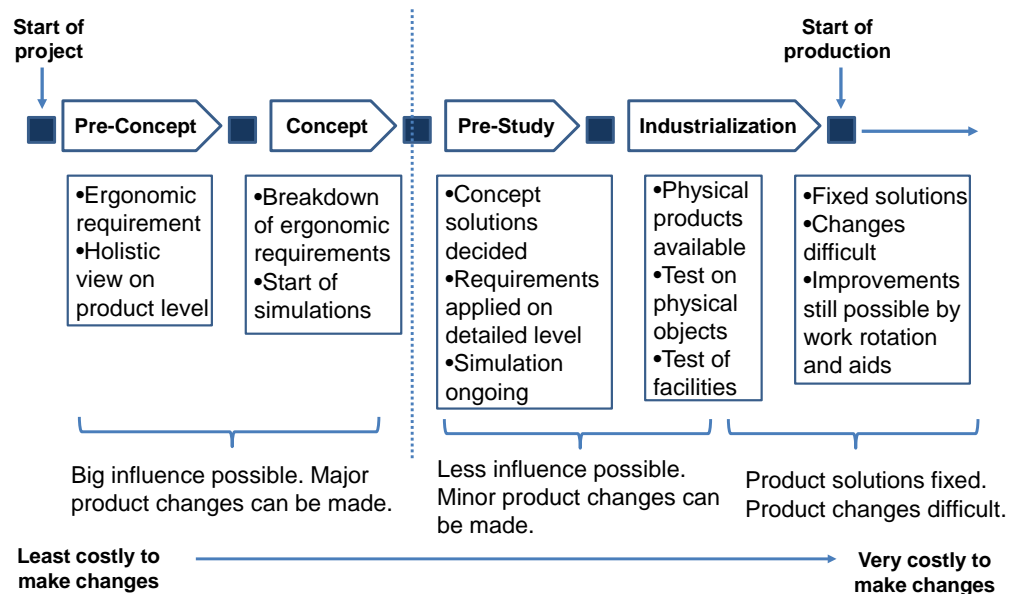


FIGURE 1.3: Description of ergonomic influence during the product development process [8].

In recent years, the advance of a series of powerful computer simulation tools has made it possible to be executed on modern desktop computers instead of expensive workstations and mainframes, thus facilitating the simulation applications in manufacturing industry. New computer simulation technologies encompass all aspects of product development (including manufacture, maintenance, product life cycle, ergonomics, etc.) with the greatest potential impact during the early stages of product design. They empower manufacturing industry with a faster and more powerful decision making process. Four immediate benefit of the computer simulation are given as follows [9]:

1. While in the design stage, designers may virtually eliminate the time and costs of expensive tooling rework or design changes.
2. Simulation also eliminates costly and time-consuming physical mockups.
3. Manufacturing engineers reduce time-to-market by visualising and validating processes digitally before committing resources and purchasing or modifying equipments and tooling after simulation is validated. Engineers may use the product and process models for training, maintenance, and documentation.
4. Ergonomics, anthropometry and physiology issues can be analysed and addressed while the system is still in the design stage.

Ergonomics simulation is used to perform ergonomics analysis for product/process validation. The main purpose of an ergonomics simulation is to apply biomechanical models and data to assess the acceptability of physical workload. The design of product and process may be changed in order to improve ergonomic conditions in manual assembly and to promote overall productivity performances.

1.1 Aim and Objectives

The aim of this thesis is to integrate ergonomic considerations into assembly process modelling and simulation in order to provide product/process design changes before their physical prototyping.

The primary research objectives of this thesis are as follows:

- to study ergonomic factors in the manual assembly process early and thoroughly in the product/process design stage by computer modelling and simulation;

- to develop an assembly posture prediction method for the practical and precise ergonomics analysis in the assembly process;
- to propose assembly posture strategies in terms of task constraints, human diversity and human performances;
- to propose new ergonomic constraints for manual assembly sequence evaluation;
- to develop an assembly sequence planning system integrated with ergonomic constraints.

1.2 Research Overview

The research in this thesis involves multidisciplinary knowledge comprising different expertise for the ergonomics simulation and analysis; human posture modelling and prediction; computer aided assembly process planning. The main research deliverable in the thesis is to apply and develop novel computer modelling and simulation technologies towards the complete and correct ergonomics analysis in the manual assembly process.

First, a state-of-the-art commercial software tool is adopted for the ergonomics simulation and analysis. Associated with its capabilities in the ergonomics solution, a series of human related issues in the manual assembly process is simulated and studied in order to demonstrate the benefits of a virtual assembly approach to the product design, workplace design, time and energy saving.

The accuracy of ergonomics analysis using a software tool is strongly dependent on the accuracy of simulated postures. However, manual manipulation of digital human postures by software users can introduce errors and lead to a poor repeatability and reproducibility. A posture prediction method based on manual assembly consideration is therefore essential to a practical and precise ergonomics analysis. The development of the posture prediction method concerned with assembly features and human diversity will not only provide an effective control of digital human in the virtual environment that closely simulates the real assembly task, but also afford a clearer understanding of human performances during the operation. When this method is verified by comparing its outcomes with the real experimental data, it can be

used to conduct a more accurate posture analysis and investigate posture strategies under different assembly conditions.

In the manual assembly process, the choice of assembly sequences is important due to its significant influence on the product quality, assembly efficiency and operator performances. A well-designed assembly sequence, for example, will be easy for operators to perform and conversely, a poorly designed assembly sequence which includes awkward manoeuvres and whose execution will injure or fatigue operators gives rise to product quality losses. Therefore, the advantages of incorporating assembly operators in a proper assembly sequencing are very exciting. Consideration of high-level ergonomic issues at the product design stage eliminates possible design faults which lead to poor assembly postures, limited visibility and hand accessibility of assembly objects. More importantly, operator's health and safety can be improved, facilitating the improvement of product quality and productivity, reducing product cost and time to market in the long term.

1.3 Structure of Thesis

The remainder of the thesis consists of five chapters, including one chapter of literature review, three chapters of original research work, and one chapter of conclusions. Figure 1.4 shows the thesis structure.

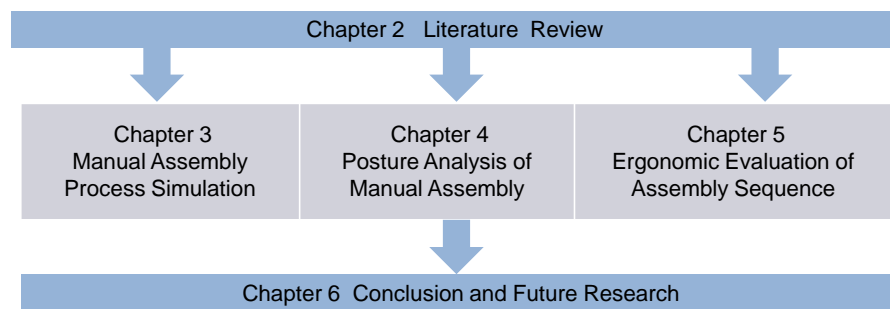


FIGURE 1.4: The thesis structure.

Chapter 2 presents a literature review on ergonomics simulation, posture prediction, and analysis and assembly process planning. In order to introduce the research work in these areas, traditional research methods, recent research achievements, research interests and in particularly the advantage and

disadvantages of previous research are reviewed and discussed.

Chapter 3 proposes a virtual assembly approach for the product assemblability analysis and the workplace design. First, a visual assembly environment is created where the ergonomics simulation and analysis is carried out utilising the commercial software tool – DELMIA. By studying two cases in the virtual environment, the influence of a series of product/process related factors and their combination to human performances in manual assembly tasks is investigated. Finally, the behaviour of DELMIA in the ergonomics simulation and analysis is evaluated.

Chapter 4 presents an optimisation-based posture prediction method in order to simulate and analyse manual assembly tasks with higher actuality and accuracy. At first, a 10-degrees-of-freedom (DOF), 4-control-points digital human model taking assembly features and human diversity into account is proposed. Next, the multi-objective optimisation method is applied to predict assembly postures and its efficiency and accuracy can be verified via experimental data. Finally, by incorporating specific constraints identified by the assembly task, posture strategies under different assembly conditions are investigated.

Chapter 5 proposes an integration of new ergonomic constraints in the objective evaluation of assembly sequencing for manual assembly tasks. Firstly, feasible assembly sequences are generated and evaluated based on the product geometry, assembly workstation layout, operator characteristics and posture. Subsequently, a new Liverpool Assembly Sequence Planning System (LASP) is developed to achieve this integration by applying two different evaluation criteria, i.e. visibility criterion, accessibility criterion or both.

Chapter 6 concludes the contribution of the research work described above. In addition, combined with the limitations which have been obtained during the research, promising directions for future research are identified.

Chapter 2

Literature Review

2.1 Introduction

Research presented in this thesis mainly consists of three parts: simulation of manual assembly process, assembly posture prediction and analysis, and ergonomics evaluation of assembly sequences. The reviewed work thus covers a wide range of areas. In this chapter, the literature related to these areas would be reviewed respectively.

In Section 2.2, the characteristics of manual assembly in manufacturing industry are summarised. Latterly, the definition of ergonomics as well as its developments and applications in manufacturing industry are introduced. Finally, a review on traditional and advanced ergonomics simulation technologies is given. The review of Section 2.2 leads to the research work of manual assembly process simulation in Chapter 3.

Human posture modelling is crucial to the realistic and accurate ergonomics simulation and analysis. In Section 2.3.1, a review on digital human modelling tools is carried out, including academic modelling tools and commercial modelling tools, which points at one limitation of them, i.e. the incapability in predicting complex human postures. In Section 2.3.2, general approaches to solve the posture prediction problem are presented. Human performance measures are often taken as the objective functions of an optimisation-based posture prediction problem and those relating to this investigation are introduced and discussed in Section 2.3.3. Postures should satisfy certain constraints which are proposed by different manual tasks, therefore in Section 2.3.4 a review is given on task-based posture prediction and analysis. The review of Section 2.3 is the

basis of the original research work in Chapter 4.

In Section 2.4, the definition and significance of assembly planning and assembly sequence planning are identified first. General approaches to generate assembly sequences and their applications in some typical assembly sequencing systems are presented later. Finally, evaluation criteria for assembly sequence optimisation are described. The literature review of the current assembly sequencing systems exposed their common limitation, i.e. considerations on human operators (including their anthropometry characteristics and working postures) are deficient. This finding will be taken into account in Chapter 5.

Figure 2.1 illustrates the structure of the literature review and the correspondence of each section to the original research in the thesis.

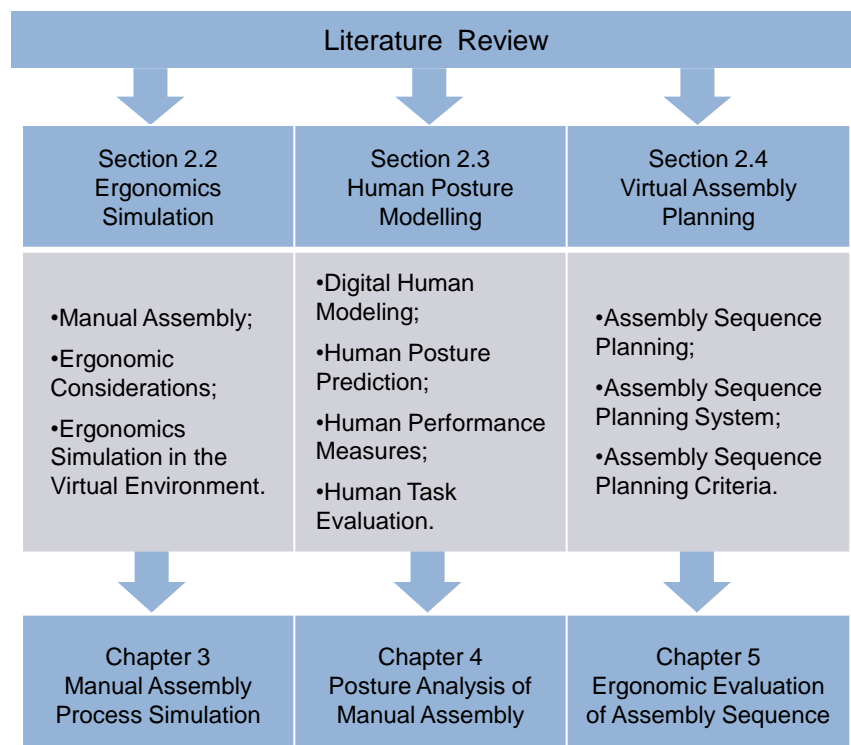


FIGURE 2.1: The literature review structure.

2.2 Ergonomic Simulation of Assembly Process

2.2.1 Manual Assembly

Assembly is the capstone process in manufacturing which brings together all the upstream processes of design, engineering, manufacturing, and logistics to create an object for desired functions [10]. Until very recently, assembly was accomplished exclusively manually. Automatic assembly systems were designed to perform high volume assembly of simple items in the twentieth century. In the 1970s, interest in robot assembly arose. High hopes were placed on robots combined with vision systems, force and touch sensors, powerful computers and artificial intelligence. Many original equipment manufacturers were even dreaming about a completely robotised assembly system. Through the years, this ideology crashed because of a lot of obstacles and imperfections, such as the technical complexity, high cost of machines and maintenance [11].

As indicated in literature [12], human operators perform better than robots over time in varying tasks and their outperformance would be substantially distinct after training. Assuming well-trained operators, their superiority (such as control of motion, decision-making capability and flexibility) in manual assembly can reduce assembly time and errors. Furthermore, the need for economical improvements in the last decade has created a paradigm shift back from automation approaches towards a focus on human factors [13]. The background for the dissatisfaction with investments in automation is shown in Figure 2.2 [1]. About 65% of the companies have taken or plan to decrease automation due to decreasing lot sizes. Those cannot be managed efficiently with highly automated facilities. The majority (57 %) of the companies demand a greater flexibility not given by automation to cover fluctuations in capacity. About 39 % report that the needed flexibility for production of parts with high complexity is not achievable with high automation. A shorter product life cycle is the reason for 14% of the companies' dissatisfaction. Particularly in markets with strong pressure on innovation, it seems impossible to develop automated facilities that are also able to produce the subsequent generation of products. Similar problems exist in flexible planning dealing with the future volume and handling part complexity. Moreover, costs for equipment modifications can exceed investments for completely new facilities. For this reasons, ergonomic considerations have become more and more critical in order to rediscover the true potential of operators and to design the manual assembly system in companies.

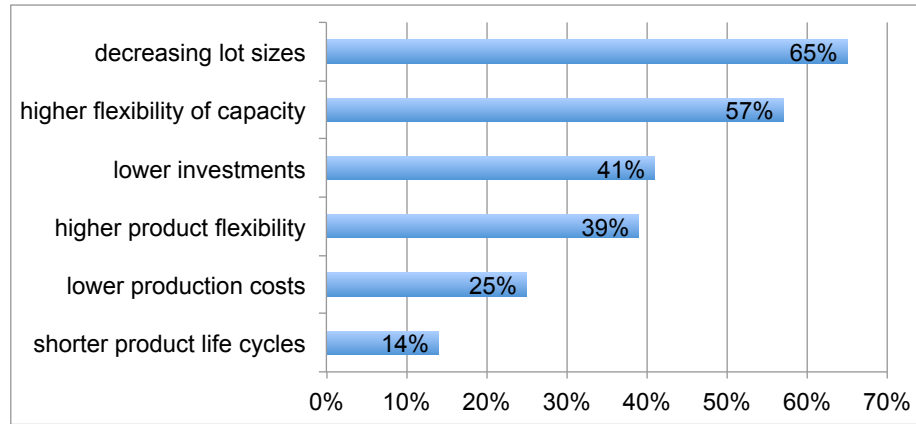


FIGURE 2.2: Reasons for reduction of automation [1].

2.2.2 Ergonomic Consideration

Ergonomics can be defined as “the branch of science that is concerned with the achievement of optimal relationships between workers and their work environment [14]”. It deals with assessments of the human’s capabilities and limitations (biomechanics and anthropometry), work and environmental stress (work physiology and industrial psychology), static and dynamic forces on the human body structure (biomechanics), design simulation and training, and design of workplace and tools (anthropometry and engineering). Therefore, ergonomics draws heavily from many areas of sciences and engineering.

The term **ergonomics** has its root in Ramazzini’s study of the ill-effects of poor postures and poorly designed tools on the health of workers in the early 1900s. Table 2.1 shows a brief history of ergonomics [15]. The goal of ergonomics is to fit work to individuals, as opposed to fitting individuals to the work. Given a body of scientific knowledge, it aims at developing efficient adaptations of work methods to the individual’s physiological and psychological characteristics. Therefore, the mission of an ergonomist is to identify and alleviate those work stresses which adversely affect the health, safety and efficiency of human operators.

In manufacturing industry, ergonomists use ergonomics principles for the following considerations [14]:

- Design, modification, replacement and maintenance of equipments for enhanced productivity and quality;
- Design and modification of workplace for ease of operation, service and maintenance;

TABLE 2.1: A brief history of ergonomics [15]

Year	Ergonomics	Social background
1900s	Time and motion study	Growth of industry
1930s	Powered conveyor line	Mass production
1940s	Human factors	World War II
1960s	Anthropometry	Growth of the consumer market
	Biomechanics	Space development
1970s	Occupational safety and health	Occupational safety and health act
		Labor Unions
1980s	Human-computer interaction	Computer
		LAN (Local Area Network)
1990s	Computer-oriented work	Personal computing
		Internet
2000s	-	Information revolution
		Globalisation industry
		Knowledge society

- Design and modification of work methods, including automation and task allocation between human operators and machines;
- Controlling physical factors (e.g., temperature, illumination, noise) in workplace for the best productivity and safety of operators.

2.2.3 Ergonomics Simulation in the Virtual Environment

Traditionally, industrial ergonomic research was implemented when products, workplace and human operators were physically and completely available. A videotaping system was used to collect data of operators performing activities in the workplace. Afterwards, ergonomic experts were consulted in the examination and evaluation of data in terms of work methods and the workplace design. The experience of an expert and the data from injuries in the workplace are therefore necessary for ergonomic studies. Examples of the traditional ergonomics research are found in literature [16–18]. In addition, ergonomics analysis was usually based on a single human performance measure (e.g. lift index, energy expenditure measure, work postures, etc.) related to a specific ergonomics standard, such as the Ovako Working Posture Analysis System (OWAS), the NIOSH (National Institute for Occupational Safety and Health) lifting equations, and the Garg analysis [19–22]. Ergonomics analyses which integrated two or more human performance measures in order to achieve multiple and simultaneous ergonomic improvements were rarely found. Thus it is obvious that the traditional ergonomics research is time-consuming, partial, and infrequently

applied.

With the development of computer science, a series of commercial software tools are available for ergonomics simulation and analysis, furthering a faster and more efficient product/process design. Those tools replace the human operator with an anthropometric articulated representation of a human being, call “manikin” [16]. This technology poses an opportunity to integrate ergonomic considerations into early design stages. Two of the main software tools, DELMIA from Dassault Systemes and Jack from Siemens Tecnomatix have been benchmarked. Table 2.2 shows a comparison between them focusing on features such as the data exchange capability, ergonomic analysis capability and typical applications.

Besides, virtual reality (VR), as an extension of simulation technologies allowing designers to immerse in a simulated environment and perform operations through various input/output devices, has been applied in ergonomics research.

TABLE 2.2: DELMIA vs. Jack.

Main properties	Software	
	DELMIA	Jack
Data exchange capability	Direct CAD interface: CATIA neutral formats: IGES,DXF, STEP,STL	Direct CAD interface: Unigraphics NX neutral formats: IGES,DXF STEP,STL
Ergonomic analysis capability	Carry analysis; Lift/lower analysis; Push/pull analysis; Reach envelop analysis; Metabolic energy expenditure; Biomechanical analysis; Vision analysis; Predetermined time standards; Rapid upper limb assessment(RULA)	Fatigue analysis; Low back analysis; Manual material handling analysis; Metabolic energy expenditure; NIOSH lifting analysis; Static strength prediction; Predetermined time standards; Rapid upper limb assessment(RULA); OWAS analysis
Typical application	Aerospace industry; military industry	Automotive industry; electronics industry

Jayaram et al. defines the key elements of VR as “ a) immersion in a 3D environment through stereoscopic viewing, b) a sense of presence in the environment through tracking and representing the user in the environment, c) presentation of information of the sense other than vision, and d) realistic behaviour of all objects in the virtual environment [23].” In a VR system, the ability to visualise realistic behaviour of CAD models and represent complex human interactions facilitates designers to identify assembly-related problems in the conceptual product design state, such as awkward reach angles, insufficient clearance for tooling, and excessive part orientation during assembly, etc. It also supports designers to analyse tooling and fixture requirements for assembly. In addition to visualisation, designers can touch and feel complex CAD models of parts and interact with them using natural and intuitive human motions with the assistance of haptic technology. With the force feedback device, collision and contact forces calculated in real-time can be transmitted to the user by robotic devices, making it possible for him to feel the simulated physical contacts that occur during assembly. These capabilities make VR tool ideal for ergonomics simulations which require frequent and intuitive manual interaction such as assembly method planning.

Rajan et al. developed a Virtual Reality-based environment JIGPRO for the analysis of product assembly and jig design [24]. 3D CAD models of assembly product, jig and a virtual hand were imported into JIGPRO for assembly process simulation and accessibility analysis. The main purpose was to analyse accessibility during assembly and to reduce the risk of musculoskeletal injuries.

Chryssolouris et al. developed an experimental virtual environment for the verification of manual assembly processes [25]. An immersive virtual environment with a CyberGlove was used to study four alternative layouts for assembling a boat propeller. The influence of a number of process parameters and their combinations on the lift capacity, energy expenditure and process cycle time were also quantified.

Sundin et al. described a case study of bus chassis assembly, which aimed to improve the efficiency and ergonomics in the early design stage of products [26]. ‘Jack’ was used for creating the computer manikin and conducting ergonomic analysis in terms of different working sequences and postures. The experience obtained in this case study showed that an ergonomics approach improves the design of product and production, leading to a better final product and better

assembly operations in the production system.

Jayaram et al. presented an integration of virtual environments and quantitative ergonomic analysis tool (Jack) into the real-time occupational ergonomic research [27]. This research allowed different postures and assembly processes to be examined in a more rigorous manner in order to identify problems in the assembly environment. In addition, the integrated technology presented in the research embedded complex ergonomics evaluation capabilities into commercial ergonomics systems and immersive VR applications.

Dukic et al. presented a case study of the manual assembly process of the XC90 car model at the Volvo Car Corporation for ergonomics evaluation in a pre-production phase [28]. The case study stressed the need to improve the ergonomics software tool in order to support users' interpretations to simulation results.

Cimino et al. proposed a methodology for the ergonomic effective design of workstation in industrial plants [29]. The actual workstations which manufacture high-pressure hydraulic hoses with alternative configurations were investigated and compared via the ergonomics analysis utilising software tool eM-workplace. The new workstation layout was characterised by ergonomic improvements in terms of energy expenditure and process time saving.

Of the above literature on the subject, the research interests in ergonomics simulations are mainly concentrated on:

1. Simulation of manual tasks and prediction of human related issues during the product life cycle such as workstation layout, tooling design, virtual training, maintenance and serviceability in order to provide suggestions and improvements for the product and process design before their physical mockups or prototypes exist;
2. Development of advanced technologies, for example, visualisation systems, human modelling systems and accurate ergonomics analysis functionalities, in order to better integrate and reinforce ergonomic considerations in the immersive or non-immersive environment.

The usage of VR technology in the ergonomics simulation and analysis is very costly since it has demanding requirements on computer software tools and equipment for the creation and visualisation of the virtual environment by means

of various sensations (visual, haptic, auditory, etc). Additionally, in order to gain the integration of CAD systems and VR environments, a time-consuming data exchange procedure is compulsory. Therefore, its application in ergonomics research is still limited, especially for those small and medium enterprises even though they have the same risk of ergonomic problems.

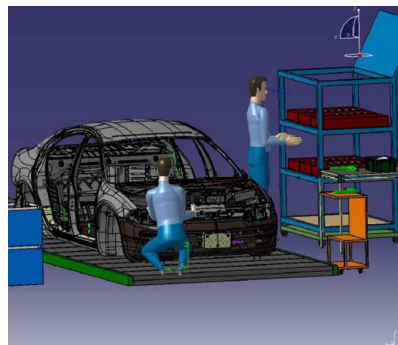
2.3 Human Posture Modelling in Manual Tasks

2.3.1 Digital Human Modelling

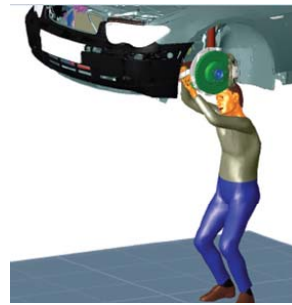
Digital human modelling (DHM) is defined as “2D or 3D graphical computer representation of the human body based on anthropometric measurements, link and joint structure, and movement characteristics [30]”. Digital human modelling includes the appearance, or skin, and the built-in characteristics, such as the skeleton system, body dimensions, vision, ranges of motion, biomechanics model, discomfort prediction model, and so on.

Research on digital human modelling spans at least two decades. *Cyberman* is one of the earliest digital humans [31]. It was developed by Chrysler Corporation for automotive industry in order to define and analyse acceptable limb and body locations for a human model within a virtual environment. Specifically, it can be used to analyse virtual drivers and passengers and their activities in and around a car. *Cyberman* is a simple wireframe model, and other digital humans of similar complexity have also been developed. *Combiman* was designed at the Aerospace Medical Research Laboratory in order to determine human reach capacity and it had been used for the aircraft cockpit-configuration design and evaluation [32]. *Sammie* was designed at the University of Nottingham for the general anthropometric analysis and design [33]. Additional anthropometric modelling programmes include *Boeman* and *CAR* at the Boeing Corporation [34], *Buford* at Rockwell International [35], and *Bubbleman* at the University of Pennsylvania [36]. As the appearance of initial virtual humans has been far from realistic, considerable research has been conducted in an effort to improve realism. For instance, Badler et al. and Thalmann developed models based on the combination of multiple cylinders [37, 38]. In addition to visual appearance, research has focused on autonomous perception, intelligence and behaviours [39, 40].

To date, several companies have developed relatively advanced digital human models on the market, as shown in Figure 2.3. For example, DELMIA's manikin (Figure 2.2(a)) and Jack (Figure 2.2(b)) from Siemens Tecnomatix as mentioned in Section 2.2.3. In DELMIA, the manikin structure consists of 99 independent segments which contribute to 148 degrees of freedom. The manikin is created by selection of gender and the percentile standard (e.g., male, 50th percentile) or editing of more than 100 editable anthropometric variables. Forward kinematics and inverse kinematics are provided at the same time so users can control manikin's movements manually. Jack is also a scalable human model with flexible segments (77 segments in total) which can be articulated through inverse kinematics and forward kinematics. Besides, digital human models offered by Ramsis (Figure 2.2(c)) and Sammie System (Figure 2.2(d)) are all manipulated by software users to execute the ergonomics simulation and analysis. Ramsis developed in collaboration with German automotive industry is used extensively for designing automobile interiors and airplane cockpits. Sammie System's manikin structure is made up of 18 joints and 21 rigid links which provide a preliminary evaluation about fit, reach, vision and posture.



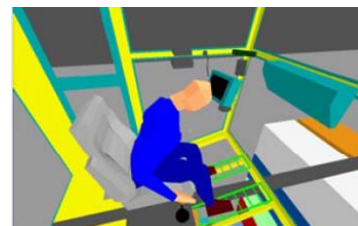
(a) DELMIA



(b) Jack



(c) Ramsis



(d) Sammie System

FIGURE 2.3: Examples of commercial digital human models.

The review of existing digital human modelling tools has revealed one limitation, i.e. the difficulty to predict complex human postures and movements in a timely and realistic manner. Research on human posture prediction using modern digital human modelling tools incorporating empirically validated, perceptual-motor and biomechanical models are under investigation. A general practical problem they face is that users were incapable of specifying how a manikin of certain demographic and anthropometric characteristics should be positioned in the virtual environment, especially when dynamic activities or motions are involved.

2.3.2 Human Posture Prediction

Human posture prediction typically involves finding a set of joint rotations and translations that results in an end-effector reaching a given target point in Cartesian space. Before a review of this problem is given, it is necessary to briefly describe the basic computational procedures used in human posture modelling, which are forward kinematics and inverse kinematics. Forward kinematics refers to the procedure of computing joint and end-effector (e.g., fingertip) coordinates from known joint or segmental angles. Inverse kinematics is the procedure of determining the joint or segmental angle from known joint coordinates, or most often end-effector coordinates. In biomechanical models of human posture, normally the number of joint angles (i.e. degrees of freedom) is greater than the dimension of end-effector position. Therefore, kinematic redundancy in inverse kinematics occurs, which gives rise to a very fundamental problem in the modelling of human posture – the so-called Bernstein’s problem.

There are two approaches to solve the posture prediction problem. The first and the more traditional one is to use the classical animation obtained from experiments or user-manipulation of manikins. Firstly, data is collected either from thousands of experiments with human subjects, or from simulations with 3D human modelling software. Then, the data is analysed statistically to form predictive posture models (e.g., regression models). These models have been implemented in simulation software tools along with various methods in order to select the most probable posture given in a specific scenario [41–43]. Although this approach is based on actual human data thus does not need to be verified in terms of realism, it involves a time-consuming data collection process often requiring thousands of human subjects.

Another approach for solving posture prediction problem is based on optimisation where various performance measures served as objective functions or cost functions are formulated to mathematically represent an optimal strategy in determining joint motions. It hypothesises that human performances govern human posture; thus the process of human posture simulation can be formulated as an optimisation problem that minimises human performance measures given at different constraints and hand loads, corresponding to a number of manual tasks. Zhao and Badler used constrained, gradient-based optimisation to minimise an objective function formed by weighted sum of components which model various factors, such as the position of the fingers (end-effector) or the orientation of the hands [44]. Limits on the joint angles were incorporated as constraints. Riffard and Chedmail used an unconstrained global optimisation approach in order to determine the optimum placement of the torso and the optimum posture of a 7 degree-of-freedoms arm [45]. Equations for target contact, collision avoidance, vision, body-orientation and torque were combined in a weighted sum to form the objective function. In addition, coupling between particular joint angles and variable joint limits was modelled. The final unconstrained problem was solved using simulated annealing, nonetheless the solution process was relatively slow. Yu used the same fundamental approach but took joint displacement and potential energy as objective functions for a 3 degree-of-freedoms arm [46]. The problem was solved using a genetic algorithm, which is also a relatively slow global optimisation technique. Mi extended the work of Yu to a 15 degree-of-freedoms arm [47]. A real-time optimisation algorithm was developed which combines predetermined genetic algorithm results with an unconstrained gradient-based algorithm.

In optimisation-based approaches, the idea of combining multiple objective functions to determine an optimal solution leads the application of multi-objective optimisation (MOO) method. Zhao and Bai used MOO method to solve problems of load distribution and joint trajectory planning, taking the minimum joint or/and load as objective functions [48]. With respect to robot motion prediction, Saramago and Steffen used this method to minimise the travel time for a robot and the mechanical energy of robotic actuators, considering dynamics and collision avoidance of moving obstacles [49, 50]. With respect to human posture prediction, Yang et al. described the use of MOO method to predict human's upper body posture, combining joint displacement, potential energy and discomfort as human performance measures [51, 52]. Ma et al. proposed the use of MOO to predict and analyse the human posture with the

consideration of physical fatigue and joint discomfort concurrently [53]. These studies adopted a weighted sum method to convert the multiple objectives into a single objective to achieve the Pareto optimal sets of the optimisation problem and then investigated the effect of various weighting factors to Pareto optimal set in order to obtain the insight of the most desirable manner to combine multiple objectives.

The accuracy of optimisation-based posture prediction is heavily dependent on the objective function. Hence there is a potential development not only within the optimisation algorithm but also within the human performance measures. In addition, inverse kinematics algorithm is not necessarily correct for prediction of posture because its theoretical foundation may violate task constraints. Therefore, the development and integration of task constraints modelled from specific task contexts into posture prediction is essential when posture-prediction approach continues to advance.

2.3.3 Human Performance Measures

Currently, there exist over 500 distinct human performance measures for evaluations of human functionalities and capacities associated with different domains, such as posture, strength, energy, fatigue, and so on [54]. In this section, posture evaluation methods and energy evaluation methods which will be used in the later investigation are reviewed separately.

a. Posture Evaluation Methods

Posture analysis is one of the most important aspects in human performance evaluations. Govindaraju mentioned that when the human body was exposed to discomfort, its natural reactions would slow down in order to minimise the accumulation of discomfort, and avoid or reduce the manifestation of pain [55]. Psychologically, when the operator starts to feel fatigue, his motivation to keep performing at optimal levels is significantly reduced. As a result of the reduced performance, human errors could increase, which in turn increases the risk of accidents and loss of quality. The analysis of posture is therefore necessary.

Posturegram is one of the first methods developed to numerically quantify human postures [56]. From repeated observation of operators, the basic body posture in a three-dimensional coordinate system, the levels at which joints and limbs are located, and the direction and amount of movements within the

three-dimensional coordinate system are defined and recorded on a Posturegram card. By creating a standard base posture, it was the first method describing the posture deviation from a start position.

The Ovako Working Posture Analysing System (OWAS) is another practical method for unsuitable working postures identification and evaluation [19, 57]. In OWAS, a coding system as shown in Table 2.3 is established to evaluate each posture corresponding to the discomfort or risk it caused. Each posture is described with a 4 digit code. After that, action categories are given a rank from 1-4 with 4 being the highest risk to the musculoskeletal discomfort. Subjective evaluations of each posture's code are categorised into one of the 4 action categories. Applied initially for a company in Finland steel industry, it has now been integrated into a substantial of ergonomics software tools for manual task investigation.

TABLE 2.3: OWAS coding system [19]

Body region	Posture or weight	Risk rank
Back	Straight	1
	Bent	2
	Twisted	3
	Bent and twisted	4
Upper Extremity	Both below shoulder height	1
	One above shoulder height	2
	Both above shoulder height	3
Lower Extremity	Sitting	1
	Both legs straight (Standing)	2
	one leg straight (Standing)	3
	Both legs bent (full squat)	4
	one leg bent	5
	Kneeling	6
	Walking	7
Force or load effort	≤ 10 kg	1
	≤ 20 kg	2
	> 20 kg	3

Similar to OWAS, a rapid upper limb assessment (RULA) method is developed which uses the concept of numbers to describe postures with an associated coding system [58]. It is of particular assistance in fulfilling the assessment requirements of the UK guidelines to prevent work-related upper limb disorders and recently has become a programming ergonomics analysis tool as

well.

Rapid Entire Body Assessment (REBA) method is developed as a practitioner field tool, which is specifically sensitive to the type of unpredictable working postures found in health care and other service industries [59]. By coding and ranking over 600 postural examples collecting from hospital industries, a final REBA score (1-15) is established with accompanying risk and action levels.

Besides these methods, some checklist tools are developed to assess postural risks rapidly, e.g. PLIBEL and Postural Checklist [60, 61]. PLIBEL (method for the identification of musculoskeletal stress factors which may have injurious effect), designed and tested in Sweden, is developed to determine tasks' contribution to WMSDs and now has been used in a variation of environments from manufacturing industries to service industries. It includes a list of seventeen total "yes/no" questions which relate to individual body regions to identify whether they cause WMSDs. Table 2.4 gives some questions relating to the low extremity in the PLIBEL. Postural Checklist was originally developed for management of automotive manufacturing. Postures in checklist are grouped according to different body segments. Qualitative stress rating responses for each of the body segments can be given as zero, check or star. A total risk score for a task was quantified by adding the total number of checks with the total number of stars, as shown in Table 2.5.

TABLE 2.4: PLIBEL questions relating to the low extremity [60]

Question number	Related question for feet, knee and hip body regions
1	Is the walking surface uneven, sloping or slippery?
2	Is the space too limited for work movements or work materials?
3	Are tools and equipment unsuitably designed for the worker or the task?
6	(If the work is performed whilst standing): Is there no possibility to sit and rest?
7	Is fatiguing foot-pedal work performed?
8	Is fatiguing leg work performed?

In reviewing the posture evaluation tools above, some limitations of the methods based on the coding system or checklist should be noted. First, a

TABLE 2.5: Stress rating response and their explanations in postural checklist [61]

Stress rating response	Explanation
Zero	Using the posture for the indicated duration presented the insignificant risk of injury or illness.
Check	Moderate exposure to postural stress was presented indicating a potential risk of injury to some workers
Star	Substantial exposure to postural stress was presented indicating significant risk of injury

flexible range of joint movement was typically divided into several sections and each section was simply assigned by a score. Furthermore, the posture score had a consistent increment of '1' according to the joint section or the number of checks. The score '1' is given to the working posture where the risk factors present are minimal and the higher scores are allocated to more extreme postures indicating an increasing presence of risk factors. For example, a calculation of lower arms score using the RULA method is shown in Figure 2.4 [59]. It is observed that only two scores (1 and 2) are used to describe the posture discomfort resulting from the lower arm movements. Though the method is easy and rapid used by the analyst, limited scores can not represent differences existing among considerable joint movements sufficiently and accurately. Also, due to the physical properties of joints, their influence on the discomfort score can not be identical. Therefore, a more detailed analysis should be conducted in order to better investigate the exclusive contribution of joint posture to the discomfort and risk.

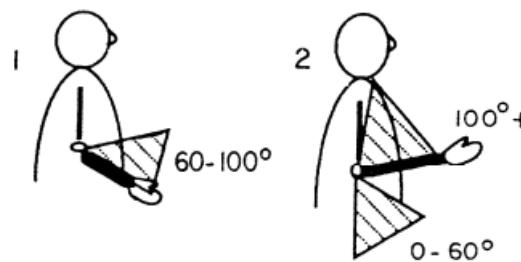


FIGURE 2.4: The lower arm posture score calculation [59].

b. Energy Evaluation Methods

Energy expenditure rates are examined typically by ergonomists to assess physiological demand on workers. In theory, if workers are required to exert less than 50% of their energy expenditure capacity during a work day, then they

should not become physiological strained. Therefore, a predictive method for assessing metabolic rate of work has appealed to practitioner as an invaluable tool due to its major advantage on the job design.

Traditionally, many researchers had used the measurement of oxygen utilisation rate to predict the metabolic energy expenditure [62, 63]. However, due to interference of measuring equipments with the normal work methods, its results may be not valid.

A table look-up approach can provide a rough approximation of the metabolic energy expenditure of average operator in performing manual activities. A large number of tables, in which occupational task and grouped together according to their metabolic demands, can be found in the literature [64, 65].

Garg proposed a metabolic rates prediction approach for manual materials handling tasks [66]. The average rate of a handling task can be estimated by summing up the basic energy require to maintain a body posture and the net energy cost for lifting, carrying and walking.

Burford developed a systematic workload estimation (SWE) method for assessment of the metabolic cost of work performed in underground mines [67]. In SWE, the analyst conducts estimation of metabolic rate by coding tasks according to schema and then the codes are converted into their caloric values.

Metabolic energy expenditure rate has been often suggested in literature for determining the maximum task intensity which can be continuously performed without accumulating an excessive amount of physical fatigue. Hence energy expenditure prediction can also be related to fatigue prediction. At the biomechanical level, literature [68] explains fatigue as loss of energy. In the human gait motion, Anderson and Pandy suggested that minimising muscle fatigue at each instant is roughly the same as minimising metabolic energy expended per unit distance travelled over the duration of the gait cycle [69]. In fact, it is well known that energy expenditure and muscle fatigue have positive correlation [70]. Therefore, minimum metabolic energy expenditure indicates less muscle fatigue as well.

2.3.4 Human Task Evaluation

The under-constrained nature of posture prediction is driven by tasks being performed. Although a large number of posture prediction methods have been proposed, most of them focused on relatively narrow range of tasks, such as walking, stair climbing, object lifting and transferring.

Within these tasks, the research on manual lifting are especially prevalent due to it is distinctly associated with either causing or aggravating musculoskeletal disorders in a large number of workers. The NIOSH Lifting Guide is the first comprehensive approach to evaluate the adverse effects of manual lifting in industry [71]. This Guide that was issued focuses on those tasks and material container characteristics that best define a hazardous lifting act. These factors were defined and given a variable designation, as follows:

1. Weight of object lifted;
2. Location of object centre of mass (or hand grip centre) measured horizontally from a point on the floor midway between the ankles;
3. Location of object centre of mass (or hand grip centre) measured at beginning (origin) of lift;
4. Vertical travel distance of hands from origin to destination (release) of object;
5. Frequency of lifting (in lifts per minute) averaged over period of lifting;
6. Duration of the period during which lifting takes place (less than one hour or on an eight-hour basis).

A series of methods for posture prediction in lifting tasks is proposed subsequently. Dysart and Woldstad presented three separate models to predict the postures of humans performing static sagittal lifting tasks [72]. The optimal posture was selected based on the criteria such as subject's total torque is minimum; the torque exerted at each joint is minimum; or the body stability is maximum. Kim et al. used an optimisation-based posture prediction method to predict and simulate realistic lifting postures [73]. Lifting postures were predicted based on the metabolic rate and joint torques and their risk level to injury was also evaluated. Extending the research from static level to dynamic level, Ayoub presented a simulation model to generated 2-D lifting motion patterns, as well as the kinematics and kinetics of motion for lifting tasks [74, 75]. Huang et al. developed a multi-body dynamics model to generate

optimal trajectories of human lifting movements based on optimal control [76]. The optimal motion was generated to minimise the loading of specific joints such as an ankle or a knee during the lifting motion. Xiang et al. developed an optimisation-based predictive dynamics formulation to predict nature lifting motion [77]. The results had demonstration the ability of the formulation to choose a realistic human lifting strategy with different objective functions and constraints.

The general constraints with respect to lifting tasks proposed and formulated in the above literature include: joint rotation limits, joint torque limits, foot locations, object's weight, horizontal or vertical travel distance of the object, which are illustrated in Figure 2.5 [78].

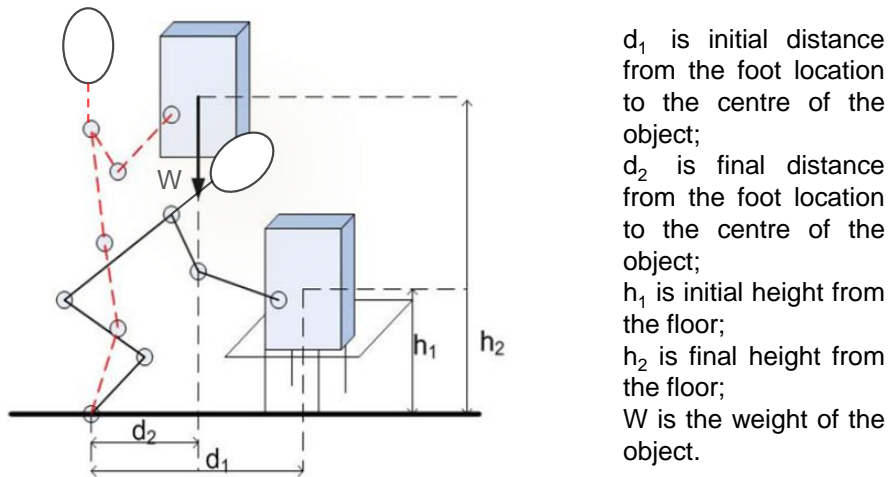


FIGURE 2.5: Constraints for lifting tasks [78].

Unlike these tasks, assembly tasks are composed of part mating and part joining (e.g. fastening screws, press fits, riveting, welding). Manual operator normally performs the assembly task in a fixed working height, in which the translation and rotation movement of his main body are not required. Moreover, the position and orientation of the assembly object with respect to the operator is not arbitrary, i.e., it should be clearly viewed by the operator during assembling in order to provide sufficient assembly guides. Therefore, it is essential to identify and propose particular constraints characterised by manual assembly in order to analyse the assembly postures precisely and efficiently.

2.4 Virtual Assembly Process Planning

2.4.1 Assembly Sequence Planning

“Assembly planning”, generally speaking, refers to the planning of any or all aspects of the assembly process by engineers and/or an automated system [79]. It is usually a hierarchical process, beginning with a broad picture of the overall assembly plan and gradually including more and more details. Clearly, the more complete and realistic the assembly plan is, the more easily the designer will be able to anticipate difficulties in assembling a product and then further improve the development of the product and of the assembly process.

Assembly sequence planning, or assembly sequencing, is one of the most fundamental aspects of assembly planning. It attempts to identify and represent the constraints on assembly plans which emerge strictly from the geometry and structure of the product itself. The result is a ordering on assembly operations that brings two or more subassemblies together for a larger subassembly. Any sequencing of the operation obeys the pre-defined constraints is called an assembly sequence. An assembly plan can be established from an assembly sequence by adding details and taking account of new constraints.

The generation of assembly sequences contains two main phases. In the first phase, all infeasible (i.e. impossible) sequences are eliminated. These are the sequences which are not complete or exclude some parts of the assembly. Once it is completed, the second phase requires engineers reveal the good sequence(s) out of the remaining sequences utilising the assembly criteria. A review of the methods for accomplishing these two phases is given in the next two sections.

2.4.2 Assembly Sequence Planning System

In the last two decades, a number of systems have been targeted specifically at assembly sequencing. These systems differ both in their representation of assembly sequence and in the reasoning techniques used to identify assembly operations which satisfy the geometric and mechanical constraints. Representation of assembly sequence will be described in Section 5.4. Several general approaches of assembly sequence identification are reviewed in this section.

Bourjault developed the first system for generating assembly sequences of a product [10]. His method starts with a liaison graph, which is a graph of connection between parts as shown in Figure 2.6. An assembly sequence corresponds to a particular order in which the liaisons can be established. Geometric reasoning is supplied by users, who answer YES/NO questions about whether certain liaisons can be established before or after others. From answers of these questions, all feasible assembly sequences of the product are generated.

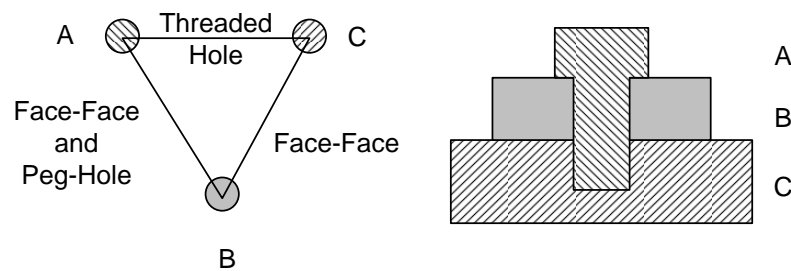


FIGURE 2.6: An example of the liaison graph [10]. (Part A is a screw that fastens part B to part C)

De Fazio and Whitney extended Bourjault's method by using specific questions to determine liaison precedence, such as "what liaisons must be done prior to doing liaison i " and "what liaisons must be left to be done after doing liaison i " [80]. This method significantly reduced the question count for determining all possible assembly sequences. Baldwin later developed simple geometric checks to answer these questions automatically, further reducing the amount of questions in the previous techniques [81]. However, an engineer is still required as a final judge of the assembly operations.

The problem of automatically generating assembly sequences is an extraordinarily difficult one, recently shown to be NP-complete in both two dimensional and three dimensional cases [82]. One common thread that appears in the assembly sequencing literature is the strategy of "assembly by disassembly", in which an assembly sequence is generated by starting with the completed product and working backwards through disassembly steps. Assuming that the parts are rigid and non-tolerance, the disassembly sequence can then be reversed to produce a valid plan of assembly sequencing.

In order to avoid the NP problems, a number of systems were developed to perform assembly sequencing only considering translation along major axes or along pre-specified trajectories [83, 84]. Hoffman, for example, created a system

called BRAEN (B-rep Assembly Engine) which took boundary representation (B-rep) models of components to derive a sequence of translational subassembly operation which would disassemble the product. The stability of subassembly under gravity was also considered to construct valid assembly sequences of the product. Later, he further extended his system to perform disassembly not only along translational trajectories in the major axes but also along specified rotational trajectories [85].

Another simplification used to avoid the NP-completeness in more general cases is to insert only one part at a time. Wolter and Dutta presented a system to automatically generate disassembly sequences for a given product by using the notation of a “disassembly tree (DT)”, in which only one part is removed at a time via single-step translations [86, 87]. Geometrical, logical and dimensional consideration was investigated for computing disassembly sequences in the system.

Using the similar approaches described by Wolter, Hoffman, and Homen de Mello, Romney developed a system called STAAT (the Stanford Assembly Analysis Tool) which was capable of computing a sequence of steps necessary to disassemble a given product; these steps could be reversed to produce the assembly sequences [88]. STAAT is a stand-alone system whose input is a geometric description of the product and only able to handle single step translations. The feasibility of the disassembly trajectories is determined by sweeping or projecting the parts in the pre-proposed directions.

A summary of the above literature on the development of assembly planning systems is shown in Table 2.6.

It is instructive to note that the computer graphics approaches are widely used to explore geometrical issues relating to assembly sequencing in the above research, for example, part separation problems, collision detection problems, and so on. The requirements for a better solution towards assembly sequencing problems can promote the development and application of computer graphics on the other hand. In this thesis, the algorithms in computer graphics would be utilised and developed to generate all feasible assembly sequences and to propose new constraints based on the geometric description of mechanical products.

TABLE 2.6: A summary of literature on the development of assembly planning systems

Authors	Year	Assumption	System input	System output	System features
Bourjault [10]	1984	Parts are rigid.	Liaison diagram	Liaison sequence diagram	Generated YES/NO questions for the computer or the engineer to answer.
De Fazio and Whitney [81]	1987	Parts are rigid.	Liaison diagram	Liaison sequence diagram	Altered the question form; reduced the question count; required the anticipation of the engineer.
Baldwin [82]	1991	Parts are rigid.	Liaison diagram	Liaison sequence diagram	Raised queries and determined answers automatically; integrated assembly sequences generating and editing.
Hoffman [86]	1990	Considered translations along X, Y and Z directions; parts are rigid.	B-rep models	Order of disassembly operations	Required no manual guidance.
Wolter [87]	1989	Parts are rigid and moved directly to their final positions; one part is removed at a time.	Disassembly tree	A program of robot assembly	Developed for robot assembly system.
Romney [89]	1995	Parts are rigid and moved directly to their final positions; one part is removed at a time.	B-rep models	AND/OR graph	Not only generated assembly sequences automatically, but also produced complexity measures for the assembly process.

2.4.3 Assembly Sequence Planning Criteria

Once all feasible sequences are available, the second phase of assembly sequence planning entails the generation and application of criteria to reveal good sequence(s). The process of selecting an optimum sequence from the feasible sequences is called sequence editing as well.

Wolter proposed a list of criteria should be considered in evaluating an assembly plan, composed of directionality, fixture complexity, manipulability, locality and tool changes [86]. Homen de Mello and Sanderson introduced two criteria to select assembly plans: the first one is to maximise the number of different assembly sequences encompassed by the assembly plan; the second is to maximise the amount of parallelism or simultaneity that is possible in the execution of the assembly tasks [89]. Baldwin reported an integration of sequence generation and evolution containing two classes of sequence editing facilities [81]. One is editing states and moves which allowed deletion of assembly states which have multiple subassemblies, deletion of moves where a particular set of simultaneous mates is made. This can quickly reduce the original large set of sequences to a reasonable few. And the other is editing all individual assembly sequences based on fixturing, refixturing, orientation, and reorientation issues.

Feasible assembly sequences can also be compared and selected based on time and cost. Kanai et al. developed a Computer Aided Assembly Sequence Planning and Evaluation system (ASPEN) which chooses an optimum sequence with the least operating time [90]. MTM (Methods Time Measurement) and DFA (Boothroyd's Design for Assembly) are used to evaluate the differences of operating time among feasible sequences explicitly. Lambert presented a dynamic programming algorithm for determining the optimum disassembly sequences of complex products with the objective of maximising the revenue [91]. Johnson and Wang introduced a procedure which integrates economical factors into the scheduling of disassembly operations aiming at improving the efficiency of the disassembly planning process and generating an optimum disassembly sequence with maximum profits [92]. Three criteria are established which are material compatibility, clustering for disposal and concurrent disassembly operations.

Meanwhile, a series of algorithms based on heuristic rules were developed in order to evaluate the assembly sequences utilising the criteria mention above. Milner et al. applied simulated annealing (SA) to find the probable least cost

assembly sequence for a mechanical product [93]. Candidate sequences are selected one at a time by the SA algorithm and their costs are estimated by designing a minimum unit cost concept assembly system. Dini et al. described a method based on genetic algorithms for the generation and the evaluation of assembly sequences [94]. Optimum assembly sequences were obtained using an appropriate fitness function which takes into account simultaneously the geometrical constraints, the minimisation of tool changes and object orientation, and the possibility of grouping similar assembly operations. Tseng et al. applied the memetic algorithm which is an extension of the traditional genetic algorithm for sequences optimisation, whose optimisation function is determined by the similarity of the engineering data of the connectors since the arrangement of similar connector can reduce the changes of assembly tools and direction, thus reducing assembly time accordingly [95].

However, most of the sequence generation and emulation systems and algorithms stated above are developed for automated assembly. Inevitably, human related factors in the manual assembly process are often ignored or even violated in the sequences evaluation and optimisation. In order to create assembly instructions which are easy to understand and implement for operators, Agrawala et al. presented a sequence planning system based on cognitive psychology[96]. By comparing the score of current parts visibility, previous parts visibility and future parts visibility, assembly sequence is selected. Wilson proposed a framework with full consideration on geometric accessibility constraints especially for a wide variety of assembly tools handled by the operator [97]. The framework can be further integrated into assembly planning. However, their research is still lack of concern on operators, such as their anthropometry characteristics and working postures. Therefore, the integration of high-level considerations on operators into an assembly sequence planning system is necessary. It will provide more sophisticated feedback to the designer, not only focusing upon the product's functionality but also upon its assemblability.

Chapter 3

Manual Assembly Process Simulation

3.1 Introduction

The importance of ergonomic considerations in the early phase of product and production system design is clearly evident, however, its implementation remains a great challenge [98]. In order to assist engineers when considering ergonomics, a number of commercial ergonomics simulation software tools have been incorporated with the basic ergonomics analysis functionalities for evaluating human factors in the design of product and process. DELMIA is one example, which allows a systematic analysis on products, processes, as well as operators in the development of products and production systems.

This chapter describes the implementation of ergonomics simulation and analysis for manual assembly in DELMIA. A brief introduction of DELMIA is presented in Section 3.2 first. Its functionalities in the ergonomics simulation and analysis are described separately in Sections 3.3, 3.4 and 3.5. Finally, the manual assembly process is simulated. General ergonomic issues identified in the process are analysed by means of two case studies: one is the manual assembly of a formula student car presented in Section 3.6, and the other is an aluminium blower assembly presented in Section 3.7.

3.2 Simulation Tool: DELMIA

DELMIA, stands for Digital Enterprise Lean Manufacturing Interactive Application, is a leading software tool for digital manufacturing solutions, which

allows manufacturers to define, plan, create, monitor, and control production processes virtually. It provides an array of dedicated applications for industries, combined with an environment for knowledge-sharing, process and resource management, and the ability to capture and implement practices for manufacturing. Its Product Lifecycle Management (PLM) technology offers five solutions in order to match users' needs in different domains, for example in aerospace and defence, architecture and engineering, transportation and mobility, and so forth. These solutions are presented as follows:

- **Resource Planning:** provides a complete 3D work-cell building solution to set up and validate tooling, perform robot feasibility studies, and associate tooling and positioning equipment, including standard robots, for a complete assessment of a manufacturing work-cell or an entire line;
- **Robotics:** delivers a comprehensive, robotic programming solution that offers advanced simulation capability with dedicated offline programming tools for arc and spot welding applications for accurate, real-world robotic welding processes. It provides an environment for teaching and simulating robotic tasks as well as the complete work cell cycle to validate the mechanical processes;
- **Assembly Planning:** enables the assembly planner or simulation engineer to plan the assembly process. It delivers assembly process tools to simulate parts and assemblies to validate the manufacturing process;
- **Ergonomics:** delivers the capability to build 3D human models to simulate human tasks, based on processes and to optimise the human workspace. In addition, users can perform risk factor analysis to maximise human comfort, safety, and performance through a wide range of advanced tools, analyse human postures, vision, reachability and biomechanics for compliance with ergonomic standards;
- **Controls:** offers Smart Device Builder capabilities for the engineer to create the mechanical, kinematical and logical behaviour of devices which can then be used to validate a PLC program in a virtual environment.

3.3 Virtual Ergonomics Solution

DELMIA's virtual ergonomics solution provides the capability to create, simulate and validate human operator interaction for manufacturing and therefore it is

adopted as a main research tool in this investigation. It consists of five workbenches, which are Human Builder, Human Task Simulation, Human Activity Analysis, Human Posture Analysis, and Human Measurements Editor. Their combination achieves a complete assembly process simulation and ergonomics analysis. These five workbenches are briefly described as follows:

a. Human Builder (MHB): permits the intuitive creation of standard digital humans for the initial operator/product interaction analysis. A user-friendly interface as shown in Figure 3.1 is provided to select a manikin's gender, percentile and population (including 7 populations which are American, Canadian, French, Japanese, Korean, German and Chinese respectively) from the pull-down menus. A manikin structure generated afterwards consists of 99 independent links, segments and ellipses. In addition, it possesses fully articulated hand, spine, shoulder, and neck models to accurately reproduce natural human movements.



FIGURE 3.1: The interface for creating standard manikins.

b. Human Measurements Editor (MHM): permits the creation of advanced, user-defined manikins via a suite of anthropometry tools. This can be used to assess the suitability of a product or process against its intended target audience.

In addition to a default manikin, users can define any human model that exists within a target population in MHM by amending the anthropometric variables manually, for example, by editing desired measurements in percentile value, unit measurement, or by an intuitive “click and drag” graphical user interface as shown in Figure 3.2.

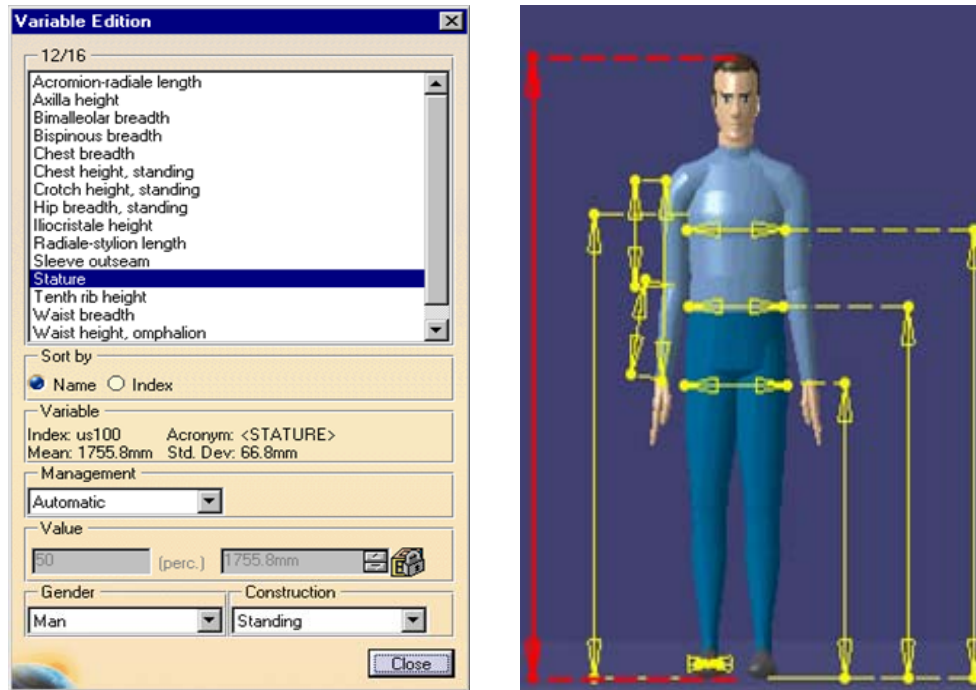


FIGURE 3.2: Anthropometry tools in MHM.

c. **Human Task Simulation (MHT)**: provides a powerful simulation tool to create and simulate activities for operators in the virtual environment. These activities are broken down into a series of target postures according to the time sequence. Users create, control and modify individual target posture via posture editing commands available in the MHT, given following:

- **Posture Editor** – to create postures by assigning a precise value to each degree of freedom of every joint in a manikin;
- **Forward Kinematics** – to control manikin's postures by dragging a selected segment in a direction and thus the segment will follow the movement exerted in that direction;
- **Inverse Kinematics** – to fix or move dedicated segments (including neck, pelvis, left foot/right foot, and left hand/right hand) on the manikin directly;
- **Reach Posture** – to locate an selected segment of the manikin to a target position via the inverse kinematics capability;
- **Standard Pose** – to apply standard poses to the manikin, which are Sit, Squat, Stoop, Twist, Lean and HandGrasp, respectively.

Utilising the commands repeatedly and interactively from one target posture to another, along with the assistance of some basic task simulation, such as walk

to a specific location, walk up and down stairs, ascend and descend ladders, users are capable of building an animation of human activities in the virtual environment. Finally, organising these activities between manikins in a time sequence via the Gantt chart as shown in Figure 3.3, a complete human task simulation is implemented.

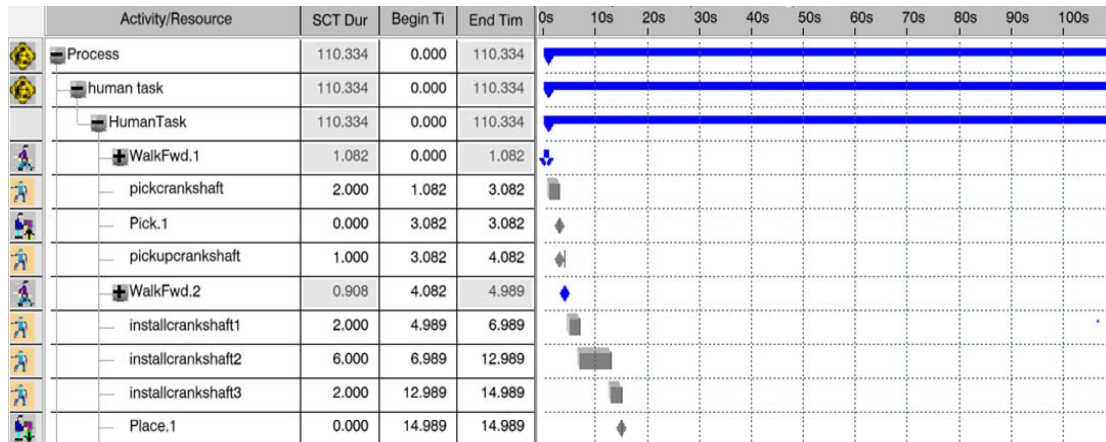


FIGURE 3.3: An example of the Gantt chart in the human task simulation.

d. Human Activity Analysis (MAA): permits users to improve the human comfort, safety, and performance through a wide range of ergonomics analysis tools and standards which comprehensively evaluate operator's interactions with a workspace. Some of these analysis tools will be further described in Section 3.5.

e. Human Posture Analysis (MHP): permits users to quantitatively and qualitatively analyse all aspects of an operator's posture. Whole body and localised postures can be examined, scored, and iterated to determine operator's comfort, safety, strength, and performance when interacting with a product in accordance with published comfort databases. Moreover, Ergonomists' knowledge regarding specific ergonomics criteria, preferred angles zones or ranges of motions can be identified in user-friendly dialogue panels and then be shared throughout the enterprise. Figure 3.4 shows an example to edit user preferred angles in MHP [99].

3.4 Virtual Assembly Environment

A complete virtual environment allows the preparation and presentation of all digital models involved in the assembly process, including product models, workplace models, mechanical resource models (e.g. models of jigs, fixtures,

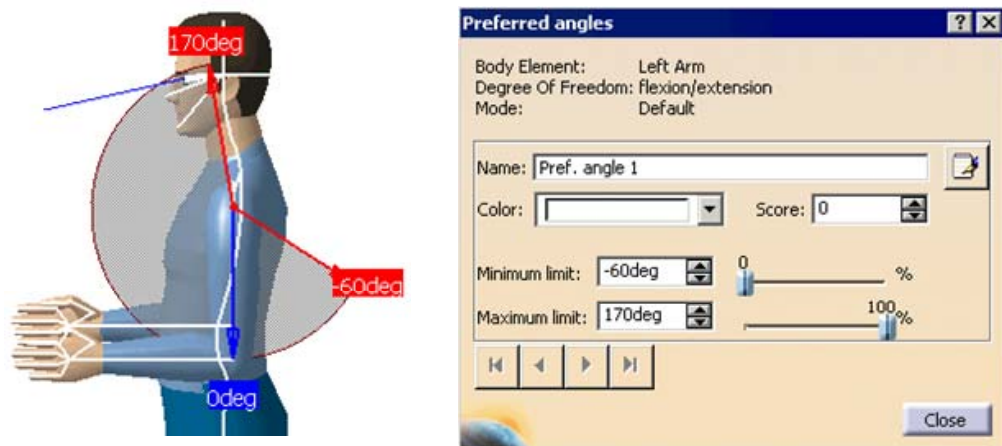


FIGURE 3.4: The angles editing panel [99].

tools, etc.) and the operator model(s). These models are loaded and located in the virtual assembly environment in order to reflect the needs and desired outcomes of the product designer.

In DELMIA, its digital manufacturing solution is built upon a Product, Process and Resource (PPR) environment which provides a central hub connecting all necessary models together. In the PPR environment, a product refers to the item being manufactured and the recourses are items resident in the environment to produce the product. Any items participating in the manufacturing process are counted as resources and arranged as required. An example of the PPR environment in DELMIA is illustrated in Figure 3.5. An engine is the product being designed in the example. The resources including the plant, tools and operators are placed in the resource list for the engine manufacturing process simulation,

Following the construction of the virtual assembly environment, a user-defined human operator is inserted. Positioning it in the virtual environment and assigning it with manual tasks, a complete assembly process simulation is carried out. This can be used to identify the feasibility of the process in terms of the ergonomic aspects of the human involvements and to optimise the human performances in the assembly process. Figure 3.6 outlines the general steps of the assembly process simulation.

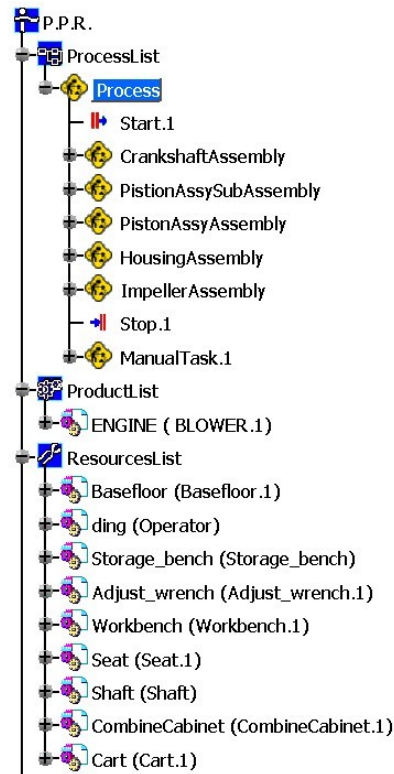


FIGURE 3.5: A PPR environment in DELMIA.

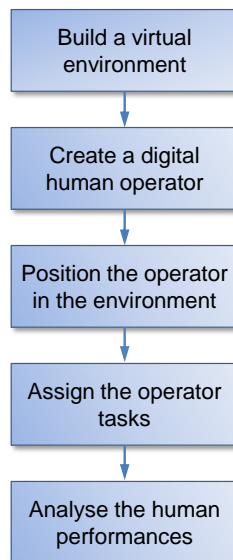


FIGURE 3.6: Steps of the assembly process simulation.

3.5 Ergonomics Analysis

3.5.1 Posture Analysis

A real-time, automatic RULA analysis can be conducted in the Human Activity Analysis workbench of DELMIA. RULA assesses the risk of upper limb disorders based on the following risk factors: working posture, the weight of loads, the muscle use factor (i.e. whether it is static or repeated), task duration and frequency. All these factors combine to provide a final score which ranges from 1 to 7:

- 1 and 2: (Green) Indicates that the posture is acceptable if it is not maintained or repeated for long periods of time.
- 3 and 4: (Yellow) Indicates that further investigation is needed and changes may be required.
- 5 and 6: (Orange) Indicates that investigation and changes are required soon.
- 7: (Red) Indicates that investigation and changes are required immediately.

There are two modes to display scores in MAA: the basic mode and the advanced mode. The data displayed in the basic mode is the final score accompanied by a colour zone. The advanced mode, in addition, also displays the intermediate scores obtained for each body segment and used to calculate the final score. Figure 3.7 indicates the score range for each segment as well as the associated colour [99]. Figure 3.8 shows an example of RULA analysis. RULA information has been transposed onto the manikin's surfaces and a dialog box shows the information in detail including the final score of manikin's current posture and the score for each body segment. It is noticeable that RULA analysis examines one side of the human body at a time and thus only one side of the manikin is coloured; secondly, the colour on the forearm corresponds to the worst score between the forearm and wrist and the colour on the neck, trunk and leg represents their combination score.

3.5.2 Cycle Time Analysis

DELMIA offers a standard time measurement to define a process time by splitting it up into steps requiring a pre-defined amount of time: e.g. grasp, move, position, release, or body motions of the operator. The measurement is based on Methods Time Measurement (MTM) and used heavily for the cycle

Segment	Score Range	Color associated to the score					
		1	2	3	4	5	6
Upper arm	1 to 6	Green	Green	Yellow	Yellow	Red	Red
Forearm	1 to 3	Green	Yellow	Red	Grey		
Wrist	1 to 4	Green	Yellow	Orange	Red		
Wrist twist	1 to 2	Green	Red				
Neck	1 to 6	Green	Green	Yellow	Yellow	Red	Red
Trunk	1 to 6	Green	Green	Yellow	Yellow	Red	Red

FIGURE 3.7: Colours representing intermediate scores [99].

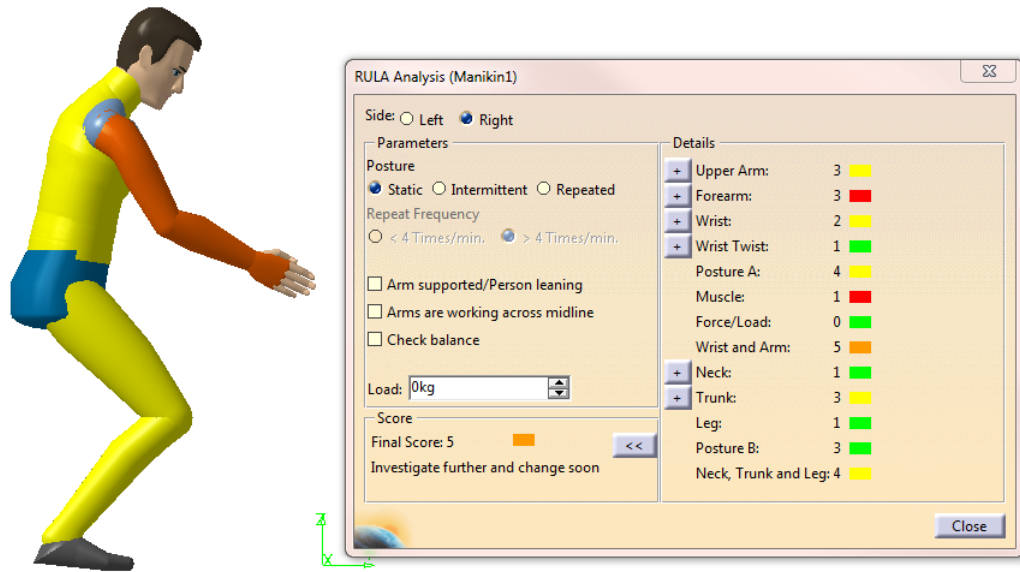


FIGURE 3.8: An example of RULA analysis.

time calculation and energy expenditure calculation [100].

Naturally, manual assembly can be divided into two components: handling (acquiring, orienting and moving of assembly parts), and insertion (mating a part to another part or a subassembly) [101]. Therefore, a functional *timer* is defined and applied in this research in order to determine the cycle time of manual assembly, which consists of handling time and insertion time as shown in Eq.(3.1).

$$\begin{aligned}
t &= t_h + t_i \\
\text{where } t &= \text{cycle time} \\
t_h &= \text{handling time} \\
t_i &= \text{insertion time}
\end{aligned} \tag{3.1}$$

3.5.3 Energy Expenditure Analysis

DELMIA's Human Activity Analysis workbench adopts Garg's energy prediction model to estimate an operator's energy consumption in kilocalories (kcal) for a given task. It assumes that a task can be divided into basic operations. Once this step has been finished, the average rate for the entire task (in kcal/min) can be estimated by summing up the energy requirements for individual operations and the energy required to maintain the posture. The equations used for different operations are described in Table 3.1.

TABLE 3.1: GARG equations

For stoop lift:
$E = 0.0109BW + (0.0012BW + 0.0052L + 0.0028S \bullet L)F$
For squat lift:
$E = 0.0109BW + (0.0019BW + 0.0081L + 0.0023S \bullet L)F$
For arm lift:
$E = 0.0109BW + (0.0002BW + 0.0103L - 0.0017S \bullet L)F$
where
E : energy expenditure (kcal/min)
BW : body weight (lb)
S : gender (female = 0; male = 1)
F : lifting frequency (lift/min)
L : load weight (lb)

3.5.4 Reach Analysis

A reach envelope tool is provided in Human Activity Analysis workbench to evaluate the manikin's arm reachability in 3D space. A reach envelope is a surface which represents all possible positions the manikin can reach using only the arm and the forearm. Practically, two kinds of reach envelope are created and visualised in real time by MAA, which are the ideal reach envelope and the 90% reach envelope.

The ideal reach envelope indicates the optimal working area for the selected manikin. It is defined as: an envelope generated from the motion of the arm limited to 45° of flexion and abduction as well as 60° of lateral (external) rotation while keeping the forearm in 90° flexed posture, as shown in Figure 3.9 [99].

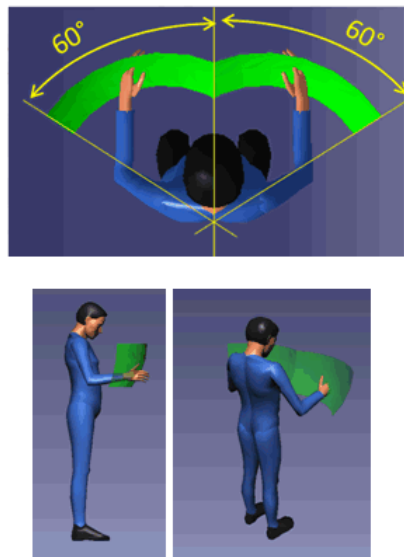


FIGURE 3.9: An ideal reach envelope [99].

The physiologically maximum reach envelope is normally of no practical use, as the operator usually does not stretch his/her joints to the full possible extent. The 90% reach envelope corresponds to 90% of the maximum reach envelope of the arm. It is defined as: 1) maximum envelope which is reduced by an allowance of 10% to take the not-fully stretched joints into account; 2) the lateral rotation is limited to 90° . Figure 3.10 gives an example of a 90% reach envelope [99].

3.5.5 Vision Analysis

A vision window is provided in DELMIA's vision function in order to display the scene through the manikin's eyes. In addition, the vision window can update itself automatically when the manikin's head is moved. The manikin's vision can be set as binocular or monocular by editing the manikin's vision attributes. For example, Figure 3.11 shows a binocular vision window of a manikin in the current position [102].

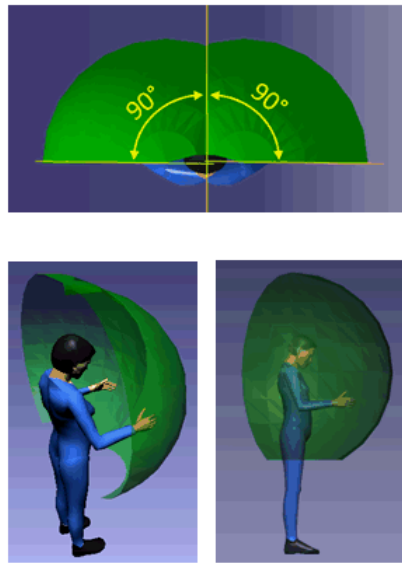


FIGURE 3.10: A 90% reach envelope [99].

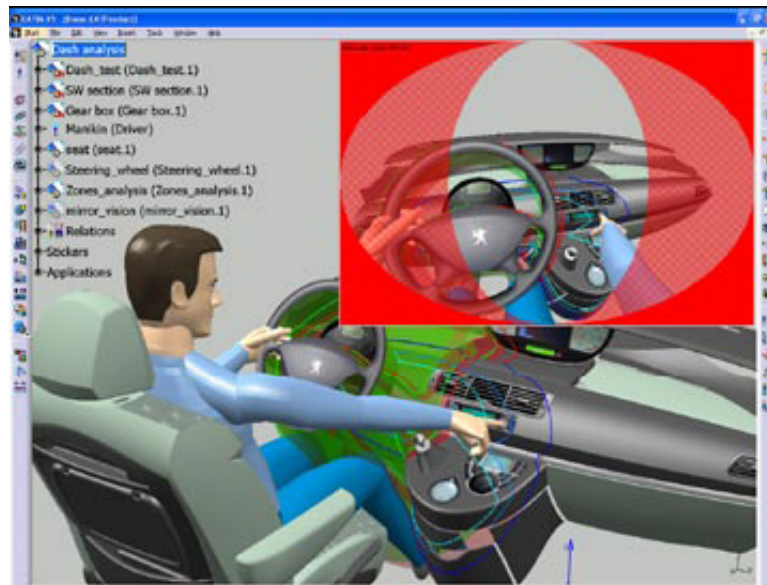


FIGURE 3.11: A binocular vision window of a manikin [102].

3.5.6 Clearance Analysis

DELMIA's distance and band analysis techniques offer valuable clearance calculation in the simulation. A distance analysis tool offers the capability to measure the minimum distance and the distance along an axis between products and/or resources. A band analysis tool allows a static visualisation of products and/or resources corresponding to a clearance examination between them. For example, Figure 3.12 shows a head clearance analysis in the car interior design [102]. The green colour indicates an area in which the user-defined clearance to

the manikin's top of the head is satisfied and the red colour corresponds to an area in which the clearance is unsatisfied.



FIGURE 3.12: A head clearance analysis [102].

3.6 Case Study: A Comparison Study of Product Assemblability

A case study of the formula student car assembly is presented as an application of DELMIA's virtual ergonomics solution. Formula Student (FS) is a worldwide university competition organised by the Society of Automotive Engineers, which encourages university teams to design, build and compete with a Formula-style race car. Participating in the competition from 2005, the Formula Student Team in the University of Liverpool designed, manufactured and tested a race car each year. Due to its fully manual operations, the formula student car assembly was chosen to investigate DELMIA's capabilities in the ergonomics simulation and analysis. The purpose of this case study is:

- to evaluate the product assemblability via the assembly process simulation and ergonomics analysis in DELMIA;
- to examine DELMIA's performances in the product assemblability evaluation in terms of the outcomes in the ergonomics solution.

3.6.1 Method and Materials

A formula student car ULM005 is shown in Figure 3.13. The project is organised in module teams comprising of 23 members drawn from the 3rd and 4th year students in the School of Engineering. Each team is responsible for different parts of the car, i.e. the chassis, suspension, engine, drivetrain and bodywork. The final assembly work is carried out by experienced students from the 4th year, lasting approximately one month.



FIGURE 3.13: Formula student car – ULM005.

As the assembly activities are planned and executed in parallel with the car design, a substantial number of ergonomic problems are found in the assembly process. Through interviewing formula students, observation and video recording of their assembly operations, all assembly tasks with unacceptable ergonomic conditions are collected.

The common requirements in automotive industry, as detailed in Table 3.2 [103], are employed for the identification and categorisation of ergonomic problems in the assembly process. Afterwards, the ergonomic problems are simulated and analysed using DELMIA associated with its capability in the ergonomics solution. Finally, a comparison study between the real operations in the workshop and the simulated operations in DELMIA can be made. Figure 3.14 shows the flow chart of the FS car assembly case study.

3.6.2 Development of Virtual Assembly Environment

Simulation and analysis model are supported by a virtual assembly environment, which is capable of creating the virtual assembly process using a series of digital models. In this case, the data collected as assembly operators, objects, and tools

TABLE 3.2: Common ergonomic requirements in automatic industry [103]

Ergonomic requirement	Definition	Test method
Visibility	Parts and/or components or operations must be able to be seen or differentiated when assembled.	Vision analysis
Weight	If weight limits are exceeded, a weight reduction of the part must be made or an adequate lifting device be developed.	Posture analysis
Working distance	In general terms, a work distance exceeding 500 mm from operator's front hip bone should not occur.	
Assembly force	Assembly of parts or other material must not exceed a force of: 15 N for one finger, 30 N for two/three fingers, 50 N for hands at average position.	
Clearance	There must be enough space for the operator(e.g., hands, machine, components for assembly) at the spot for assembly.	Clearance analysis

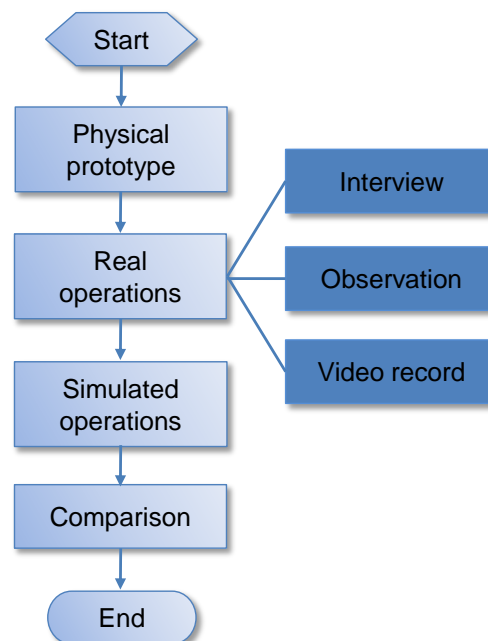


FIGURE 3.14: The simulation flow chart of the FS car assembly process.

are used to reproduce and visualise the FS car assembly place in DELMIA.

Assembly students' height and weight are collected and used to build the human models in DELMIA. Therefore, digital human operators are capable of representing student's characteristics as much as possible. Besides, the CAD model of the FS car ULM005 and assembly tools are created and inserted into the virtual environment. As a consequence, all necessary information (e.g. dimensions and weights of assembly parts/components and tools) is available when performing the ergonomics analysis. Figure 3.15 shows the final virtual assembly environment of the FS car.

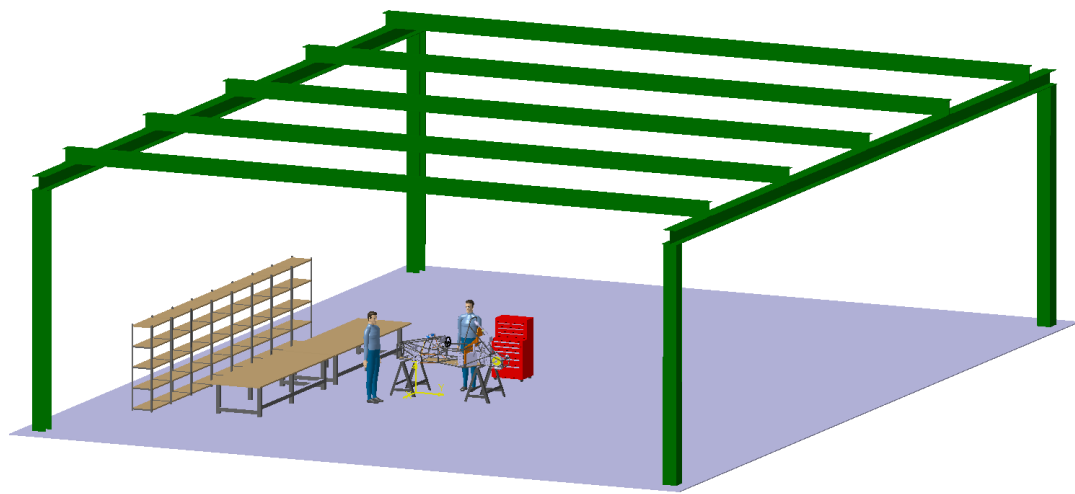


FIGURE 3.15: The virtual assembly environment of the FS car.

3.6.3 Results

a. Engine Assembly

Engine assembly is a case with plenty of complaints from assembly students, which requires at least two students' involvement. Figure 3.16 shows five operations in this process from the real environment versus the virtual environment. RULA test is conducted to analyse operator's current working conditions. The scores of body segments and the whole body with regard to the operation are calculated and shown in Figure 3.17.

The engine weighs 16.98 kg. For the first and second operations, the engine load is imposed completely on the left operator as shown in Figure 3.16. From the third to fifth operations, assuming the load is distributed equally on the left

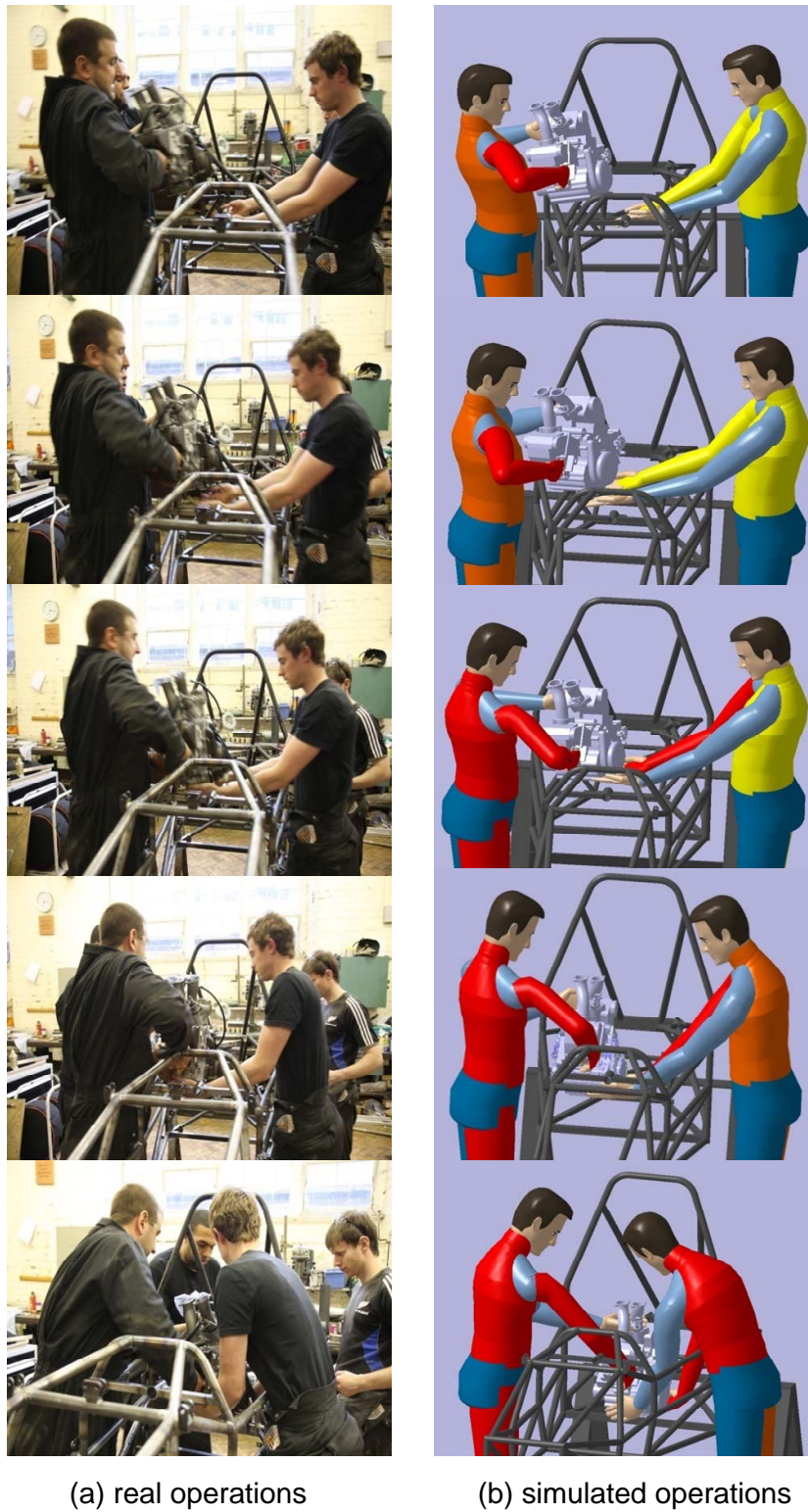


FIGURE 3.16: Operations in the engine assembly process.


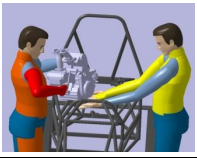
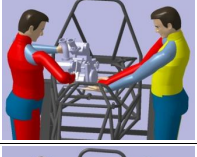
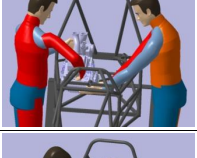
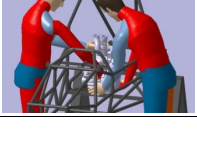
Unit	Operation	Operator	Upper arm	Fore arm	Wrist	Wrist Twist	Neck	Trunk	Leg	Final Score
1		Left	3	3	4	1	2	1	1	7
		Right	2	2	2	1	2	2	1	3
2		Left	3	3	2	1	2	2	1	7
		Right	2	2	2	1	2	1	1	3
3		Left	3	3	2	1	2	3	1	7
		Right	2	3	2	1	2	1	1	6
4		Left	4	2	2	1	2	3	1	7
		Right	3	2	4	1	1	2	1	7
5		Left	4	3	4	1	2	3	1	7
		Right	3	2	4	1	4	4	1	7

FIGURE 3.17: RULA scores of operations in the engine assembly process.

and the right operator (approximately 85 N for each), it is still far more than the limitation in ergonomic requirement. This generates a high burden on the body segments, especially on the upper extremity. As illustrated in Figure 3.17, red colours appear on the upper and fore arm during the whole process, which indicate that changes are required immediately. Additionally, in order to avoid the collision with the chassis frame, the operator on the left has to raise the engine to a certain height which results in an awkward working posture, for instance, the arm extending upwards over the shoulder as shown in operation 4 of Figure 3.17. Meanwhile, for the operator on the right, in order to move and fit the engine in its assembly location, his arms are forced to stretch out of the comfortable reach zone with the twisted neck and truck, as illustrated in operation 5 of Figure 3.17. It is clearly evident that the majority of operators' extended body movements are encountered in the upper body.

In order to reduce the stressful working postures, several improvements should be considered in the new car design, for example: 1) provide an auxiliary device for the engine lifting, 2) decrease the working height or 3) shorten the distance

between the engine's assembly location and the operator.

b. Firewall Assembly

Firewall assembly is identified as a time-consuming assembly case with uncomfortable working postures by assembly students. Four operations in the process are chosen to perform RULA analysis. Figure 3.18 displays the scenarios obtained from the real environment versus the virtual environment. Figure 3.19 displays the RULA results for each body segment and the whole body of the operation.

The firewall which separates the driver compartment from the engine bay is made from the ABS/PC material and weighs 4.93 kg. Although the weight satisfies the ergonomic requirement in whatever way of loading on one or two operators, RULA scores indicate that changes are required immediately. Inappropriate working height and working distance are the two main factors contributing to the awkward postures as shown in Figure 3.19. In the first operation, the operator's arms are above his shoulders when raising the firewall to avoid collision with the chassis frame; in the fourth operation, the operator's neck is bent and the back is twisted when fitting the firewall. The final scores of operators' postures combining all segments' contributions are 7 for the entire assembly process, which indicate that changes are required immediately.

c. Plenum Assembly

Blind assembly is not allowed in manual assembly, which means that no visibility of the task is available. It will cause extra time, quality deviations and risks of physically stressful working postures for assembly operators. However, due to the complexity of the ULM005 development project, numerous of blind assemblies are reported, for instance, in the process of plenum assembly. Figure 3.20 (a) captured from the reality shows the student's hand manoeuvres during the process. Reproducing the scenario in the virtual environment and performing the vision analysis, simulated results are shown in Figure 3.20 (b), (c), (d). It is observed from the vision window that the location of assembly part (a screw), which should be visible in order to steer a screwdriver towards it, was obstructed by the plenum chamber in the assembly process. A blind assembly for the screw was detected - no visibility for it as well as the hand's movement to manipulate it, which resulted in difficulty to install the inlet stack to the engine. For the next generation car, the shape of plenum chamber causing the visibility deficiency should be redesigned in

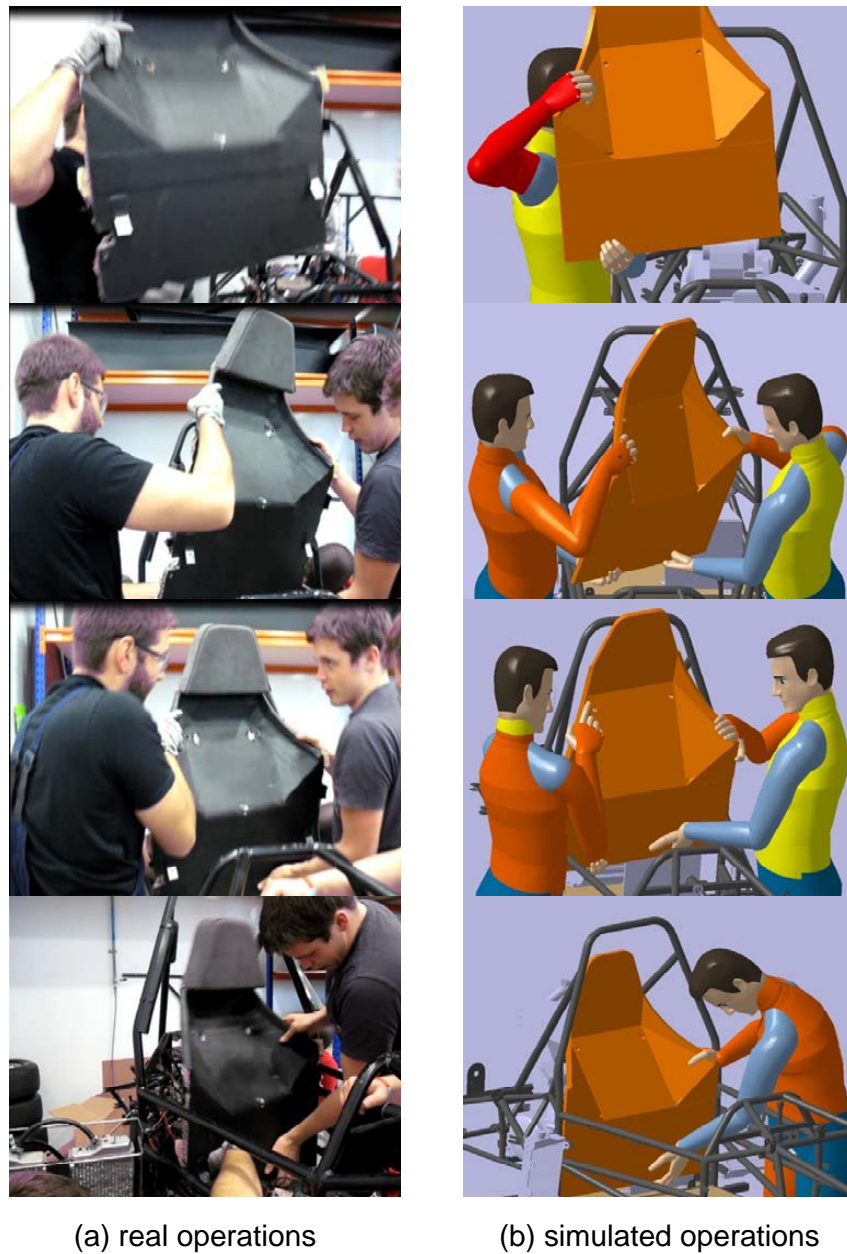


FIGURE 3.18: Operations in the firewall assembly process.

order to provide a better vision condition for assembly operators, improving their manipulation efficiency and quality.

d. Bodywork Assembly

Hand/tool access problems are often encountered due to the insufficient concern on assembly process planning for the ULM005 development project. One example is the bodywork assembly. When fitting the top and bottom panels onto the chassis, particular holes are cut on the bodywork and therefore, assembly tools





Unit	Operation	Operator	Upper arm	Fore arm	Wrist	Wrist Twist	Neck	Trunk	Leg	Final Score
1		Left	5	2	4	1	3	2	1	7
2		Left	4	3	3	1	3	3	1	7
		Right	4	3	3	1	2	2	1	7
3		Left	2	3	4	1	3	3	1	7
		Right	4	3	3	1	2	2	1	7
4		Right	3	3	4	1	2	4	1	7

FIGURE 3.19: RULA scores of operations in the firewall assembly process.

(the wrench and the alley key) can access the assembly object (a screw). This induces a hand/tool access problem. When representing the real scene of the task (Figure 3.21 (a)) in the virtual environment, a clearance analysis can be conducted and the clearance from the obstructing surface to the hole centre is obtained, which is 11.491 mm (Figure 3.21 (b), (c)). The clearance is less than the unrestricted access standard in the manual assembly, which is 16mm as defined by Fujita [104]. Based on the experiences of assembly students, inadequate tool manipulation space in manual assembly has a devastating effect on the assembly time and the product quality. Consequently, it is necessary to take the assembly process planning into account during the FS car design stage.

3.6.4 Discussion

- Posture studies

The simulation of FS car assembly has proven to reflect the ergonomics conditions in reality. A good agreement is achieved between the results in the real environments and those in the virtual environments (Figures 3.16 and 3.18). Moreover, a detailed feedback from RULA results (Figures 3.17 and 3.19) offers a thorough explanation and evaluation of each body segment's conditions under the assembly workloads. For a successful simulation, there are two vital requirements: one is the correct data

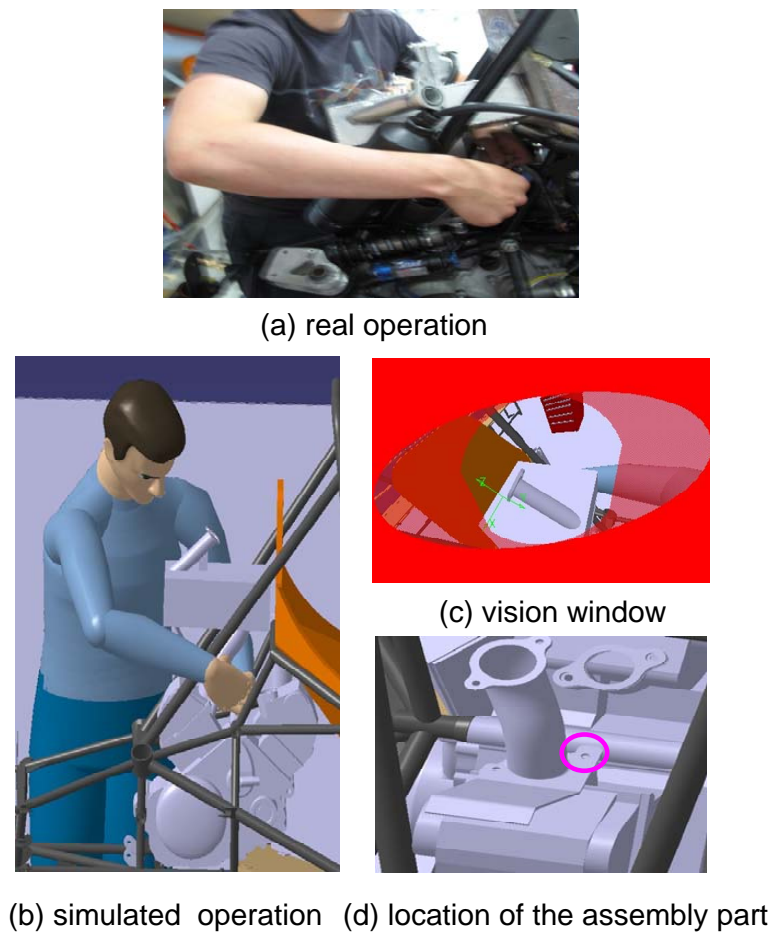


FIGURE 3.20: Task of the plenum assembly.

collection regarding the assembly tasks and the assembly environment, and the other is the correct manipulation of the simulation and analysis tool – DELMIA. To a certain extent, DELMIA' manipulation, i.e. creating and positioning digital humans in the virtual environment and assigning them the assembly tasks, gives a higher impact on the analysis results than the former one. This could be seen as an experience-based process which relies heavily upon the users' familiarity of DELMIA.

This case study shows a strong relationship between the working height/working distance and the assembly postures. The unsuitable working height and working distance force the operator to occupy awkward postures. These postures often consist of a bent or twisted neck and back, arms above or at the shoulder height, or out of the comfortable reach zone. Therefore, the working height and working distance should be purposeful

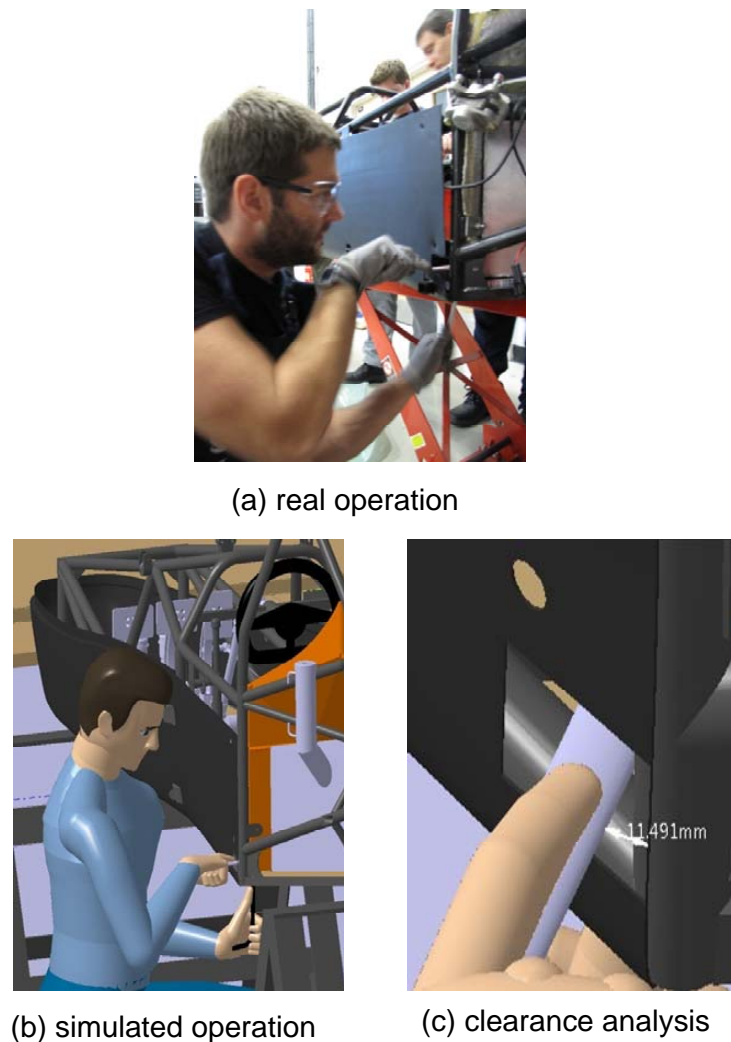


FIGURE 3.21: Task of the bodywork assembly.

investigated in the design of the workplace. This would be further studied in Section 3.7.

- Vision studies

According to the ergonomic requirement, parts/components and operations must be seen or differentiated when assembled or manipulated. This will provide a fully technical guidance to facilitate the accuracy and efficiency of assemblies. DELMIA includes the functionality to display the manikin's field of view. It is also capable of setting different attributes of human vision (i.e. binocular versus monocular). However, it does not give any interpretation regarding the simulated results, which in turn set high demands on users' knowledge and experiences upon the human vision requirements or standards. This limitation often leads to erroneous

decisions [105]. In order to better assist users during ergonomics analysis, an improvement in the vision analysis tool is necessary. For example, an evaluation regarding the visibility of parts/components associating with the vision related parameters (such as the geometry of the assembly product, working height/working distance, working postures, etc.) should be developed in order to confirm design solutions automatically. This is studied further in Chapter 5.

- Hand access studies

The size of the hand/tool clearance affects several performance parameters. Studies performed by Kama have shown that the time taken to remove and replace a component decreases sharply as the aperture available for the hand clearance increases [106, 107]. Additionally, the literature in [108] shows that the hand torque capability is affected by the clearance between the hand and any physical obstruction. As reported by formula students, insufficient hand manipulation space especially when sharp edges are present, for example assembling car bodies made of joined metal sheets, decreases the efficiency and comfort in assembly tasks. Hence the hand accessibility is significant for a smooth manual assembly process. DELMIA offers the capability to calculate and visualise the hand clearance with respect to the obstructed objects. Also, several hand activities (e.g. grasping) are modelled in DELMIA in order to reproduce a realistic scenario. However, the basic constraints regarding the hand accessibility as well as the accessibility for a series of hand tools are not defined. Knowledge and experiences from assembly operators are therefore essential to determine or predict an access problem. Several researchers have emphasised the need to improve hand access modelling and simulation capability for ergonomics studies [109, 110]. Further investigations would be given in Chapter 5.

3.7 Case Study: Ergonomic Design of Manual Assembly Workplace

Ergonomics solutions in the workplace design attempt to minimise the incompatibilities between the capabilities of operators and the demands of their jobs. The improved solutions would increase productivity, enhance safety performance, and reduce overall cost. An effective workplace can be achieved by the computer simulation with digital human models in the virtual assembly

environment [111, 112]. In order to demonstrate DELMIA's functionalities in the ergonomics design of workplace, a case study of assembling an aluminium blower is given. The objective of this study is twofold:

- to achieve an effective ergonomic design of workplace through the assembly process simulation in the virtual environment;
- to investigate the impact of a series of process related factors and their combination on the human performances.

3.7.1 General Workplace Design Procedure

The following are the general steps which should be obeyed in a systematic workplace design procedure [113].

1. Preparation: all necessary information with regard to the tasks to be performed in the workplace, which should include types of job functions and the descriptions of work populations.
2. Identification of all feasible design alternatives: the collected information is assembled to link the design components together to explore all feasible design alternatives that effectively combine components to satisfy the design constraints.
3. Selection of the optimum design alternative: all identified alternatives are compared to select the optimum alternative. The criteria used for comparison and selection should include: economy of production, efficiency of operations, easy of assembly.
4. Examination of the final alternative: the selected final design alternative should be evaluated to insure that the design objectives have been achieved and the constraints are satisfied.

3.7.2 Method and Materials

The blower, as shown in Figure 3.22, was designed for remote control model aircraft applications [114]. Its assembly process simulation consists of five tasks: 1) crankshaft assembly, 2) piston sub-assembly; 3) piston assembly; 4) housing assembly; and 5) impeller assembly. Each task requires the operator to acquire a part from the storage bench, transport it, and insert it into the subassembly on the work bench. The weight of assembly part is given in Table 3.3. As the process involves handling parts weighing more than 4.5 kg, a standing

workstation is recommended [115]. Utilising the design-for-average principle for the workplace design, a 50th percentile US male digital operator is chosen provided by the DELMIA database [14]. The operator has a height of 175.58 cm and weighs 78.49 kg. Table 3.4 displays the screenshots captured from each individual step in the assembly process simulation.




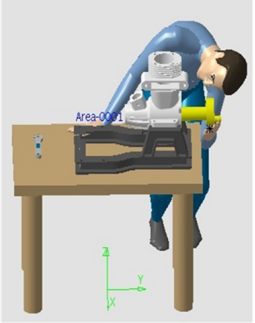
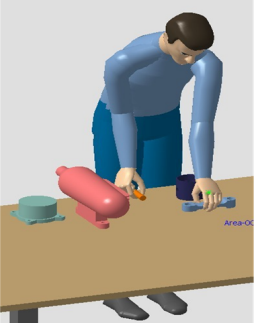


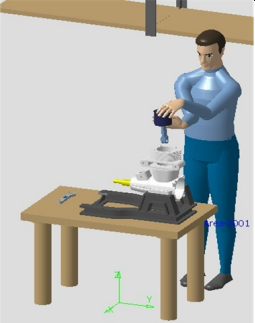

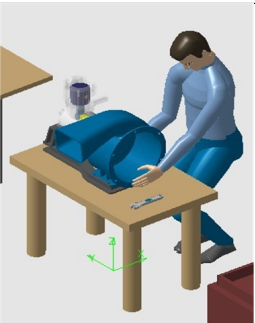


FIGURE 3.22: The blower model for manual assembly [114].

TABLE 3.3: Weights of the assembly part or component

Part	Weight(kg)
Impeller	6.262
Housing	5.695
Crankshaft	2.033
Piston	0.147
Connecting rod	0.157
Piston pin	0.039
Piston assy	0.504

The major factors, which are considered influencing the operator performances in the assembly process, are the work bench height (BH), the workplace layout (WL), and the part location (PL). These factors and their levels are given in Table 3.5. The level 1 and level 3 of the factor BH (Figure 3.23) are obtained from the quantitative measure of the bench height in reality, i.e. in the office and in the workshop. The level 2 of BH (Figure 3.23) is proposed based on the hypothesis that the operator's effort is minimum when his elbows keep horizontal in performing activities. As shown in Figure 3.24, the working height in this case is the work bench height plus half of the product height and thereby equals to the operator elbow's height, which is 1085.583mm for a 50 percentile US male obtained in DELMIA anthropometric database. According to Eq. (3.2), the level 2 of BH is settled. The levels of the factor WL refer to alternative layout designs involving different relevant locations of the storage bench and the work bench (Figure 3.25).

TABLE 3.4: The assembly process of the blower

Task	Handling	Inserting
Crankshaft assembly		
Piston sub-assembly		
Piston assembly		
Housing assembly		
Impeller assembly		

The levels of PL are set according to the assembly sequence and the weight of assembly part (Figure 3.26) respectively: for the level 1, the first assembly part is arranged closest to the operator; for the level 2, the heaviest part is arranged closest to the operator as an attempt to minimise the energy expenditure.

TABLE 3.5: Design factors and their levels

Factor	1	2	3
Work bench height (BH)	700mm	850mm	900mm
Workplace Layout (WL)	Layout1 (Fig.3.25)	Layout2 (Fig.3.25)	Layout3 (Fig.3.25)
Part location (PL)	PL1 (Fig.3.26)	PL2 (Fig.3.26)	-

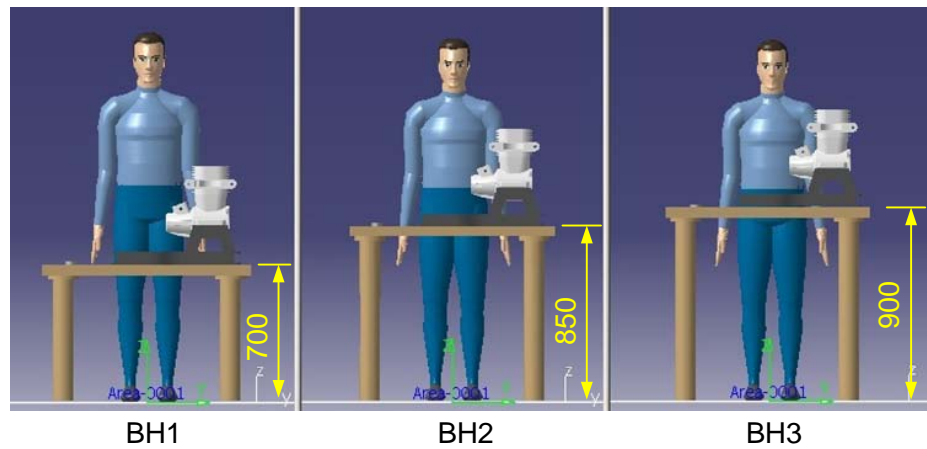


FIGURE 3.23: The alternative work bench height designs.

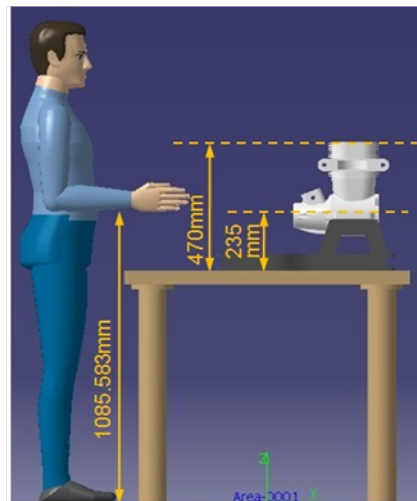


FIGURE 3.24: The determination of level 2 of work bench height.

$$BH2 = 850 \approx 1085.583 - 235 \quad (mm) \quad (3.2)$$

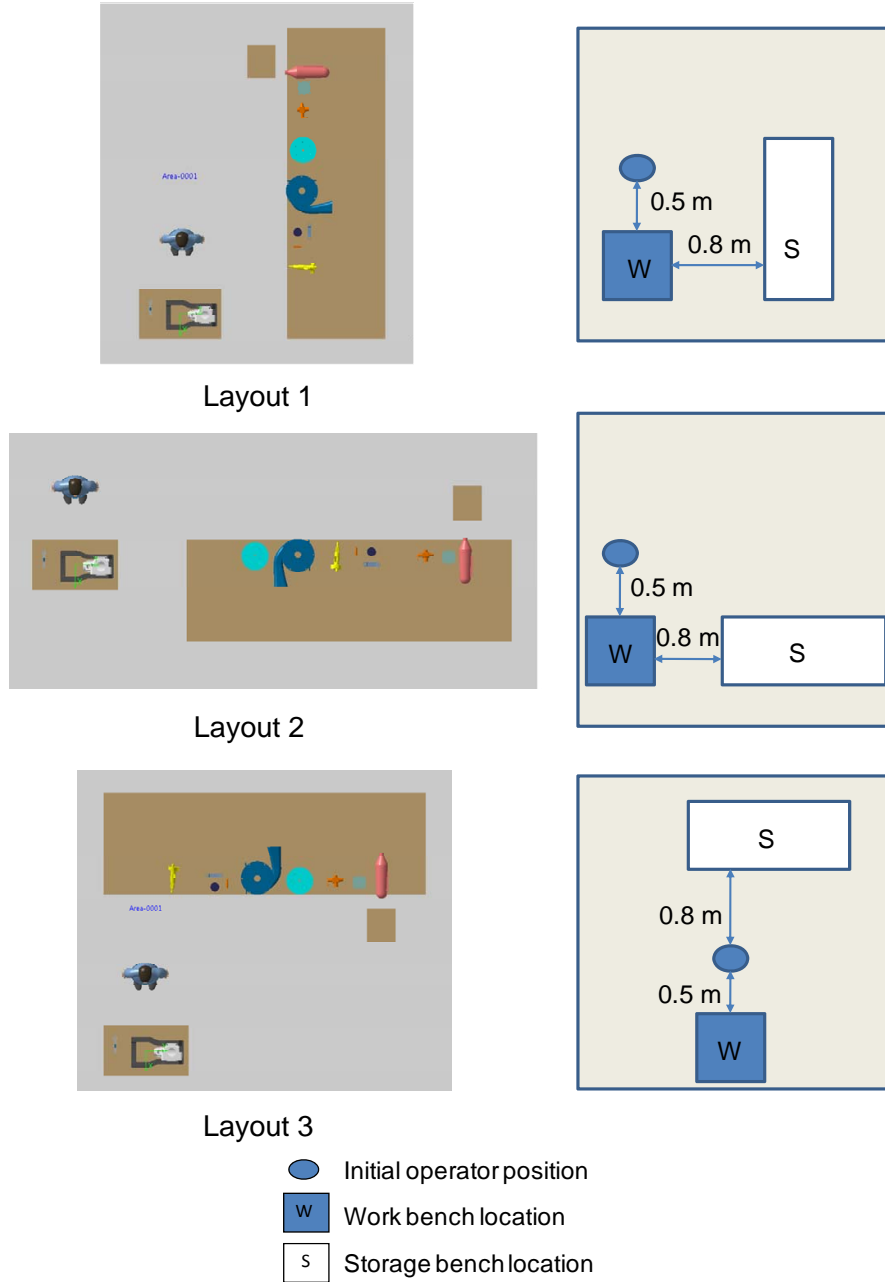
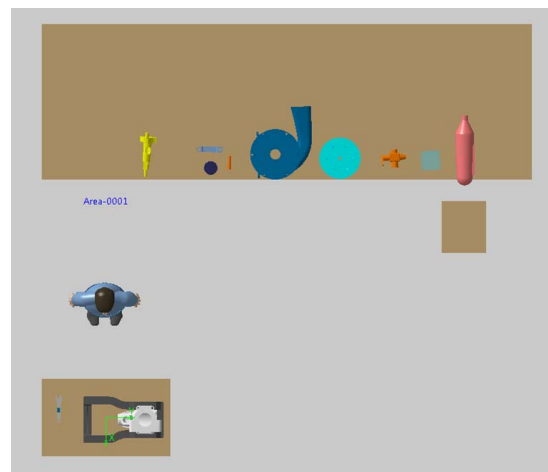
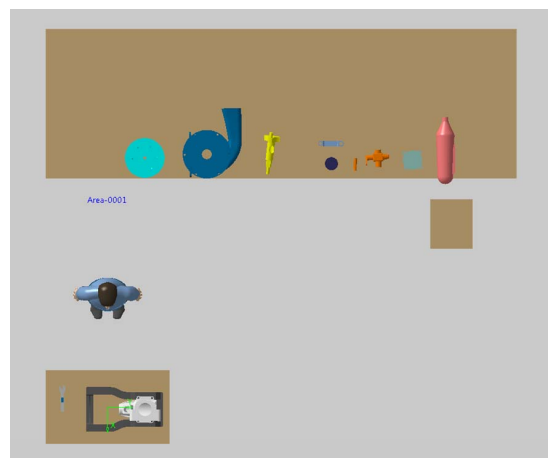


FIGURE 3.25: The alternative workplace layout designs.

In order to establish an optimum workplace design and estimate the contribution of individual process related factor, an orthogonal array experiment is carried out, which allows a significant reduction in simulation amounts [116]. The orthogonal array selected for the simulation is the $L_9(3^4)$. Following techniques suggested by Phadke, the fourth column of the array is neglected



PL1: Part location according to assembly sequence



PL2: Part location according to part's weight

FIGURE 3.26: The alternative part location designs.

[117]. The resulting array used for the simulation is presented in Table 3.6. During the assembly process simulation, the operator performances such as RULA scores, process cycle time and energy expenditure are calculated as the criteria to evaluate each workplace alternative and to validate the final design. Figure 3.27 outlines the flow chart of the blower assembly case study.

3.7.3 Results

The simulation results are presented in Figure 3.28, where “√” denotes that the posture is acceptable and “×” denotes that the posture is unacceptable, changes are required. Using these results along with necessary calculations, an analysis of

TABLE 3.6: Factor levels for each simulation

No.	Levels of factors		
	BH	WL	PL
1	1	1	1
2	1	2	2
3	1	3	1
4	2	1	2
5	2	2	1
6	2	3	1
7	3	1	1
8	3	2	1
9	3	3	2

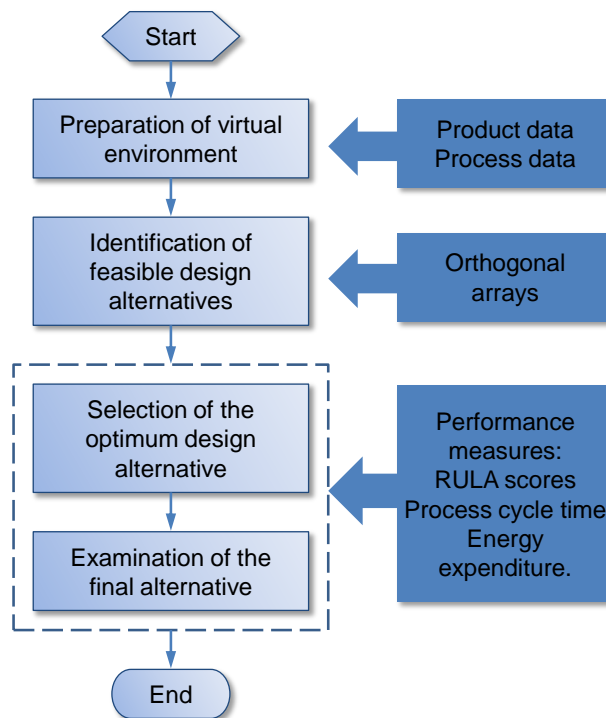


FIGURE 3.27: The simulation flow chart of workplace design.

means (ANOM) diagram of each performance measure is created (Figures 3.29 and 3.30), which graphically shows the average values for each level of the design factors. From Figures 3.29 and 3.30, the levels of the factors representing the best process cycle time and energy expenditure could be easily identified, which are BH2, WL3 and PL2 (Table 3.9).

In order to determine the effect of each design factors on the performance measures, a range analysis is carried out. Table 3.7 and Table 3.8 describe the results of range analysis, where range $R = \max(I, II, III) - \min(I, II, III)$. Table 3.7

Simulation			1	2	3	4	5	6	7	8	9	
Crank-shaft	Handle	RULA test	✓	✓	✓	✓	✓	✓	✓	✓	✓	
	Fasten		✗	✗	✗	✓	✓	✓	✓	✓	✓	
Sub-piston	Handle		✓	✓	✓	✓	✓	✓	✓	✓	✓	
	Fasten		✓	✓	✓	✓	✓	✓	✓	✓	✓	
Piston	Handle		✓	✓	✓	✓	✓	✓	✓	✓	✓	
	Fasten		✓	✓	✓	✓	✓	✓	✗	✗	✗	
Housing	Handle		✓	✓	✓	✓	✓	✓	✓	✓	✓	
	Fasten		✓	✓	✓	✓	✓	✓	✓	✓	✓	
Impeller	Handle		✓	✓	✓	✓	✓	✓	✓	✓	✓	
	Fasten		✓	✓	✓	✓	✓	✓	✓	✓	✓	
Total			Hand-ling time (s)	41.33	50.68	39.48	40.82	50.20	40.72	45.72	56.63	42.93
			Insert-ion time (s)	69	69	69	49	49	49	55	55	55
			Cycle time (s)	110.33	119.68	108.48	89.82	99.20	89.72	100.76	111.63	97.93
			Energy (kcal)	5.59	6.29	5.46	4.93	5.78	4.86	5.45	6.50	5.22

FIGURE 3.28: Simulation results.

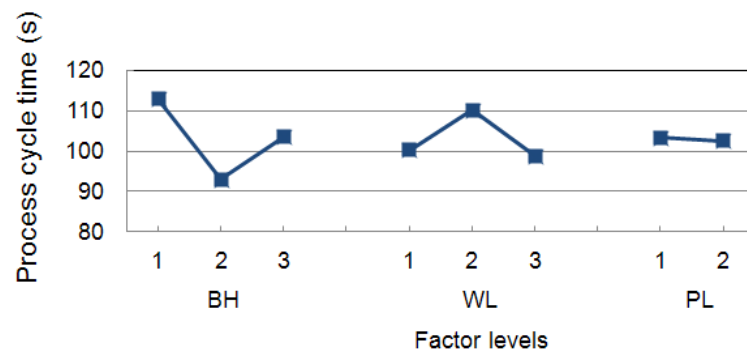


FIGURE 3.29: ANOM diagram of process cycle time.

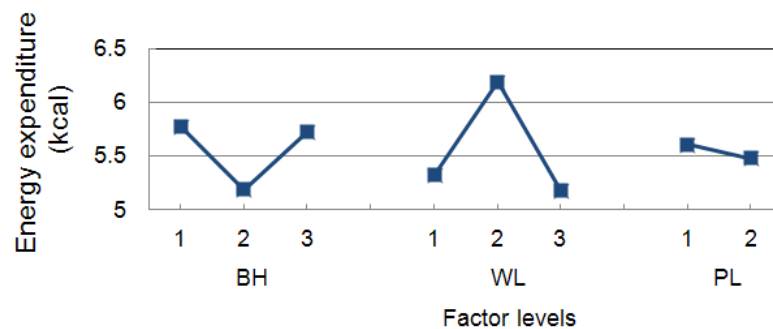


FIGURE 3.30: ANOM diagram of energy expenditure.

illustrates that the factors significance to process cycle time is $BH > WL > PL$ and thereby the optimum workplace design is BH2WL3PL2. The relative importance of the three factors to energy expenditure is that $WL > BH > PL$ observed from Table 3.8 and therefore the optimum design is WL3BH2PL2. It is evident that the optimum levels of each factor constructed from range analysis is consistent with that from the ANOM diagram, which are detailed in Table 3.9.

TABLE 3.7: Range analysis of process cycle time (s)

Mean	BH	WL	PL
I	112.83	100.30	103.35
II	92.91	110.17	102.47
III	103.44	98.71	-
R	19.92	11.46	0.88

TABLE 3.8: Range analysis of energy expenditure (kcal)

Mean	BH	WL	PL
I	5.78	5.32	5.61
II	5.19	6.19	5.48
III	5.72	5.18	-
R	0.59	1.01	0.13

TABLE 3.9: Optimum factor values

Factor	Level	Value
BH	2	850
WL	3	Layout3
PL	2	PL2

The optimum factor levels are examined in terms of their contributions to the operator performances (i.e. RULA scores, process cycle time and energy expenditure) via an updated simulation in the final workplace design. The process cycle time and energy expenditure are both further reduced, which are 78.23 s and 4.62 kcal respectively. This confirms that the final alternative of workplace design is time and energy efficient. Figure 3.31 shows this final ergonomic effective workplace design.

3.7.4 Discussions

- Posture studies

The unsuitable working height and working distance are two main reasons



FIGURE 3.31: The optimum workplace design.

give rise to the unacceptable postures. Among them, working distance issues could be detected easily by using the reach analysis. As shown in Figure 3.32, the 90% reach envelope was created and visualised during the assembly process simulation, which represents all possible reach positions for operator assembling objects. Therefore by locating the operator close to the current assembling part covered by the reach envelope, awkward postures attributed to the improper working distance could be eliminated.

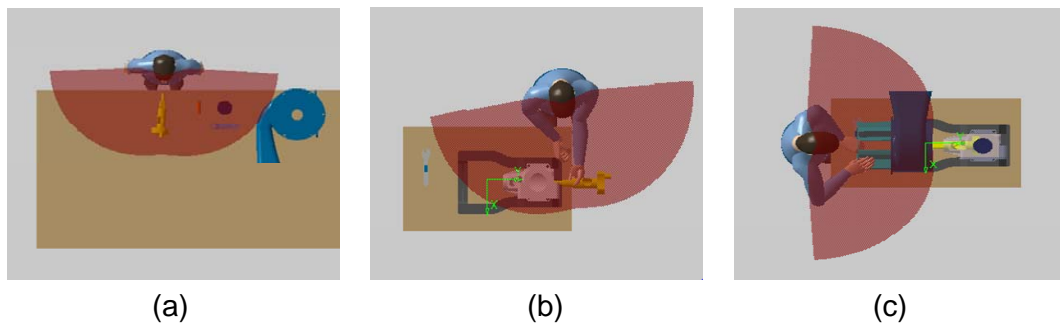


FIGURE 3.32: Reach analysis in the assembly process simulation.

When working distance issues are excluded, the working height is the only determination of the unacceptable postures, which are found in level 1 and level 3 of the work bench height (simulation 1,2,3,7,8,9 in Figure 3.28). If the working level is too low, undesirable postures of squatting and stooping occur. In addition, the neck and head are inclined forward. They would consequently pose stress on the spine and legs, as shown in Figure 3.33.

However, if the working level is too high, the shoulders and upper limbs will be raised, leading to fatigue and strain in the shoulder region, as shown in Figure 3.34. Between the working level that is too high and the one that is too low, a suitable compromise is established in level 2 of the work bench height. Supposing the working height equals to the elbow's height when performing assembly activities, a great improvement is demonstrated with RULA test, at which neither the shoulders nor the back are subjected to excessive postural stress.

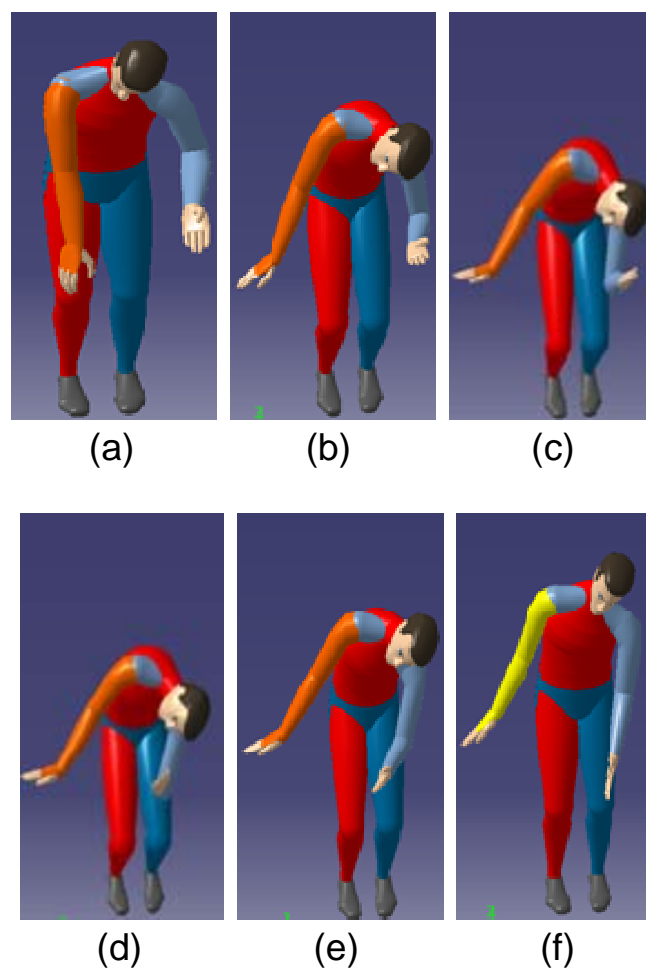


FIGURE 3.33: Unacceptable postures in level 1 of work bench height.

Finally, it is important to distinguish between the working height and the work bench height. The former may be substantially higher than the latter if hand tools are used or parts/components are manipulated during the assembly. It is the working height for the tasks to be performed that should be settled first when designing a workplace, rather than the height

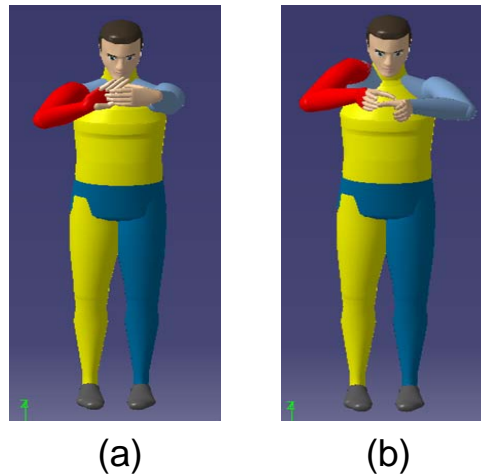


FIGURE 3.34: Unacceptable postures in level 3 of work bench height.

of the bench in itself. Once the working height is determined, the bench height could be designed accordingly. Assuming that the product is manipulated or held at an intermediate height, the bench height is equal to the elbow height of the operator minus half of the product height.

- Cycle time studies

As shown in Table 3.7, the work bench height and the workplace layout have proved to be two significant influential factors to the process cycle time. The effect of work bench height on the process cycle time is attributed to the postures and effort that required for orientating and positioning assembly objects. Figure 3.29 shows a reduction of cycle time in level 2 of the work bench height due to the removal of undesirable and stressful postures, for example squatting, stooping or raising of shoulders.

As shown in Figure 3.28, the workplace layout causes the fluctuation of handling time when the work bench height is constant. Assuming that the operator's walking speed remains the same under different workplace alternatives, which is 80 m/min without load and 60 m/min with load as recommended by Grandjean [118], it is the walking distance resulted from different workplace layouts that cause the cycle time variation. Table 3.10 lists the walking distance calculated for different workplace layouts, which further reveals that level 3 of workplace layout is the most time-efficient.

TABLE 3.10: Walking distance of workplace layout

Level of workplace layout	Walking distance (m)
1	20.322
2	30.843
3	18.259

- Energy expenditure studies

As illustrated in Table 3.8, the workplace layout results as the most important factor to the energy expenditure. The amount of energy expended in the workplace is reduced significantly when the process cycle time as well as the walking distance is decreased. The work bench height has proved to be the second most influential factor. Based on GARG equation in Table 3.1, the energy expenditure per min of arm lift is lower than stoop and squat lift when other parameters, i.e. the body weight, operator gender, lifting frequency and load weight remain unchanged. Therefore, the energy expenditure will decline correspondingly after the removal of uncomfortable movements (squat and stoop). The part location has a minor effect on the energy consumption. It affects the energy expenditure by adjusting the time distribution on carrying workloads. The amount of energy could be further reduced by reducing the time spend on carrying heavier assembly objects.

3.8 Conclusions

Research work presented in this chapter refers to the implementation of the manual assembly process simulation and ergonomics analysis utilising DELMIA in order to study the product assemblability and the workplace design. Based on the functionalities of DELMIA, a virtual assembly environment was developed and a series of ergonomics analysis models were embedded into the environment. Therefore, the product assemblability and workplace design in terms of human performance measurers could be quantitatively and qualitatively evaluated in the virtual environment.

A comparison study of product assemblability was presented in Section 3.6. The product's assemblability for manual assembly was evaluated via the assembly process simulation and ergonomics analysis. Moreover, by comparing the operations which were obtained from the ergonomics simulation and those in

reality, DELMIA's capabilities and performances were fully studied and examined.

An approach for the ergonomic design of the manual assembly workplace was proposed in Section 3.7. This approach allowed an effective design of the manual assembly workplace and evaluation of the impact of each design factor on the multiple performance measures. The result of the case study is a completely new workplace characterised by several ergonomic improvements in terms of RULA scores, cycle time and energy expenditure.

The application of DELMIA for the manual assembly process simulation has proven to be beneficial to the product and workplace design. However, for more sophisticated posture simulations, the usage of DELMIA requires more care in order to prevent unrealistic results. This relies on experiences in software manipulation and the recognition of different assembly tasks undertaken. Furthermore, several limitations of DELMIA have been revealed in this chapter, i.e. vision analysis and hand access analysis, which require further improvements in order to provide better support during the ergonomics analysis.

Chapter 4

Posture Analysis of Manual Assembly

4.1 Introduction

An accurate simulation of assembly posture is critical for ergonomic assessments because posture has a dominant effect on the analysis. However, current ergonomics simulation software tools require the manual manipulation of digital human models, resulting in errors and low efficiencies. With a posture prediction method, the accuracy, repeatability and reproducibility of the ergonomic simulation could be improved. More importantly, the method can produce realistic assembly postures automatically in a variety of assembly conditions and provide a more profound understanding on human performances in conducting the ergonomic analysis.

The purpose of this chapter is to develop a general assembly posture prediction method which closely simulates manual assembly tasks. First, a digital human model associated with assembly features is proposed in Section 4.2, in which the human body is represented as a kinematic system including a series of links connected by revolute joints. Considering the human diversity, the anthropometric characteristics of digital human, for example, body dimensions, masses of body segments, are illustrated as well.

Following digital human modelling, a procedure for assembly posture prediction using the multi-objective optimisation (MOO) method is described. Multiple objectives given in Section 4.3.2 refer to joint discomfort and metabolic energy expenditure: the former one deals with the human postures locating

joints and limbs as predictors of pain and musculoskeletal disorders and the later one deals with the endurance capacities for the body as predictors of fatigue. They are both important for designing assembly tasks without excessive strain or fatigue. In Section 4.3.2, modelling individual objective function and combining them via the weighted sum method are separately described. In section 4.3.3, the SQP (sequential quadratic programming) algorithm is introduced for optimisation solutions. In order to examine the proposed method, a verification experiment comparing predicted postures and postures captured in the real environment is presented in Section 4.3.4.

Constraints, presenting boundaries or restrictions on the optimisation problems, are identified by a variety of manual tasks. In addition to the basic constraints for optimisation-based posture prediction problems, i.e., an end-effector (i.e. hand) in contact with a target object and limits on the joint angles, new constraints characterised by manual assembly are proposed and formulated in Section 4.4. Finally, satisfying manual assembly constraints, a series of posture strategies in terms of different assembly conditions are investigated in Section 4.5.

4.2 Digital Human Modelling

4.2.1 Model Simplifications

Associated with the assembly features, the digital human model is simplified initially as follows:

- Extension and flexion movements of the head are not considered.
Based on the guidelines upon working postures, forward inclination of the head should be avoided [119]. Under this circumstance, visibility could be controlled by forward inclination of the trunk when performing some assembly tasks with high visual demands.
- Movements on the right and left equivalent segments are symmetrical with respect to the midsagittal plane.
An asymmetrical posture could cause musculoskeletal disorders especially if it lasts for long periods [120]. Hence it should be avoided in manual assembly. In the following modelling and simulation, only symmetrical postures are considered.
- The rotation movement of the trunk is not considered.
A twisted posture is commonly caused by the poor location of materials,

controls or storage bins, or the poor layout of components [121]. However, it could be prevented by improvements of operator orientations in the materials handling process. An operator can move to align with the assembly object and thereby the rotation movement of his/her truck can be eliminated.

4.2.2 A 10-DOF, 4-Control-Points Human Model

A simplified, 10-DOF human model is proposed as illustrated in Figure 4.1 and its body dimensions are defined in Table 4.1. Essentially, the human body is modelled as a kinematic system, a series of links connected by revolute joints that represent musculoskeletal joints, such as the ankle, knee, hip, trunk, shoulder, elbow and wrist. Each joint is assigned to one or more reference frames in order to describe its movable capacity and the Z axis is in its rotation direction. It is important to note that the index number for the z -axis of joint i is $i - 1$. The 10 degrees of freedom and their descriptions are given in Table 4.2.

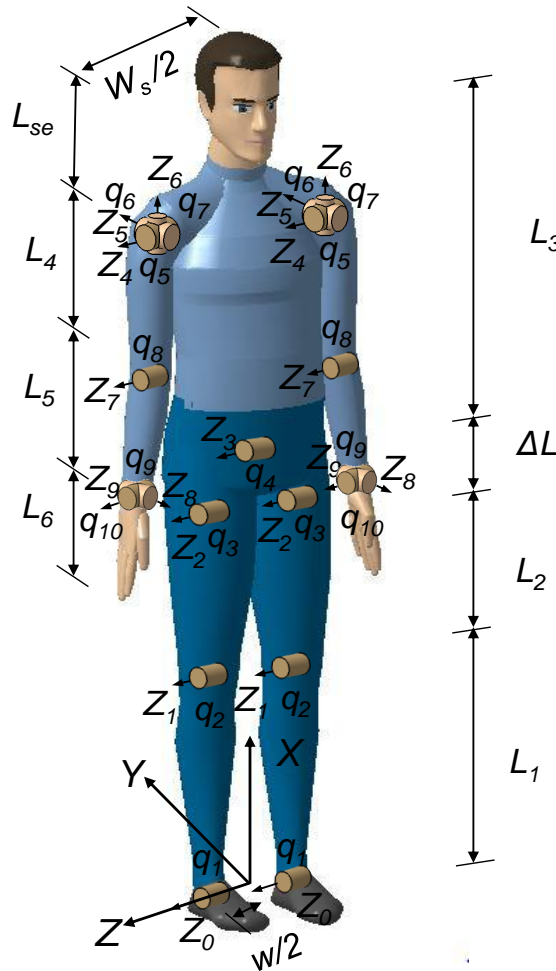


FIGURE 4.1: A 10-DOF human model.

TABLE 4.1: List of body dimensions and their definitions

Dimension	Definition
L_1	Vertical distance between the floor and the centre of the knee.
L_2	Vertical distance between the centre of the knee and the trochanterion on the hip.
ΔL	Vertical distance between the trochanterion on the hip and the flexion and extension axis on the truck.
L_3	Vertical distance between the flexion and extension axis on the truck and the inner corner of the eye.
L_{se}	Distance between the inner corner of the eye and the tip of the shoulder.
L_4	Distance between the tip of the shoulder and the bottom of the elbow.
L_5	Distance between the bottom of the elbow and the base of the hand.
L_6	Distance between the base of the hand and the tip of the middle finger.
W	Horizontal distance between the centres of the ankles.
W_s	Horizontal distance between the centres of the shoulders.

TABLE 4.2: 10 degrees of freedom and their descriptions

DOF	Joints	Description
1	ankle	dorsal flexion/plantar flexion
2	knee	flexion/extension
3	hip	flexion/extension
4	trunk	flexion/extension
5	shoulder	flexion/extension
6	shoulder	abduction/adduction
7	shoulder	pronation/supination
8	elbow	flexion/extension
9	wrist	flexion/extension
10	wrist	adduction/abduction

In order to define a general procedure to describe transformations between joints, the Denavit-Hartenberg (D-H) method is applied [122]. It offers a convenient and systematic representation of transformations and has been reported as a proven method in modelling human biomechanics and kinematics [53, 123–125].

According to the D-H method, the following four parameters completely describe the position and orientation of the $(i + 1)$ th reference frame with respect to the i th reference frame (Figure 4.2):

- the angle θ_i between the $(i - 1)$ th and the i th x -axis about the $(i - 1)$ th z -axis.
- the distance d_i from the $(i - 1)$ th to the i th x -axis along the $(i - 1)$ th z -axis.
- the angle α_i between the $(i - 1)$ th and the i th z -axis about the i th x -axis.
- the distance a_i from the $(i - 1)$ th to the i th x -axis along the i th x -axis.

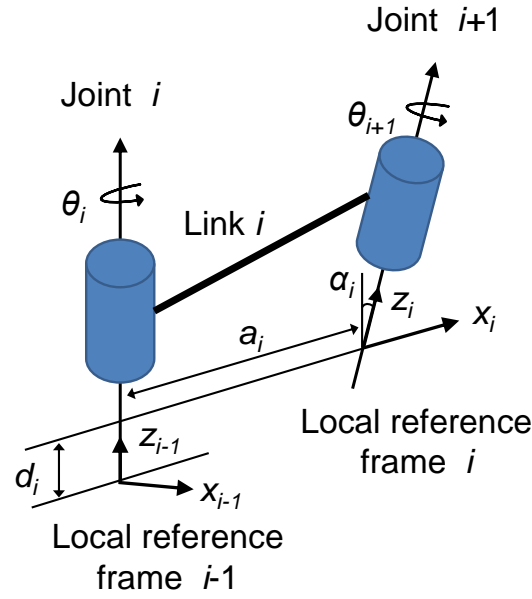


FIGURE 4.2: Parameters for the D-H method.

A homogeneous matrix defined by the D-H method describing the transformation from the $(i + 1)$ th local reference frame to the i th reference frame is shown in Eq.(4.1):

$${}^{i-1}\mathbf{T}_i = \begin{bmatrix} \cos \theta_i & -\cos \alpha_i \sin \theta_i & \sin \alpha_i \sin \theta_i & a_i \cos \theta_i \\ \sin \theta_i & \cos \alpha_i \cos \theta_i & -\sin \alpha_i \cos \theta_i & a_i \sin \theta_i \\ 0 & \sin \alpha_i & \cos \alpha_i & d_i \\ 0 & 0 & 0 & 1 \end{bmatrix} \quad (4.1)$$

The position vector of a point of interest on the end-effector of the human model, e.g., a point on the thumb with respect to the shoulder, can be written in terms of frame coordinates as Eq.(4.2).

$$\mathbf{X} = \Phi(\mathbf{q}) \quad (4.2)$$

where $\mathbf{q} \in \mathbf{R}^n$ is the vector of n -generalised coordinates, and $\Phi(\mathbf{q})$ can be obtained from the multiplication of the homogeneous transformation matrices, as shown in Eq.(4.3).

$${}^0\mathbf{T}_n = {}^0\mathbf{T}_1 {}^1\mathbf{T}_2 \dots {}^{n-1}\mathbf{T}_n = \begin{bmatrix} {}^0\mathbf{R}_n(\mathbf{q}) & \Phi(\mathbf{q}) \\ 0 & 1 \end{bmatrix} \quad (4.3)$$

where ${}^i\mathbf{R}_j$ is the rotation matrix and ${}^i\mathbf{T}_j$ is the homogeneous transformation matrix relating frame i to j .

Manual manipulation of digital human models has proven to be a difficult, time-consuming and experience-based process. In order to facilitate this process, 4 control points are proposed in this research, which are placed on the foot, hip, eye and hand, respectively. In particular, as shown in Figure 4.3, the foot and hip control points are on the coronal plane; the eye control point is on the intersection of the coronal plane and the midsagittal plane; the hand control point is on the tip of the middle finger. In addition, individual reference frame is applied to each control point. Assuming the orientations of the four reference frames are consistent with the global reference frame, they are only determined by their position vectors, i.e. $\mathbf{X}(foot)$, $\mathbf{X}(hip)$, $\mathbf{X}(eye)$ and $\mathbf{X}(hand)$.

An assembly object (e.g., a screw), represented by a point in the workspace, is aligned with the operator and hence it is on the midsagittal plane. Let H denotes its height from the floor and D the distance to the operator, its position vector in the global reference frame is shown in Figure 4.4.

The position vector of the foot control point in the global reference frame is given in Eq.(4.4). During manual assembly, the operator is required to handle and fasten the assembly object and thereby, the position vector of his/her hand could be simply specified as the object's position vector, which is given in Eq.(4.5).

$$\mathbf{X}(foot) = (X_{foot}, Y_{foot}, Z_{foot})^T = \left(0, 0, \frac{W}{2}\right)^T \quad (4.4)$$

$$\mathbf{X}(hand) = (X_{hand}, Y_{hand}, Z_{hand})^T = (H, -D, 0)^T \quad (4.5)$$



FIGURE 4.3: 4 control points in the human model.

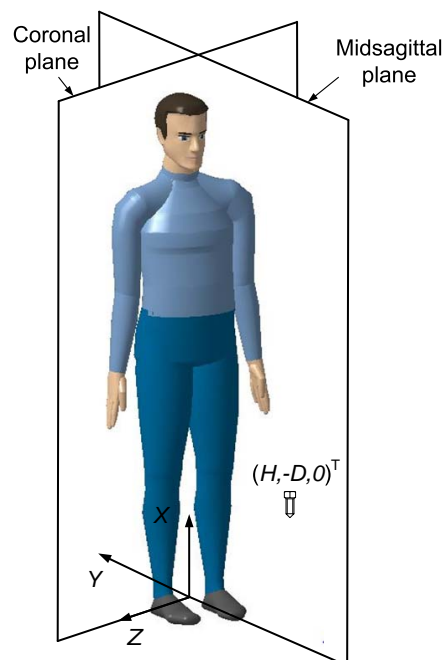


FIGURE 4.4: The position of assembly object.

TABLE 4.3: D-H parameters table between the foot and the hip

	θ	d	a	α
1	$-q_1$	0	L_1	0
2	q_2	0	L_2	0

Table 4.3 shows a D-H table that describes the joint and link parameters between the foot and the hip. Substituting each row into Eq. (4.1) yields the following transformation matrices:

$${}^0\mathbf{T}_1 = \begin{bmatrix} \cos \theta_1 & -\sin \theta_1 & 0 & L_1 \cos \theta_1 \\ \sin \theta_1 & \cos \theta_1 & 0 & L_1 \sin \theta_1 \\ 0 & 0 & 1 & 0 \\ 0 & 0 & 0 & 1 \end{bmatrix} \quad (4.6)$$

$${}^1\mathbf{T}_2 = \begin{bmatrix} \cos \theta_2 & -\sin \theta_2 & 0 & L_2 \cos \theta_2 \\ \sin \theta_2 & \cos \theta_2 & 0 & L_2 \sin \theta_2 \\ 0 & 0 & 1 & 0 \\ 0 & 0 & 0 & 1 \end{bmatrix} \quad (4.7)$$

Performing the multiplication and obtaining the position vector of the hip yields Eq.(4.8).

$$\begin{bmatrix} \mathbf{X}(hip) \\ \mathbf{1} \end{bmatrix} = {}^0\mathbf{T}_1 {}^1\mathbf{T}_2 \begin{bmatrix} \mathbf{X}(foot) \\ \mathbf{1} \end{bmatrix} \quad (4.8)$$

From inspection it is noted that q_1 , q_2 and q_3 are exclusively determined by the hip position vector ($\mathbf{X}(hip)$) in the global frame where $q_3 = q_2 - q_1$. Thus, q_1 , q_2 and q_3 can be controlled by the hip control point.

Similarly, the transformation matrix relating the eye to the 3rd local reference frame is shown as follows:

$${}^3\mathbf{T}_{eye} = \begin{bmatrix} \cos \theta_4 & -\sin \theta_4 & 0 & L_3 \cos \theta_4 \\ \sin \theta_4 & \cos \theta_4 & 0 & L_3 \sin \theta_4 \\ 0 & 0 & 1 & 0 \\ 0 & 0 & 0 & 1 \end{bmatrix} \quad (4.9)$$

The position vector of the eye is obtained by Eq.(4.10).

$$\begin{bmatrix} \mathbf{X}(eye) \\ \mathbf{1} \end{bmatrix} = {}^3\mathbf{T}_{eye} \begin{bmatrix} \mathbf{X}(q_4) \\ \mathbf{1} \end{bmatrix} \quad (4.10)$$

where:

$$\mathbf{X}(q_4) = (X_{hip} + \Delta L, 0, 0)^T \quad (4.11)$$

It can be readily found that q_4 is specified by the eye position vector ($\mathbf{X}(eye)$) and thus the eye control point can control q_4 .

TABLE 4.4: D-H parameters table between the shoulder and the hand

	θ	d	a	α
1	q_5	0	0	$\frac{\pi}{2}$
2	$-q_6$	0	0	$\frac{\pi}{2}$
3	q_7	0	$-L_4$	$\frac{\pi}{2}$
4	$-q_8$	0	$-L_5$	$\frac{\pi}{2}$
5	$-q_9$	0	0	$\frac{\pi}{2}$
6	q_{10}	0	$-L_6$	$\frac{\pi}{2}$

Finally, the parameters describing the transformation from the shoulder to the hand are shown in Table 4.4 and substituted in Eq.(4.1) that yield the following transformation matrices:

$${}^4\mathbf{T}_5 = \begin{bmatrix} \cos \theta_5 & 0 & \sin \theta_5 & 0 \\ \sin \theta_5 & 0 & -\cos \theta_5 & 0 \\ 0 & 1 & 0 & 0 \\ 0 & 0 & 0 & 1 \end{bmatrix} \quad (4.12)$$

$${}^5\mathbf{T}_6 = \begin{bmatrix} \cos \theta_6 & 0 & \sin \theta_6 & 0 \\ \sin \theta_6 & 0 & -\cos \theta_6 & 0 \\ 0 & 1 & 0 & 0 \\ 0 & 0 & 0 & 1 \end{bmatrix} \quad (4.13)$$

$${}^6\mathbf{T}_7 = \begin{bmatrix} \cos \theta_7 & 0 & \sin \theta_7 & -L_4 \cos \theta_7 \\ \sin \theta_7 & 0 & -\cos \theta_7 & -L_4 \sin \theta_7 \\ 0 & 1 & 0 & 0 \\ 0 & 0 & 0 & 1 \end{bmatrix} \quad (4.14)$$

$${}^7\mathbf{T}_8 = \begin{bmatrix} \cos \theta_8 & 0 & -\sin \theta_8 & -L_5 \cos \theta_8 \\ \sin \theta_8 & 0 & \cos \theta_8 & -L_5 \sin \theta_8 \\ 0 & 1 & 0 & 0 \\ 0 & 0 & 0 & 1 \end{bmatrix} \quad (4.15)$$

$${}^8\mathbf{T}_9 = \begin{bmatrix} \cos \theta_9 & 0 & \sin \theta_9 & 0 \\ \sin \theta_9 & 0 & -\cos \theta_9 & 0 \\ 0 & 1 & 0 & 0 \\ 0 & 0 & 0 & 1 \end{bmatrix} \quad (4.16)$$

$${}^9\mathbf{T}_{hand} = \begin{bmatrix} \cos \theta_{10} & 0 & -\sin \theta_{10} & -L_6 \cos \theta_{10} \\ \sin \theta_{10} & 0 & \cos \theta_{10} & -L_6 \sin \theta_{10} \\ 0 & 1 & 0 & 0 \\ 0 & 0 & 0 & 1 \end{bmatrix} \quad (4.17)$$

Performing the multiplication and obtaining the position vector of the hand yields Eq.(4.18).

$$\begin{bmatrix} \mathbf{X}(hand) \\ \mathbf{1} \end{bmatrix} = {}^4\mathbf{T}_5 {}^5\mathbf{T}_6 {}^6\mathbf{T}_7 {}^7\mathbf{T}_8 {}^8\mathbf{T}_9 {}^9\mathbf{T}_{hand} \begin{bmatrix} \mathbf{X}(q_5) \\ \mathbf{1} \end{bmatrix} \quad (4.18)$$

where:

$$\mathbf{X}(q_5) = \left(X_{eye} - L_{se} \sin q_4, Y_{eye} - L_{se} \cos q_4, \frac{W_s}{2} \right)^T \quad (4.19)$$

Obviously, a series of joint rotation variables on the arm (i.e. q_5, q_6, q_7, q_8, q_9 and q_{10}) is determined by the hand position vector ($\mathbf{X}(hand)$). Therefore the hand control point can control q_5, q_6, q_7, q_8, q_9 and q_{10} .

The construction of control points offers an intuitive and immediate approach to position digital human's segments (i.e. the foot, hip, eye and hand) in the virtual environment. A new constraint can be established when a control point is activated, allowing the fixing of the relevant body segments directly instead of fixing quantities of rotational variables between joints. This decreases the number of undetermined variables significantly and therefore enhances the efficiency for digital human manipulation.

4.2.3 Human Diversity

Differences of anthropometric characteristics between human beings are represented by their ages, sexes, geographical regions, and so on. Hence it is necessary to define the population being studied. British male, aged 19 to 65 years, is chosen as the modelling and simulation target in this chapter. Its body dimensions as shown in Figure 4.1 and defined in Table 4.1 are calculated according to a compilation of the data sources available [30, 126, 127]. The calculation results are given in Table 4.5.

TABLE 4.5: Anthropometric data for British male, aged 19 to 65 years.
(all dimensions in millimetres, except for body weight, given in kilograms)

Dimension	5th %ile	50th %ile	95th %ile	SD
L_1	490	545	595	32
L_2	345	375	405	18
ΔL	125	130	135	3
L_3	550	580	610	18
L_{se}	170	175	180	3
L_4	330	365	395	20
L_5	265	285	305	12
L_6	175	190	205	10
W	85	95	110	6
W_s	365	400	430	20
Stature	1625	1740	1855	70
Body weight	55	75	94	12

Besides, the locations of the centres of mass of body segments as a percentage of the length of their corresponding body segments are shown graphically in Figure 4.5 [128].

Based on Winter, the mass of each body segment can be expressed in terms of a percentage of the total body mass, since the mass of each individual segment increases with the total body mass increase [129]. Data on the masses of body segments (Table 4.6) are obtained from the published literature [130].

Human anthropometric characteristics are usually assumed in a standard normal deviation. Let variable x represents a specific anthropometric measure (e.g., body weight) and x_p is the p th percentile of x . Thus the p th percentile value of the body weight can be defined by the following equation:

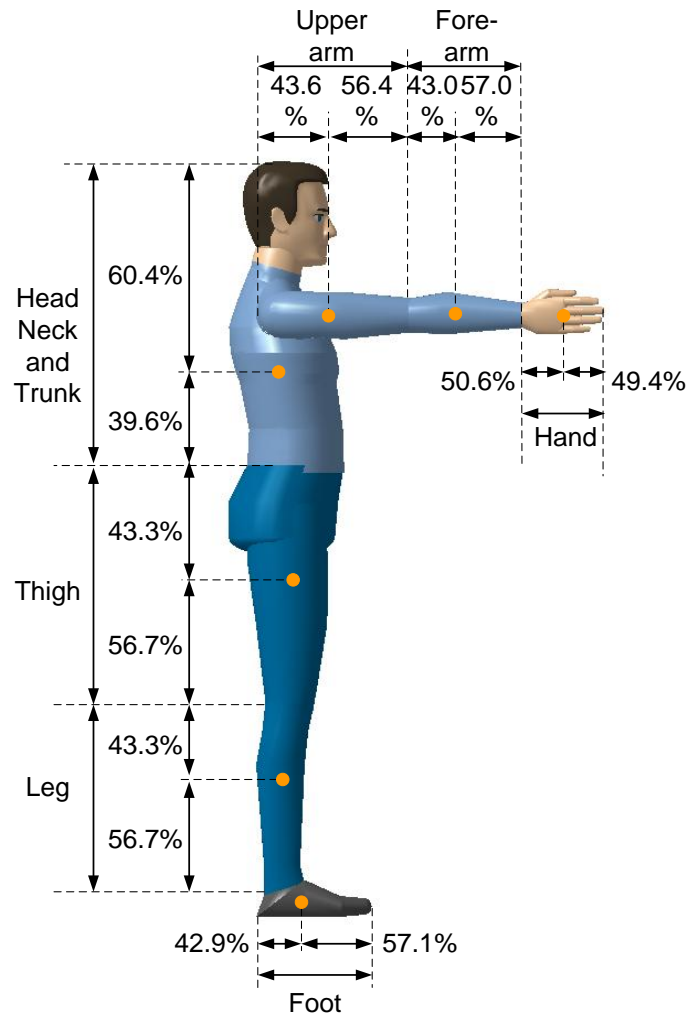


FIGURE 4.5: The locations of centres of mass in the body segments in the sagittal plane [128].

TABLE 4.6: Masses of body segments as a percentage of the whole body mass [130]

Group body segments	Total body mass (%)	Individual body segments	Total body mass (%)
Head and neck	8.4	Head	6.2
		Neck	2.2
Trunk	50.0	Thorax	21.9
		Lumbar	14.7
		Pelvis	13.4
Each arm	5.1	Upper arm	2.8
		Forearm	1.7
		Hand	0.6
Each leg	15.7	Thigh	10.0
		Lower leg	4.3
		Foot	1.4

$$\begin{aligned}
x_p &= \bar{x} + z_p \cdot s \\
\text{where } \bar{x} &= \text{sample mean} \\
s &= \text{sample standard deviation} \\
x_p &= p\text{th percentile value of the variable } x \\
z_p &= \text{standard normal value corresponding to} \\
&\quad \text{the } p\text{th percentile value of } x
\end{aligned} \tag{4.20}$$

According to the definition and calculation of the anthropometric data for the UK population, a British male operator can be specified by his percentile value based on Eq.(4.20). This can be taken as supplement of DELMIA's population database since DELMIA has no data on the UK population yet as described in the previous chapter.

4.3 Multi-Objective Optimisation Method for Posture Prediction

4.3.1 Overview of Multi-Objective Optimisation

The general MOO problem is posed as follows:

$$\begin{aligned}
&\text{Find: } \mathbf{q} \in R^{DOF} \\
&\text{To minimize: } \mathbf{f}(\mathbf{q}) = [f_1(\mathbf{q}) \quad f_2(\mathbf{q}) \quad \dots \quad f_k(\mathbf{q})]^T \\
&\text{Subject to: } \begin{aligned} &g_i(\mathbf{q}) \leq 0 \quad i = 1, 2, \dots, m \\ &h_j(\mathbf{q}) = 0 \quad j = 1, 2, \dots, e \end{aligned}
\end{aligned} \tag{4.21}$$

where k is the number of objective functions, m is the number of inequality constraints, and e is the number of equality constraints. $\mathbf{q} \in E^{DOF}$ is a vector of design variables. $\mathbf{f}(\mathbf{q}) \in E^k$ is a vector of objective functions $f_i(\mathbf{q}) : E^{DOF} \rightarrow E^1$.

The feasible design space is defined as

$\Pi = \{\mathbf{q} | g_j(\mathbf{q}) \leq 0, j = 1, 2, \dots, m; \text{ and } h_i(\mathbf{q}) = 0, i = 1, 2, \dots, e\}$. The feasible criterion space is defined as $\mathbf{Z} = \{\mathbf{f} \in R^k \text{ such that } \mathbf{f} = \mathbf{f}(\mathbf{q}), \mathbf{q} \in \Pi\}$. The point in the criterion space where all of the objectives have the minimum values simultaneously is called the utopia point \mathbf{f}° . In general, \mathbf{f}° is unattainable; it is rarely possible to fully optimise each individual objective function independently and simultaneously, whether the problem is constrained or not.

The idea of a solution for Eq.(4.21), where multiple objectives may conflict with one another, is unclear. Consequently, the idea of Pareto optimality is used to describe solutions for MOO problems. A solution point is Pareto optimal if it is not possible to move from that point and improve at least one objective function without detriment to any other objective functions. Based on this definition, the minimum of a single objective function is Pareto optimal if it is unique. Alternatively, a point is weakly Pareto optimal if it is not possible to move from that point and improve all objective functions simultaneously.

Typically, there are infinitely many Pareto optimal solutions for a MOO problem. Thus it is often necessary to incorporate user preferences in order to determine or select a single suitable solution. With methods that incorporate a priori articulation of preferences, the user indicates the relative importance of the objective functions or desired goals before running the optimisation algorithm. Different methods allow one to articulate preferences in different ways, but the most common approach is to exploit the user set parameters such as weights. Although the exact solution point provided by such methods is somewhat arbitrary, these types of methods can provide useful benchmark results for the multi-objective analysis.

Generally, the posture prediction based on the MOO method involves determining a set of joint rotations to minimise a given human performance measures(s), constrained by the range of joint rotations and by the requirement that hands are in contact with the target object. For the 10-DOF, 4-control-points human model, its optimal posture is obtained by solving the following optimisation problem:

$$\begin{aligned}
 &\text{Find: } \mathbf{q} \in R^{10} \\
 &\text{To minimise: Human performance measures} \\
 &\text{Subject to: } \|\mathbf{X}(\text{hand}) - \mathbf{X}(\text{object})\| \leq \varepsilon \\
 &\quad q_i^L \leq q_i \leq q_i^U \quad i = 1, 2, \dots, 10
 \end{aligned} \tag{4.22}$$

In this chapter, human performance measures refer to joint discomfort and metabolic energy expenditure. ε is a positive infinitesimal value approximates zero. q_i^U and q_i^L represent the upper and lower limits for q_i , respectively. These

limits ensure that the digital human does not assume a position that is completely unrealistic given by actual human joints.

4.3.2 Optimisation Objectives

a. Joint discomfort

The discomfort measure model is taken from Marler et al. [131], which has been adopted by numerous researchers as an objective function in the human posture prediction and proven to be effective and accurate [52, 53, 132].

This model evaluates joint discomfort in its rotational position associated with its comfortable neutral position and its rotation limits as formulated in Eq. (4.23). It shows that joint discomfort obtains the minimum value in the neutral position and increases when approaching the upper limit and the lower limit by adding QU and QL , where QU (Eq.(4.25)) and QL (Eq.(4.26)) are specially designed penalty terms corresponding to the upper limit and the lower limit of each joint. The notation of the variables in the discomfort model is detailed in Table 4.7. The weighting values of joints are detailed in Table 4.8. The neutral position of the digital human is illustrated in Figure 4.6 and the values of joint neutral positions and upper/lower limits are given in Table 4.9.

$$f_{discomfort} = \frac{1}{G} \sum_{i=1}^{DOF} [\gamma_i (\Delta q_i^{norm})^2 + G \times QU_i + G \times QL_i] \quad (4.23)$$

where:

$$\Delta q_i^{norm} = \frac{q_i - q_i^N}{q_i^U - q_i^L} \quad (4.24)$$

$$QU_i = \left(0.5 \sin \left(\frac{5.0 (q_i^U - q_i)}{q_i^U - q_i^L} + 1.571 \right) + 1 \right)^{100} \quad (4.25)$$

$$QL_i = \left(0.5 \sin \left(\frac{5.0 (q_i - q_i^L)}{q_i^U - q_i^L} + 1.571 \right) + 1 \right)^{100} \quad (4.26)$$

TABLE 4.7: Parameters in the joint discomfort model

Parameters	Unit	Description
q_i	degree	current position of joint i
q_i^U	degree	upper limit of joint i
q_i^L	degree	lower limit of joint i
q_i^N	degree	neutral position of joint i
G	—	constant, 10^6
QU_i	—	penalty term of upper limits
QL_i	—	penalty term of lower limits
γ_i	—	weighting value of joint i

TABLE 4.8: Joint weights for discomfort

Joint DOF	Joint Weight
q_1, \dots, q_4	10^8
q_5, \dots, q_{10}	10^4

TABLE 4.9: Joint neutral position and movement ranges (degree)

Joint DOF	Neutral Position	Lower Limit	Upper Limit
1	0	-50	38
2	0	0	135
3	0	-18	113
4	0	-19	56
5	0	-60	170
6	0	-18	80
7	0	-20	97
8	90	0	140
9	0	-70	80
10	0	-30	20

Figure 4.7 is an example of the hip discomfort measure, graphically depicting the trend of joint discomfort from its lower limit to its upper limit. Joint discomfort reaches the minimum value in the neutral position and increases significantly when approaching the upper and lower limits. It should be noted that when a joint neutral position equals to the lower limit, QL is substituted by zero directly. An example of the knee discomfort measure is shown in Figure 4.8, where the neutral position equals to the lower limit, and therefore joint discomfort reaches the minimum value at its lower limit as well.



FIGURE 4.6: The neutral position of the digital human.

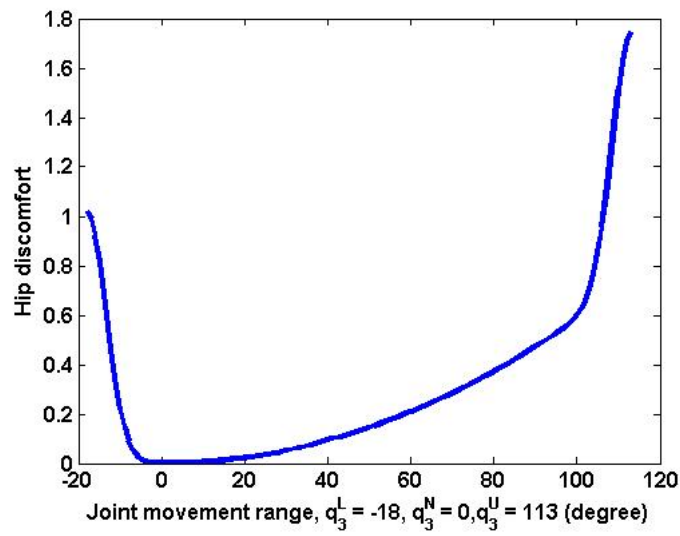


FIGURE 4.7: Hip discomfort measure.

b. Metabolic energy expenditure

Based upon the traditional approach of partitioning muscle energy liberation [68, 133–135], the total rate of muscle energy expenditure (\dot{E}), expressed in

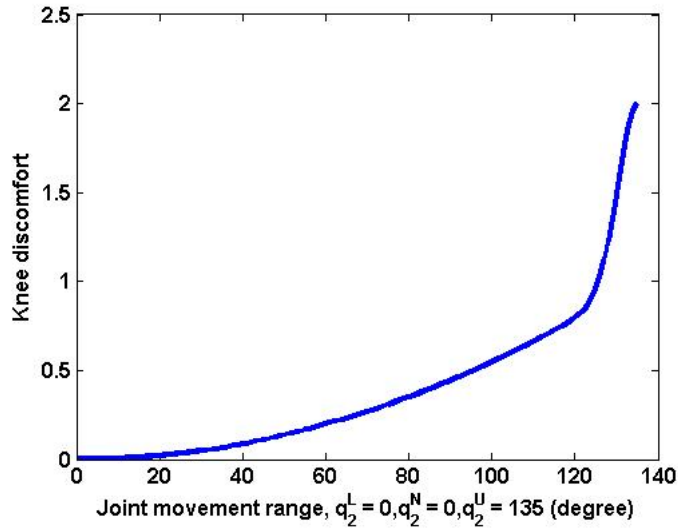


FIGURE 4.8: Knee discomfort measure.

Watts per kilogram, is divided as follows:

$$\dot{E} = \dot{E}_W + \dot{E}_M + \dot{E}_S + \dot{E}_B \quad (4.27)$$

where \dot{E}_W is the muscle mechanical power, \dot{E}_M is the muscle maintenance heat rate, \dot{E}_S is the muscle shortening heat rate, and \dot{E}_B is the basal metabolic rate (BMR).

Force calculation at the muscle level is complex and imprecise since muscles, arranged in groups around a joint, provide not only movements at the joint but also the stability and control for an activity. In addition, different properties of each individual muscle, e.g. muscle length, types of muscle fibres and the muscle contraction velocity, increase the complexity of the calculation at the muscle level. Generally, only force in the joint space is considered in a simplified energy expenditure model [73, 136]. Following Kim et al. [73], the mechanical power is defined as the product of the joint torque (τ_i) and the joint velocity (\dot{q}_i). The total mechanical power \dot{E}_M is thereby the sum of the mechanical power for all joints, as follows:

$$\dot{E}_W = \sum_{i=1}^{DOF} |\tau_i \dot{q}_i| \quad (4.28)$$

In the case of static loading, the mechanical power done by joints is zero.

Hence the energy is all dissipated as heat.

For a given muscle, the muscle maintenance heat rate is calculated as the product of a constant and the muscle activation. In terms of joint space, it is approximately proportional to the joint torque according to the research of Anderson et al. [69] and Kim et al. [73]. Therefore it can be expressed as follows:

$$\dot{E}_M \approx \sum_{i=1}^{DOF} \xi_i |\tau_i| \quad (4.29)$$

where ξ_i is the coefficient of the maintenance heat rate at joint i , which is inversely proportional to the joint torque limits. The joint torque limits are given in Table 4.10 [137].

TABLE 4.10: Joint torque limit [137]

Joint	Joint torque (N · m)	
	Upper limit	Lower Limit
ankle	100	-100
knee	100	-100
hip	100	-100
trunk	100	-100
shoulder	60	-60
elbow	50	-50
wrist	10	-10

The basal metabolic rate (BMR) is defined as the metabolic rate of an individual in a resting state. It indicates the minimum amount of energy required to keep an individual functioning, but not performing any external work. The following BMR model is presented from Hase [136]:

$$\dot{E}_B = 0.685BW + 29.8 \quad (4.30)$$

where BW is the body weight (kilogram).

The contribution of the muscle shortening heat is considered insignificant compared to that of the maintenance heat [69, 138]. Therefore the muscle shortening heat rate is neglected. The final metabolic energy expenditure rate is the sum of the maintenance heat rate and BMR, expressed as follows:

$$f_{metabolic} \approx \sum_{i=1}^{DOF} \xi_i |\tau_i| + \dot{E}_B \quad (4.31)$$

From Eq. (4.31), it is observed that the total metabolic energy rate refers to a weighted sum of joint torques implicitly. Therefore the minimum energy expenditure indicates the minimum joint torque as well.

The determination of joint torques is based on a multiple-link static model developed by Chaffin et al. [139], which is specially applicable to symmetric sagittal plane activities as depicted in Figure 4.9.

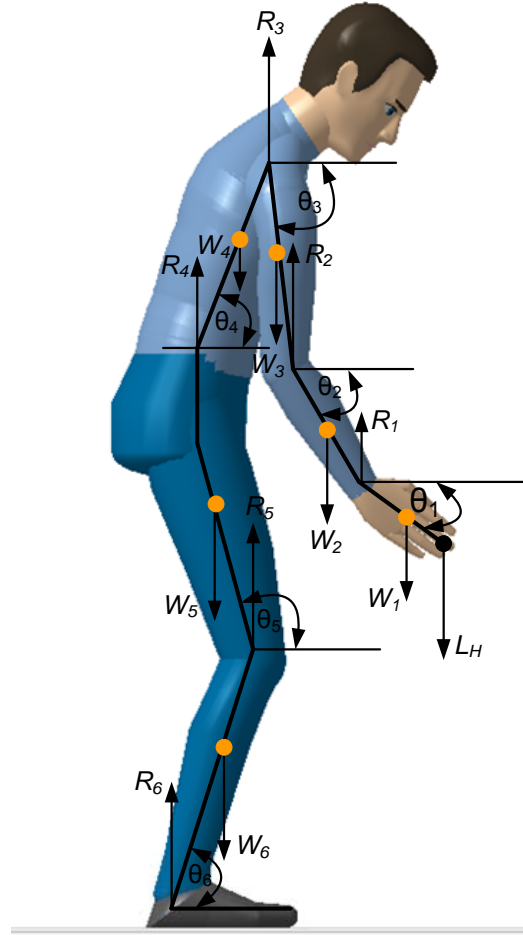


FIGURE 4.9: Static force modelling on the sagittal plane.

In this model, the forces are considered to act in parallel, producing only one force equilibrium condition in the vertical direction. The moment equilibrium conditions can then be expressed in the following general form:

$$\sum \mathbf{M}_j = 0$$

$$\mathbf{M}_j = \mathbf{M}_{j-1} + [\overline{jCM_L} \cos \theta_j \mathbf{W}_L] + [\overline{jj-1} \cos \theta_j \mathbf{R}_{j-1}] \quad (4.32)$$

where:

\mathbf{M}_j	the reactive load moments at each joint j .
$\overline{jCM_L}$	the distances from joint j to the centre of mass of link L , which are calculated based on the anthropometric data (Table 4.5) and locations of CoM (Figure 4.5).
θ_j	the postural angles of the L links at each joint j with respect to horizontal axis, which are calculated based on the value of q_i . Calculation formulae are shown in Table 4.11.
\mathbf{W}_L	the body segment weights for each link L , which are obtained directly from Table 4.6.
$\overline{jj-1}$	the body segment link lengths measured from joint j to the adjoining joint $j-1$, which are obtained from Table 4.5.
\mathbf{R}_{j-1}	the reactive forces at the adjacent joints $j-1$.

TABLE 4.11: Calculating formulae of $\theta_j (j = 1, 2, \dots, 6)$

$$\begin{aligned} \theta_1 &= \theta_2 - q_{10} \\ \theta_2 &= \theta_3 - q_8 \\ \theta_3 &= q_4 + 90 - q_5 \\ \theta_4 &= 90 - q_4 \\ \theta_5 &= 90 + q_3 \\ \theta_6 &= q_3 + 90 - q_2 \end{aligned}$$

When considering the additional workload on the hands, the moments at each joint will increase in proportion to the moment arm distances that the workload is applied to each joint. Thus the moment values can be expanded as follows:

$$\mathbf{M}_{j/L} = \mathbf{M}_j + \overline{j-h} \mathbf{L}_H \quad (4.33)$$

where:

$\mathbf{M}_{j/L}$	the load moments at each joint j with a workload held on the hands
$\overline{j-h}$	the arm distances from each joint j to the workload held on the hands
\mathbf{L}_H	the magnitude of the workload held on the hands

c. Objective function determination

Finally, the objective function is formulated in Eq. (4.34) utilising the weighted sum method, which is the most common approach to obtain solutions for MOO problems [140].

$$\mathbf{f}(\mathbf{q}) = \sum_{i=1}^k w_i f_i^N(\mathbf{q}) \quad (4.34)$$

where: w_i is the weight assigned to the i th objective, and $\sum w_i = 1$ ($w_i \geq 0$). In this context, the minimum of Eq.(4.34) is Parato optimal [141]. $f_i^N(\mathbf{q})$ is the i th normalised objective, expressed as follows:

$$f_i^N(\mathbf{q}) = \frac{f_i(\mathbf{q}) - \min f_i(\mathbf{q})}{|\max f_i(\mathbf{q}) - \min f_i(\mathbf{q})|} \quad (4.35)$$

where, $\max f_i$ and $\min f_i$ are the absolute maximum and minimum of the i th objective, respectively. After normalisation, the value of any objective $f^N(\mathbf{q})$ will vary from zero to one.

The role of weights serves to express the preference of each objective relative to the others. Hence the assignment of weights is significant to the final solution. In this research, the ranking method developed by Yoon and Hwang is adopted to select weights according to the relative importance of each objective systematically [142]. Generally, in this method different objectives are arranged in a rank order. The least important objective receives a weight of one, and integer weights with consistent increments are assigned to objectives which are more important. The procedure to determine weights when $k = 2$ is described mathematically as follow:

Step 1: Let $f_1^1 = \min f_1^N(\mathbf{q}_1)$; $f_2^2 = \min f_2^N(\mathbf{q}_2)$. It is obvious that the minimum value of a normalised objective function $f_i^N(\mathbf{q})$ equals to zero.

Step 2: Get $f_1^2 = f_1^N(\mathbf{q}_2)$; $f_2^1 = f_2^N(\mathbf{q}_1)$. Since no utopia point \mathbf{f}° exists for Eq. (4.22), f_1^1 , f_1^2 , f_2^1 and f_2^2 must satisfy the following conditions:

$$\begin{cases} f_1^2 > f_1^1 \\ f_2^1 > f_2^2 \end{cases} \quad (4.36)$$

Step 3: Get mean deviation m_i , where $m_i = f_i^j - f_i^i = f_i^j$ ($i, j = 1, 2; i \neq j$)

Step 4: Get weight w_i by Eq.(4.37)

$$w_i = \frac{m_i}{\sum_{i=1}^2 m_i} \quad (i = 1, 2) \quad (4.37)$$

4.3.3 Optimisation Algorithm

Considering the constrained optimisation problem, i.e. Eq. (4.21), an efficient gradient based optimisation method - SQP (sequential quadratic programming) method is applied and implemented in the subroutine *fmincon* in the optimisation toolbox for MATLAB.

In nonlinear programming, the objective function (\mathbf{f}) is minimised subject to equality and inequality constraints (\mathbf{G}). The Lagrangian, \mathbf{L} is formulated as follow:

$$\begin{aligned} \text{To minimize:} \quad & \mathbf{L}(x) = \mathbf{f}(x) + \sum_{i=1}^m \lambda_i \mathbf{G}_i(x) \\ \text{Subject to:} \quad & \nabla \mathbf{L}(x) = \nabla \mathbf{f}(x) + \sum_{i=1}^m \lambda_i \nabla \mathbf{G}_i(x) = 0 \\ \text{where:} \quad & \lambda_i \geq 0 \end{aligned} \quad (4.38)$$

and where λ_i are the Lagrangian Multipliers. The Lagrangian can therefore be viewed as a linear weighted sum between the objective and the constraints. Eq. (4.38) are the Kuhn-Tucker (KKT) conditions. Due to the nonlinear nature of the Lagrangian, it is approximated as follow:

$$\mathbf{L}(x_k + \Delta x) \approx \mathbf{L}(x_k) + \nabla \mathbf{L}(x_k)^T \Delta x + \frac{1}{2} \Delta x^T H \Delta x \quad (4.39)$$

The problem is then transformed to a quadratic programme (QP) which is convex. For non-convex Lagrange functions, the chance of finding local optima still exists. However, for convex functions, the transformation shown in Eq. (4.39) preserves the convexity. Note, in Eq. (4.39) H is an approximation to the Hessian, the matrix of second order derivatives. The matrix H is updated as follows:

$$H_{k+1} = H_k + \frac{q_k q_k^T}{q_k^T s_k} - \frac{H_k^T s_k^T s_k H_k}{s_k^T H_k s_k} \quad (4.40)$$

where:

$$s_k = x_{k+1} - x_k \quad (4.41)$$

and,

$$q_k = \left(\nabla \mathbf{f}(x_{k+1}) + \sum_{i=1}^m \lambda_i \nabla \mathbf{G}_i(x_{k+1}) \right) - \left(\nabla \mathbf{f}(x_k) + \sum_{i=1}^m \lambda_i \nabla \mathbf{G}_i(x_k) \right) \quad (4.42)$$

Thus s_k can be seen as the change in the solution vector. Additionally, q_k is the difference between the gradient of the Lagrangian function between the k th and $(k + 1)$ th iteration. The solution to the QP (defined by Eq. (4.38)) sub-problem produces a vector d_k , which is used to form a recursive step:

$$x_{k+1} = x_k + \alpha_k d_k \quad (4.43)$$

The step length parameter α_k is determined in order to produce a sufficient decrease in the so called merit function used by *fmincon* in MATLAB. The merit function is defined as follow:

$$\Psi(x) = \mathbf{f}(x) + \sum_{i=1}^{m_e} r_i g_i + \sum_{i=m_e+1}^{m_e} r_i \max(0, g_i(x)) \quad (4.44)$$

where:

$$r_i = r(k+1)_i = \max_i \left\{ \lambda_i, \frac{(r_k)_i + \lambda_i}{2} \right\} \quad \text{where } i = 1, \dots, m \quad (4.45)$$

and noting that λ_i is the i th Lagrange multiplier. The procedure outlined above continues until the KKT conditions are satisfied.

From the above description, it is observed that the SQP method which utilises the analytically determined gradients can improve computation efficiency even for large design space of joint rotations. Also, it is capable of achieving a (local) optimum from any arbitrary starting point, which is particularly useful to anticipate a possible solution in the posture prediction problem. In this context, the neutral posture of the digital human is specified as an initial starting point

and the local optimum obtained later is used for a new search until the global optimum is determined. Figure 4.10 shows the procedure for posture prediction via the SQP method, which takes the input of the anthropometry data (i.e. p th percentile value of the stature and the body mass) as well as the target object data (i.e. its position and weight), using the pre-defined human performance measure and the ranking method to solve the MOO-based posture prediction problem. The SQP method is employed twice in the procedure: first obtaining the absolute minimum/maximum values of a single objective function and then calculating the final solution after the automatic determination of weights for objective functions. The results of joint variables can be applied to construct digital human posture in forward kinematics directly. MATLAB code for the posture prediction procedure is detailed in Appendix B.

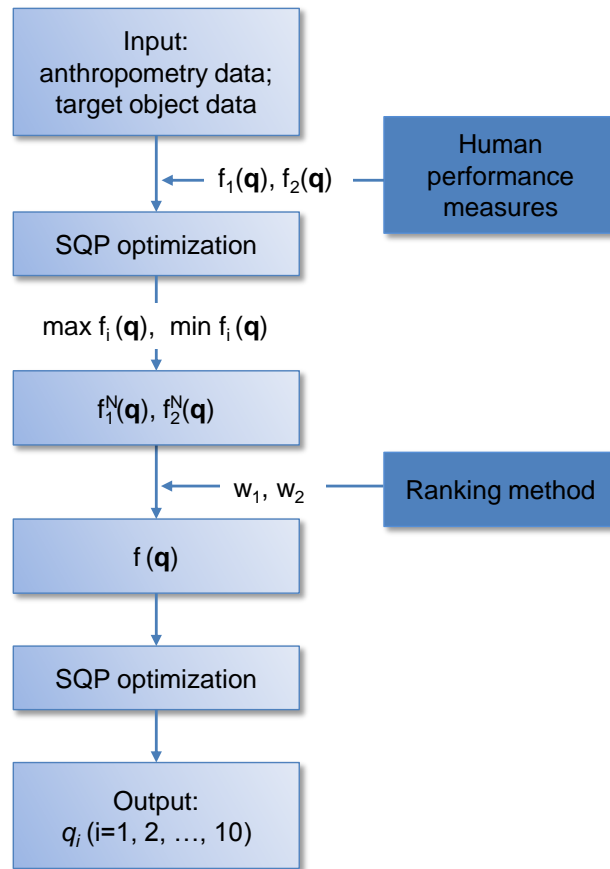


FIGURE 4.10: The procedure for posture prediction via the SQP method.

4.3.4 Model Verification

In order to evaluate the performance of the posture prediction method with the 10-DOF, 4-control-points digital human model, a verification experiment was carried out in the Virtual Engineering Centre (VEC) in the Daresbury Laboratory. The aims of the experiment are:

- To examine the validity of the 10-DOF, 4-control-points digital human model in posture presentation.
- To examine the accuracy of the optimisation-based posture prediction method, including the individual objective function and the final objective function constructed via the weight sum method.

a. Experimental protocols

Six subjects participated in the experiment where four target objects were located in front of them. The subjects were all healthy male, right-hand dominant. Table 4.12 shows their summary attributes. As stated above, objects were placed on the midsagittal plane and thus their locations were determined by the height from floor and the distance to the subjects (Figure 4.4). The height (H) and distance (D) of the objects were selected randomly, as given in Table 4.13. All subjects were instructed to touch the four target objects with their middle finger tips at a comfortable pace. Figure 4.11 shows an example of a subject and a target object in the experiment.

TABLE 4.12: Subject summary statistics

Subject	Stature		Body Mass
	(mm)	(%ile)	(kg)
1	1740	50.00	70
2	1760	61.22	75
3	1700	19.49	70
4	1720	38.78	72
5	1730	33.72	62
6	1710	23.89	68

Human posture data were captured, visualised and processed using an interactive VR system in the VEC, which comprises a stereo vision system, a motion tracking system and a software tool – Haption RTI (real-time interaction) for DELMIA human (RTID human).

TABLE 4.13: Target Objects in the experiment

Target	H (mm)	D (mm)
1	1200	550
2	750	350
3	850	450
4	1000	600

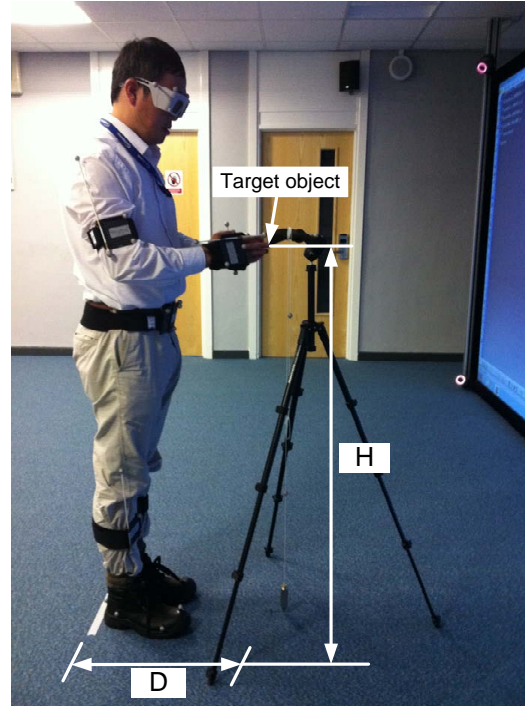


FIGURE 4.11: Illustration of locations of subjects and objects in the experiment.

A 6-meters-wide, 2.1-meters-high power-wall screen with dual stereo projectors placed at the back, as shown in Figure 4.12, was used for human posture visualisation. It provides a display of 3.6 million pixels with a refresh rate of 120Hz. A stereoscopic vision can be received when wearing stereo glasses.

A 12 Vicon-Bonita-camera, optical based motion tracking system was used for whole-body posture capture. The Vicon Bonita cameras have a 0.3 megapixel resolution, a shutter time from 0.5 ms, and an accuracy up to 1 mm in a $5\text{ m} \times 3\text{ m}$ tracking envelope. The whole-body posture is captured by positioning a series of retro-reflective markers on the subject. As the subject moves in the tracking envelope, his posture data are collected and streamed to DELMIA, where a digital human replicates his movement via data post-processing in RTID human. In order to animate the digital human in DELMIA in real-time, RTID human requires several markers being grouped to a prop and worn on the subject's body segments. Each prop represents a tracking object in the tracking system and

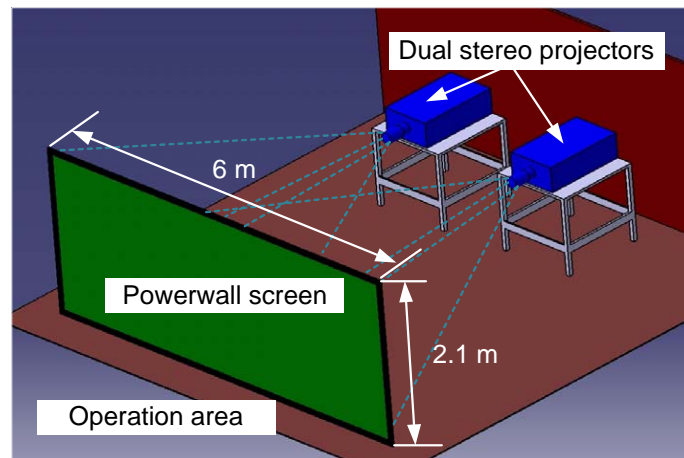


FIGURE 4.12: The stereo vision system.

then matches to relevant limbs of the digital human using a “suit configuration tool”, as shown in Figure 4.13. In this experiment, 10 props were created and added to the tracking object list as shown in Figure 4.14 and their locations are shown in Figure 4.15.

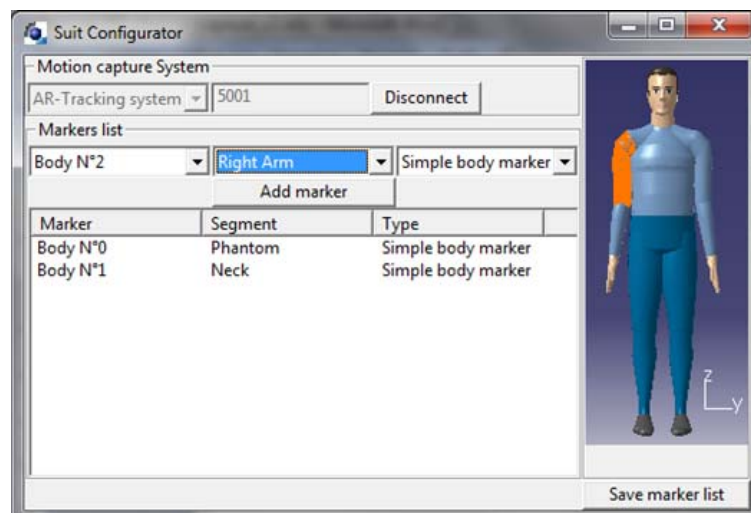


FIGURE 4.13: A suit configuration tool.

The experiment procedure is illustrated schematically in Figure 4.16. Two digital humans were created and scaled to match the subject based on the percentile and therefore potential errors which result from the calculation of segment lengths can be avoided. Among the digital humans, one in the blue shirt was animated by the motion tracking system and the other in the yellow shirt was used to display the predicted results. Due to the hypothesis that postures are symmetrical with respect to the midsagittal plane in human modelling, only

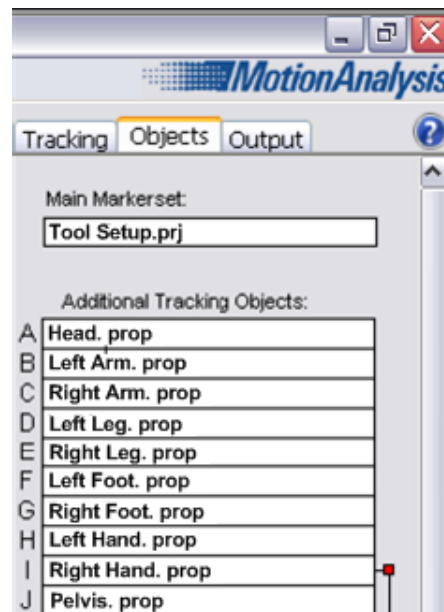


FIGURE 4.14: 10 props for tracking objects.

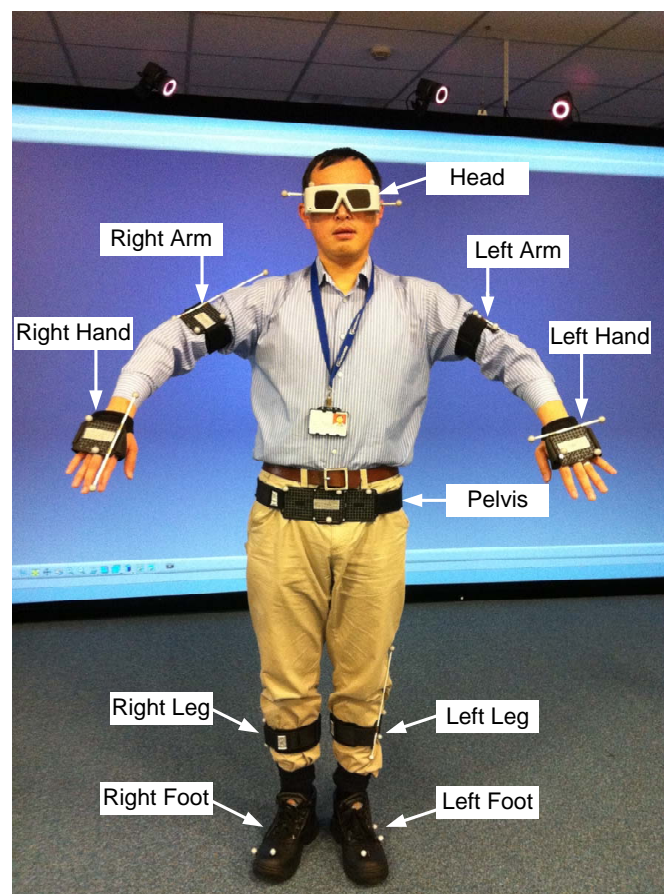


FIGURE 4.15: The location of ten props.

the right hand data of subjects were collected and compared with the predicted data.

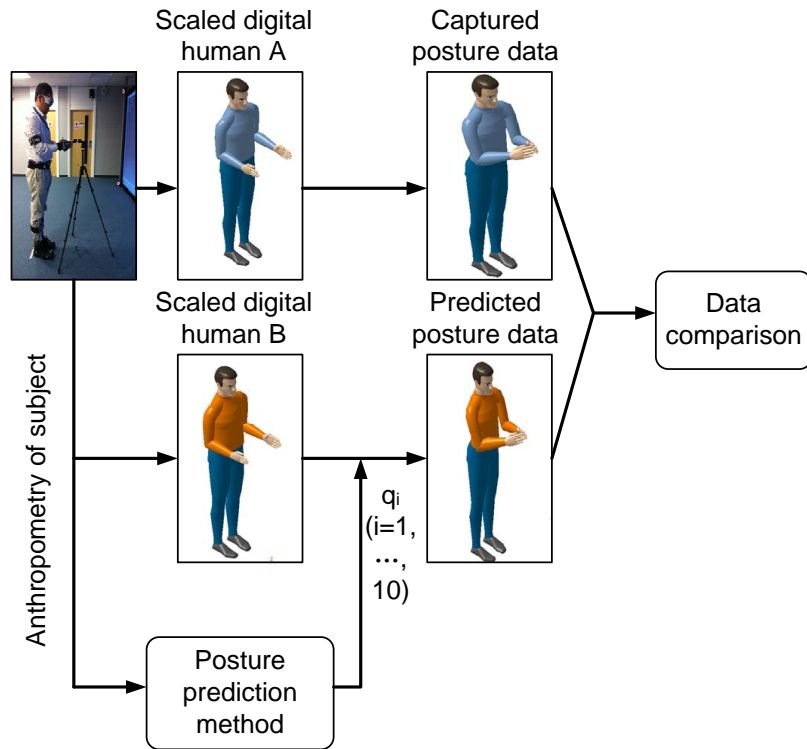


FIGURE 4.16: A schematic plot of the experiment procedure.

b. Qualitative comparative results

Figures 4.17-4.20 exhibit sets of comparative postures obtained from the motion tracking system (in the blue shirt) and from the posture prediction method (in the yellow shirt) graphically. Six subjects are randomly selected for illustration and hence the performance of the posture prediction method can be evaluated across subjects and objects. From observation of Figures 4.17 - 4.20, no significant differences are found between both postures when the objects and the subjects varying. This provides a preliminary verification regarding the accuracy of the posture prediction method. In order to further investigate the method, a quantitative comparison in terms of joint rotations is carried out.

c. Quantitative comparative results

Only upper extremity's movements were observed when subjects touching varied objects in the experiment. Hence the rotation variables corresponding to the upper extremity (from q_5 to q_{10}) are compared quantitatively. Figure 4.21 shows the captured angles versus the predicted angles of the six joint rotation variables

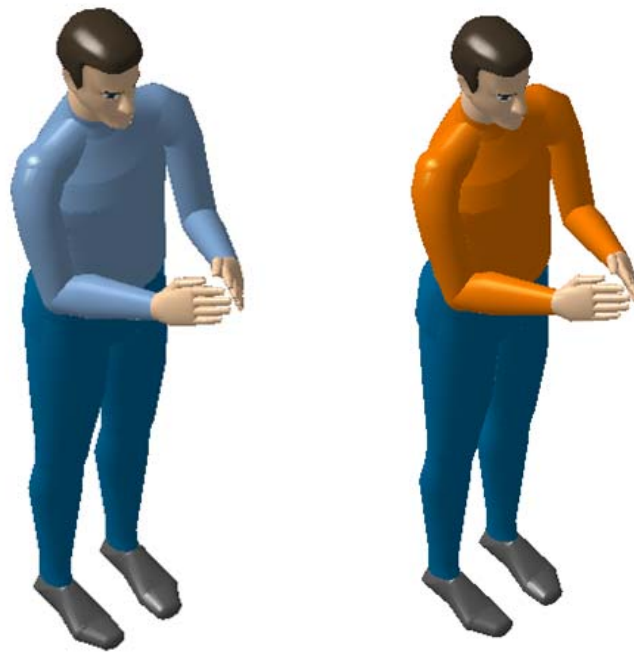


FIGURE 4.17: Qualitative comparative results for target 1.

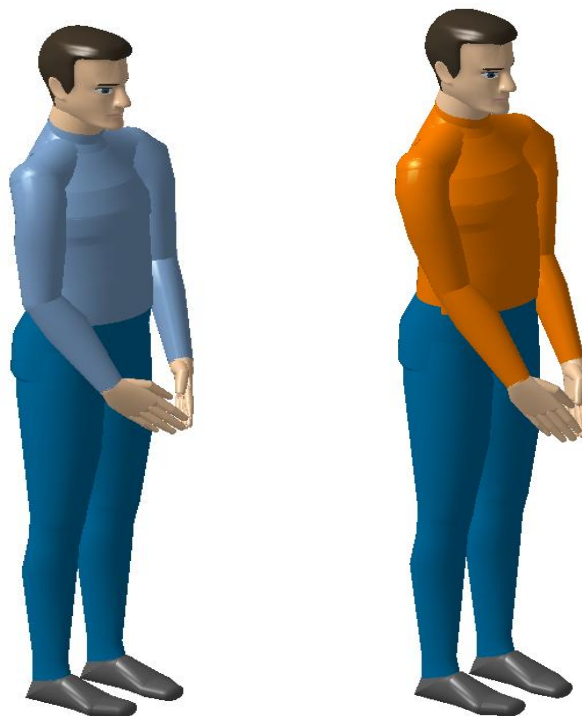


FIGURE 4.18: Qualitative comparative results for target 2.

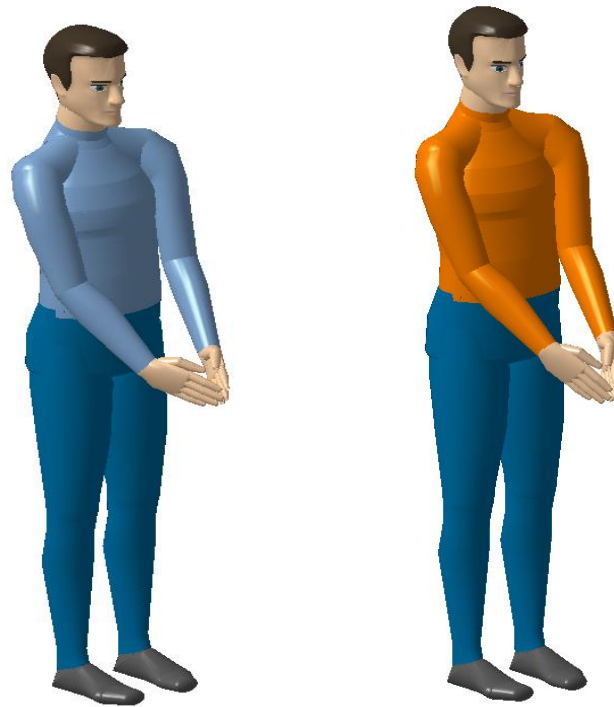


FIGURE 4.19: Qualitative comparative results for target 3.

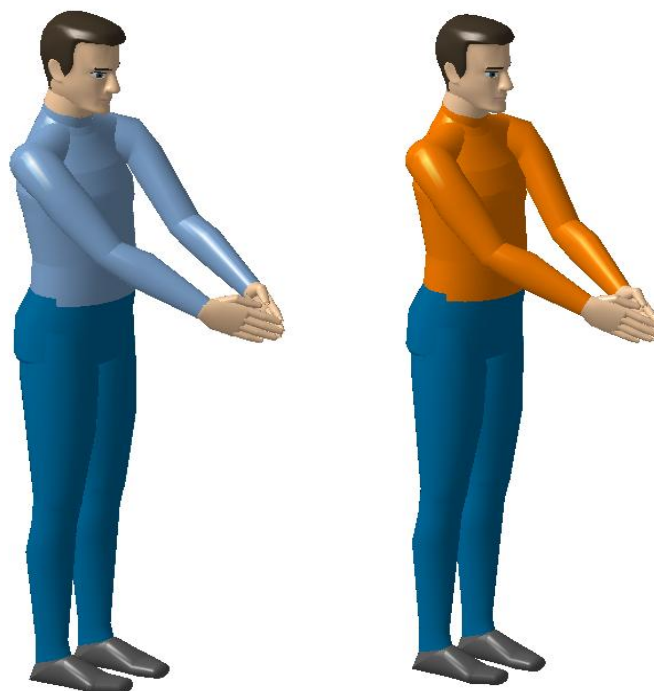


FIGURE 4.20: Qualitative comparative results for target 4.

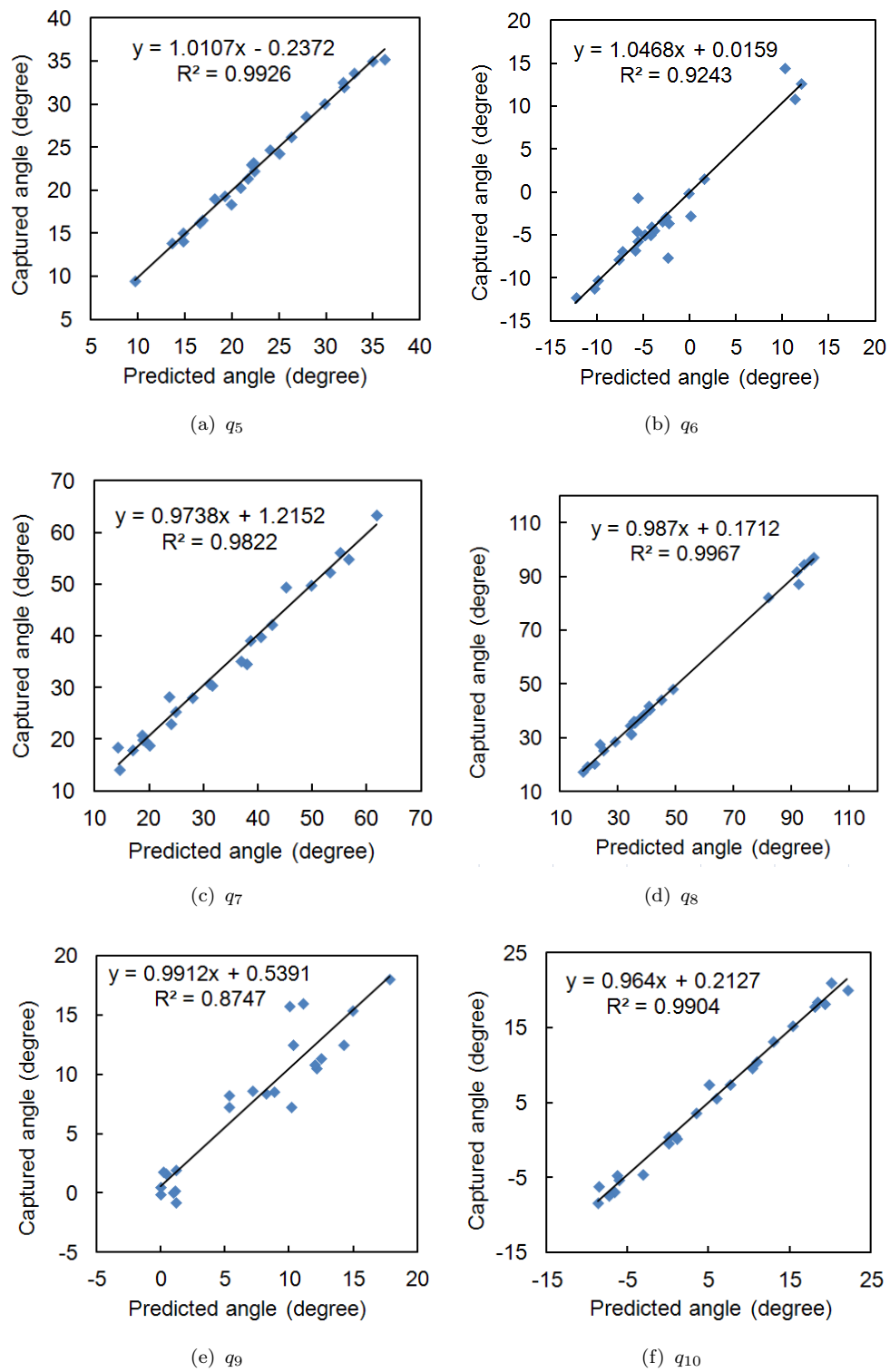


FIGURE 4.21: Regression plot of joint rotation variables

across all trials (6 subjects \times 4 objects) as well as the linear regression lines. It can be seen that the slopes of the regression lines for six variables are approximately 45° and additionally, the values of R^2 all exceed 0.8, indicating a fair accurate reflection of the predictive postures to the real postures.

TABLE 4.14: Wilcoxon Signed-Rank tests of joint variables

Comparison	Test statistics		
	N	Z	Asymp.Sig. (2-tailed)
q_5	24	-0.286	0.775
q_6	24	-1.329	0.184
q_7	24	-0.343	0.732
q_8	24	-1.771	0.076
q_9	24	-0.514	0.607
q_{10}	24	-0.486	0.627

Also, the differences between two sets of joint variables are explored using the Wilcoxon Signed-Rank test for SPSS. As the non-parametric alternative to the paired samples t-test, the Wilcoxon Signed-Rank test is suitable for small samples examination without the stringent assumptions of the scores distribution for the variables, i.e. normal distribution. The results of the test as detailed in Table 4.14 shows that the associated significance levels, presented as Asymp.Sig.(2-tailed), is greater than 0.05, suggesting that the joint angles from the posture prediction method and that from the real human postures are not significantly different at $\alpha = 0.05$.

d. Discussion

The qualitative and quantitative comparative results demonstrated that the predicted postures obtained from the MOO method are general in good agreement with the captured postures for ranges of objects and subjects. The construction of final objective function via the weighted sum method had proven to be correct and effective, which can assign the weight to each objective (i.e. joint discomfort, metabolic energy expenditure) automatically based on their relative importance. The joint discomfort model evaluates postures according to rotational position of each joint relating to its neutral position, upper limit and lower limit. The metabolic energy expenditure model indicates a calculation of joint torques on the sagittal plane at a certain posture. They both behave well for governing postures of the digital human as realistic as possible. Figure 4.22 shows the range of mean differences between the predicted data and the captured

data from q_5 to q_{10} . It was found that the predicted results for q_5 , q_8 and q_{10} out-performed than the results for q_6 , q_7 and q_9 . That is because the joint torques calculation only considered the joint rotations on the sagittal plane (i.e. q_5, q_8, q_{10}) and hence the other joint rotations (i.e. q_6, q_7, q_9) are not constrained as sufficiently as the ones on the sagittal plane in the objective model. In order to further improve the prediction performance, individual objective function could be refined, for instance, considering three-dimensional modelling of joint torques.

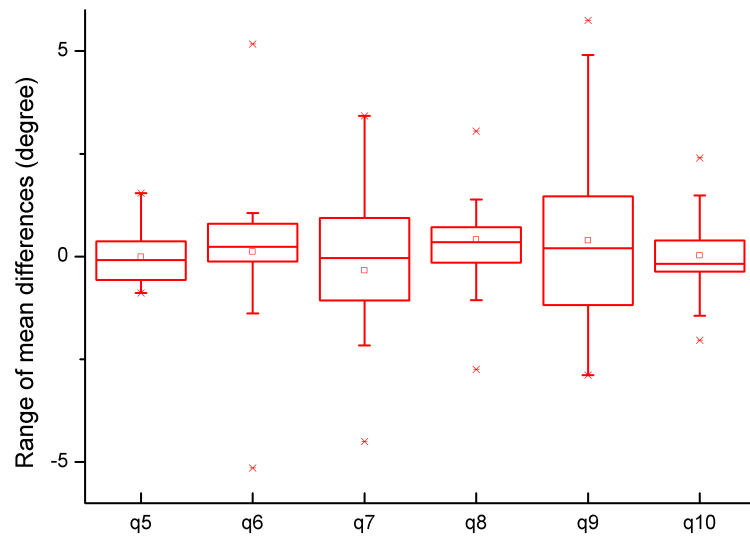


FIGURE 4.22: The range of mean differences from q_5 to q_{10} .

4.4 Task-Based Posture Analysis

The under-constrained nature of posture prediction on highly redundant human models allows human performance measures to drive the resulting posture, which satisfies a large range of constraints proposed by task conditions. In manual assembly, the visual demands of the assembly task are important not only because they provide a clear view of the assembly object to secure assembly quality and efficiency, but also because they largely determine the assembly postures of operators, for instance, the inclination of the neck and trunk. The visual demands require that the central region of both eyes is convergent directly upon the task. Furthermore, the eyes must accommodate to an appropriate distance from the object [30]. Therefore the assembly posture is not only

constrained by the hands contacting with the assembly object, but also by the eyes' location which obeys specific visual demands.

As illustrated in Figure 4.23, the eye control point ($\mathbf{X}(\text{eye})$) which is supposed to be on the intersection of the coronal plane and the midsagittal plane has aligned with the assembly object ($\mathbf{X}(\text{object})$). Let d denotes a desirable distance between the eye control point and the assembly object. When the position vector of the hip control point ($\mathbf{X}(\text{hip})$) is determined, the virtual demand will be obtained exclusively by the trunk's inclination (q_4) since the extension and flexion movements of the head have been avoided initially in the human modelling simplifications. It is evident from Section 4.2.2 that the hip control point controls joint variables q_1 , q_2 and q_3 and the eye control point controls q_4 . Therefore, the MOO-based posture prediction problem constrained by the additional visual requirement can be redefined as follows:

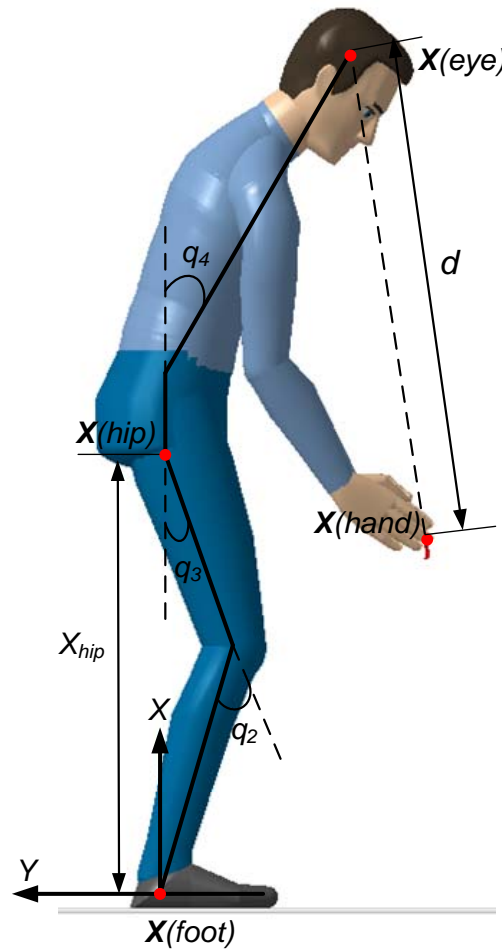


FIGURE 4.23: Illustration of the visual demands.

$$\begin{aligned}
&\text{Find: } \mathbf{X}(hip), \quad q_i (i = 5, \dots, 10) \\
&\text{To minimize: } f = w_1 f_1^N + w_2 f_2^N \\
&\quad \|\mathbf{X}(hand) - \mathbf{X}(object)\| \leq \varepsilon \\
&\text{Subject to: } \|\mathbf{X}(eye) - \mathbf{X}(hand)\| = d + \varepsilon \\
&\quad q_i^L \leq q_i \leq q_i^U \quad i = 5, \dots, 10 \\
&\quad \sin(q_2^U - q_3^U)L_1 \leq X_{hip} \leq (L_1 + L_2)
\end{aligned} \tag{4.46}$$

where f_1^N represents the normalised joint discomfort function and f_2^N the normalised energy expenditure rate function. ε is a positive infinitesimal value approximates zero. The range of the hip control point is determined by the joint motion range and the dimensions of anthropometry data.

4.5 Results

4.5.1 Optimum Posture Analysis

The squat and stoop postures are sometimes necessary for the operator because of the layout of workplaces, for instance, when an assembly object is placed below the operator's upper extremity reach envelope. As illustrated in Figure 4.23, the inclination of truck correlating with a required visual distance (d) can be reduced in adopting squat postures. This can reduce the stress on the low-back region which contributes to the development of low-back pain and injury. However, the stresses on the hip, knee and ankle are increased correspondingly during squatting. In the contradiction of reducing stress on the low-back region and that on the lower extremity, an optimum posture with the minimum total joint discomfort and moment can be predicted using the MOO method.

Figure 4.24 shows sets of optimum hip displacement (which equals to the hip height determined by the anthropometry data minus the optimum X_{hip}) for different operators varying from 5th percentile to 95th percentile in a certain assembly condition, i.e., the object height (H) from the floor is 700mm, the distance (D) to the operator is 500mm, the weight (L_H) is 0.1kg, and the visual demand (d) is 500mm. As illustrated in the figure, a squatting assembly posture should be adopted for various operators in terms of minimum joint discomfort and minimum energy expenditure. Also, three curves show the same trend of substantially increasing hip displacement with increasing percentile. This indicates a preference of adopting squat postures for taller operators in order to

reduce the discomfort and energy expenditure. The optimum postures for operators from 5th percentile to 95th percentile are shown in Appendix C.

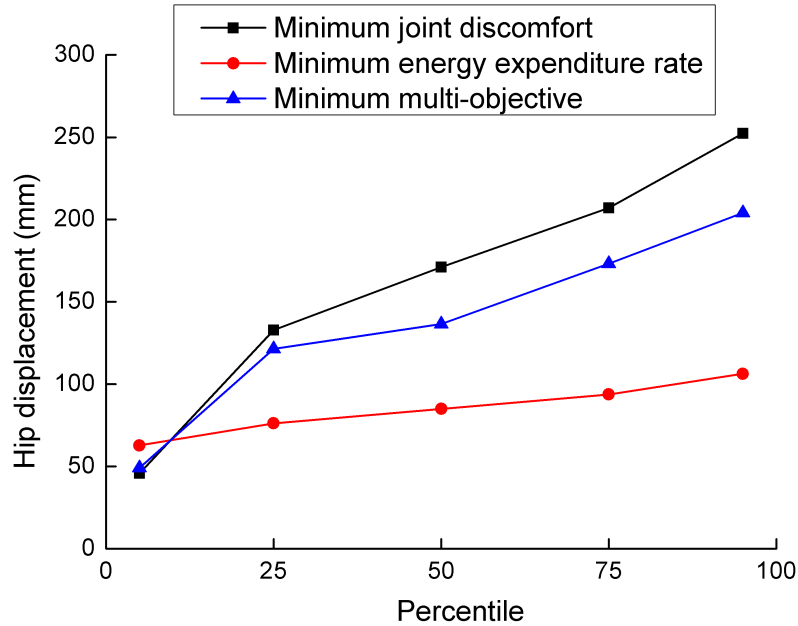


FIGURE 4.24: Optimum hip displacement for different operators.

4.5.2 Effect of Object Height

For a 50th percentile UK male operator assembling the object below his upper extremity's reach envelope (i.e. the object height $H \leq 700$ mm), the optimum assembly postures in terms of minimum joint discomfort and minimum energy expenditure are investigated with constraints due to certain visual demands (i.e. $d = 400$ mm, 500 mm and 600 mm, respectively). Figure 4.25 shows the optimum hip displacements versus object heights for three different visual demands where the object distance to the operator $D = 500$ mm and the weight $L_H = 0.1$ kg. An increase of hip displacement with the decrease of object height is observed and the trend is constant for different visual demands. This indicates a reduction of joint discomfort and energy expenditure when adopting squat postures to assemble objects in lower positions.

4.5.3 Effect of Distance to Object

The effect of the object distance to the operator on the assembly posture is investigated when certain visual demands are satisfied. The optimum hip

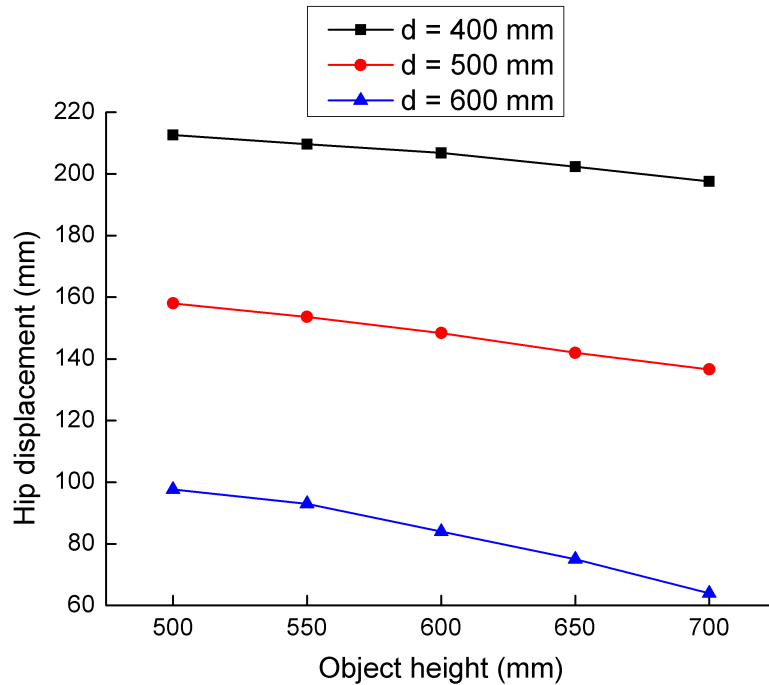


FIGURE 4.25: The effect of object height.

displacements of the 50th percentile UK male operator versus varying distances are shown in Figure 4.25, where the object height $H = 700$ mm and the weight $L_H = 0.1$ kg. Figure 4.25 displays a trend of increased hip displacement with a decreasing distance between the object and the operator for three different visual demands. It can be concluded that adopting a squat posture to assemble an object closer to the operator is recommended in terms of reduced joint discomfort and energy expenditure.

4.5.4 Effect of Object Weight

The effect of the object weight on the assembly posture satisfying certain visual demand is investigated. Based on the ergonomic requirements of manual assembly, workload on hands must not exceed 50 N at the average position (Table 3.2) and hence the object weight can vary between 0.1 kg and 5 kg. Its effect on the optimum hip displacement is shown in Figure 4.27 where the object height $H = 700$ mm and the distance $D = 500$ mm. In this diagram, more hip displacement is required when the object weight increases in order to satisfy different visual demands. As stated in Section 4.3.2, a load on hands only affects energy expenditure rate and does not interfere with joint discomfort. Consequently, the trend of optimum hip displacement leads to a recommendation of a squat posture based on the reduced total joint moment as well as the energy

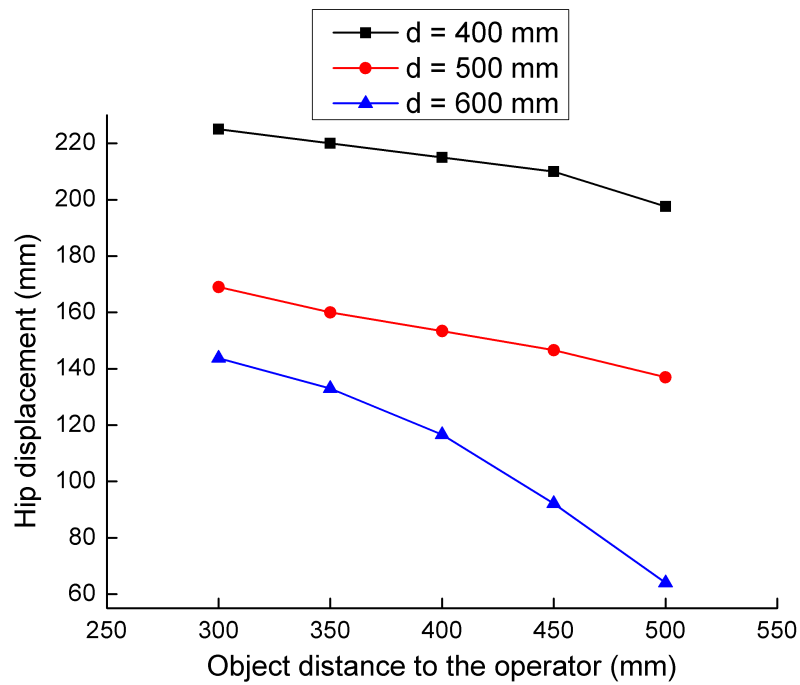


FIGURE 4.26: The effect of distance to the operator.

expenditure rate when the object weight increases.

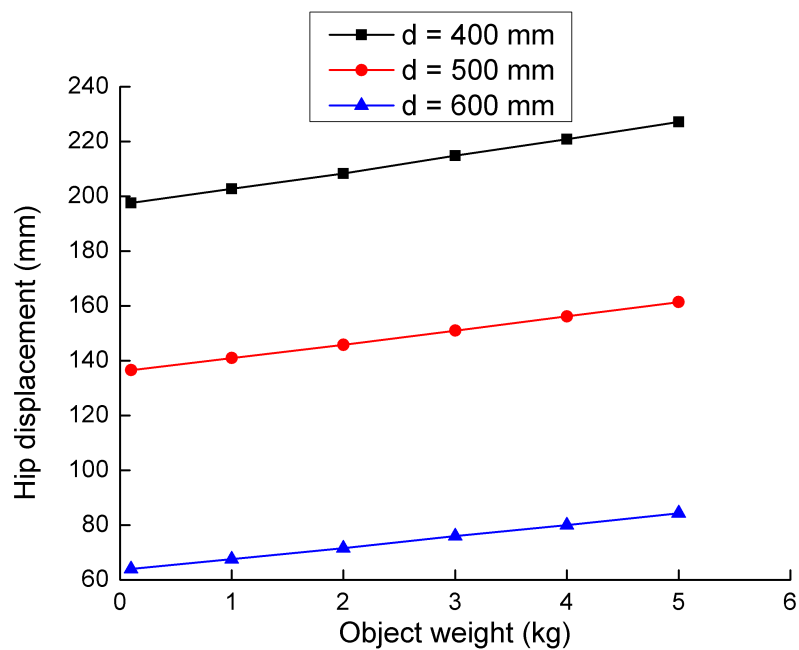


FIGURE 4.27: The effect of object weight.

4.6 Conclusions

Assembly posture modelling using multi-objective optimisation (MOO) method was achieved in this chapter in order to improve the actuality and accuracy of manual assembly simulation and analysis. A 10-DOF, 4 control-points human model associated with the assembly features was proposed and demonstrated to represent assembly postures and task constraints correctly and effectively. The proposition of 4 control points allowed a more convenient and active manipulation of human model in the virtual environment. Its advantages can be summarised as: 1) establishing new constraints readily, for example, the hand control point and eye control point are used as the equality constraints respectively for the MOO solution; 2) reducing the number of unknown variables greatly and enhancing the optimisation efficiency.

Subsequently, optimum assembly postures were predicted using the MOO method. Two main problems were considered in the posture prediction, i.e. how to model the performance measures and how to combine them together. In this chapter, the joint discomfort model based on previous work by Marler et al. evaluated joint discomfort in its rotation position associated with its comfortable neutral position and its respective rotation limits. By arranging the metabolic energy rate formula, the energy expenditure model was simplified and established as a sum of weighted joint torques and the basal metabolic rate (BMR). A weighted sum method developed by Yoon and Hwang was applied for multi-objective combination. It was capable of assigning weight to each objective function automatically without a priori knowledge about its relative importance. The procedure of assembly posture prediction using the MOO method was verified via experiments in the Virtual Engineering Centre. The results have shown a high consistence on predicted postures and those captured from real operators. After verification, a series of assembly posture analysis was conducted in terms of different assembly constraints and conditions.

Stoop and squat postures had been studied widely in manual lifting tasks in order to reduce work related injuries and increase work efficiency [143–147]. In these studies, Garg suggested that the squat posture was superior to the stoop posture when the load to be lifted was close to the operator [143]. Park showed that the stoop posture was more favourable than the squat posture for loads greater than 5 kg [144]. Compared with manual lifting, manual assembly has higher demands on object positions (i.e. visual demands) which are summarised

and formulated in this research. When constrained by certain visual requirements, there is a trade-off between the squat posture and the stoop posture. In order to minimise joint discomfort and metabolic energy expenditure, the MOO method was applied to predict optimum squat depths for varying operators from 5th percentile to 95th percentile and the results indicate a preference of adopting squat postures for taller operators.

Analyses in Chapter 3 revealed that the height of assembly object from the floor, the distance to the operator and the weight played significant roles to the assembly postures. Assembly posture strategies for varying object heights, distances and weights were investigated under certain visual constraints. The results show that in order to reduce joint discomfort and energy expenditure, a squat posture is recommended when assembling 1) objects in lower positions, 2) objects which are closer to the operator, and 3) heavier objects (less than 5 kg).

Chapter 5

Ergonomic Evaluation of Assembly Sequence

5.1 Introduction

Assembly sequencing plays a key role in the strategic and operational aspects of integrative product design and production planning. Any delays in or modifications to assembly sequence planning after the completion of product design could lead to costly changes for rectification.

It is notable that in the past two decades, research in computer-aided assembly sequencing and planning has increased significantly. Advances have been made in both theory and practice of assembly sequencing as demonstrated by the emergence of new assembly planning systems [80–82, 86, 87]. However, such systems were mainly developed for automatic assembly. Ergonomic requirements for manual assembly are normally neglected or even violated in the system design. For instance, the visibility of the product and its components in the assembly environment and the accessibility of operator's hands when performing assembly tasks, which are crucial to the assembly efficiency, product quality and operator well-being, are not always fulfilled.

DELMIA presents the basic vision analysis and hand access analysis functionalities as described in Chapter 3. In the vision analysis, the manikin's field of view is provided through a vision window when its position and posture in the virtual assembly environment are determined; in the hand access analysis, the clearance between the manikin's hand and obstructed assembly objects is detected. However, they are both lack of necessary evaluations regarding the

analysis results and hence leave ambiguous decisions to the analyst.

In this chapter, high-level consideration of the ergonomic requirements in the manual assembly process will be integrated into the assembly sequence planning. In sections 5.2, 5.3 and 5.4, several types of assembly sequences, assembly planning descriptions and representations of assembly sequences are described. Thus a general procedure to create all feasible assembly sequences can be set up and represented in Section 5.6, which only obeys the constraint arising strictly from the geometry of the assembly product itself. In Section 5.7, new ergonomic constraints considering assembly workstation layout, operator characteristics and working posture are proposed for objective evaluation and selection of manual assembly sequences, which consist of visibility criterion, accessibility criterion and both. Finally, a system called Liverpool Assembly Sequence Planning (LASP) is developed to achieve the integration by utilising different evaluation criteria. With LASP, optimum assembly sequences with the maximum viability and/or accessibility score are obtainable during the design stage and an illustrative case study of an air conditioner assembly is also presented in Section 5.8.

5.2 Type of Assembly Sequences

An assembly sequence τ can be divided into a set of assembly operations $\{\tau_1, \dots, \tau_n\}$. This representation allows additional restrictions to be placed on the operation τ_i , thereby defining types of assembly sequences. Several such types will be considered below, including binary, monotone and linear assembly sequences. Much of the terminology is taken from Wolter [86] and Wilson [79].

5.2.1 Number of Hands

Let τ_i be an operation in an assembly sequence of product P . A moved set of τ_i is a maximal set of parts S that the relative positions of parts in S stay constant during τ_i . The moved sets of any operation are a partition of the parts of the product. An operation τ_i is *m-handed* if there are m moved sets of τ_i . An assembly sequence is *m-handed* if it can be divided into *m-handed* operations. For example, if a single subassembly is being removed from the rest of the product, then two hands are required: one for moving subassembly, and one for the fixed subassembly.

A two-handed assembly sequence (i.e. no operation requires three or more subassemblies to move in different directions simultaneously) is also called **binary**. As most products can be built with two hands, all assembly planners to date have restricted to binary assembly sequences.

5.2.2 Monotonicity

The number of hands required is only one aspect of the difficulty to generate an assembly sequence. Another is the number of intermediate positions that parts may take before they are placed in their goal positions. An assembly sequence is **monotone** if each operation requiring m hands joints m subassemblies to make a larger subassembly. In other words, a monotone sequence consists of operations placing parts into their final positions relative to each other. An operation, once constructed, is final and can not be modified by subsequent operations. For example, a latch assembly in Figure 5.1 can not be built within a monotone sequence, because the inner rectangle must be temporarily inserted fully onto the left part so that the right part can be inserted and can only then be moved to its goal position [148].

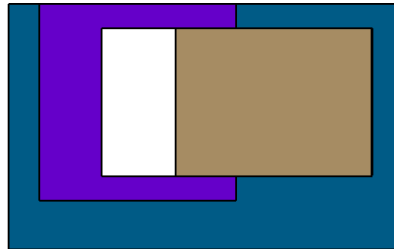


FIGURE 5.1: An example of no monotone binary assembly sequence [148].

In a monotone binary sequence, each operation brings exactly two subassemblies together; hence the monotone binary sequence consists of $n - 1$ operations.

5.2.3 Linearity

Further restrictions on assembly sequences are possible to simplify the assembly sequencing problem. One that is imposed by several assembly planning systems is linearity [86, 88]. A binary assembly sequence is **linear** if one of the two moved sets of each operation is a single part. Hence the linear monotone sequence consists of $n - 1$ operations, each mating a single part with a

subassembly. Figure 5.2 shows a monotone binary assembly with no linear assembly sequence [148]. Under the linear assumption, a disassembly planner only considers removing single parts, instead of identifying removable subassemblies. This simplifies the planning process considerable and allows additional optimisation, as will be discussed in Section 5.7.

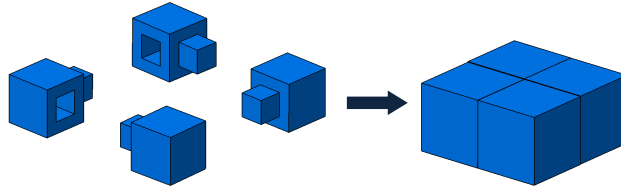


FIGURE 5.2: An example of no linear assembly sequence [148].

5.3 Assembly Planning Description

5.3.1 Local Motion

A **local motion** is an arbitrarily infinitesimal motion of a part. The local motions of a part at a given position in space form a 6-dimensional vector space [79]. For instance, a local motion $\Delta\mathbf{X}$ can be described as a 6-vector with three degrees of translation and three of rotation:

$$\Delta\mathbf{X} = (\Delta\mathbf{x}, \Delta\mathbf{y}, \Delta\mathbf{z}, \Delta\alpha, \Delta\beta, \Delta\gamma) \quad (5.1)$$

where $\Delta\alpha$, $\Delta\beta$ and $\Delta\gamma$ are the rotational components of $\Delta\mathbf{X}$ around the X , Y , and Z axes, respectively. If $\Delta\mathbf{X}$ only consists of a single motion it is called **one-step motion** and if the rotation is null, it is called a **one-step translation**.

The **local freedom** of a part p_1 with respect to a part p_2 is the set of local motions $\Delta\mathbf{X}$ in which the part p_1 can undergo a motion in $\Delta\mathbf{X}$ without interfering with p_2 .

5.3.2 Global Motion

A **global motion** is an infinite motion of a part. The globally valid translations to remove a part p_1 from a product P constitute the **global translational freedom** of p_1 with respect to its complement $S = P - p_1$. The global translational freedom

G is the set of directions in which p_1 can translate infinitely without intersecting S .

5.3.3 Sweeping

A procedure to calculate G efficiently and accurately is sweeping. A locally free part p_1 is swept along its local free directions, from its current position to infinity. If any directions is free of collisions with the rest of the product S , it constitutes a valid removal path for p_1 . During the procedure, the faces of the part p_1 will be compared pairwise with faces of S . If the two faces intersect when projected onto the plane perpendicular to the vector of translation, and the face being swept is behind the interfering face at one or more of intersection points, a collision is detected and the motion is infeasible. Figure 5.3 shows a sweeping procedure for a red part [88]. The faces of the red part are compared pairwise with the faces of the green part and two faces intersect on a plane when projecting them along the arrow's direction. Because the red face being swept is behind the green face in the arrow's direction, a collision exists and therefore the red part is globally constrained.

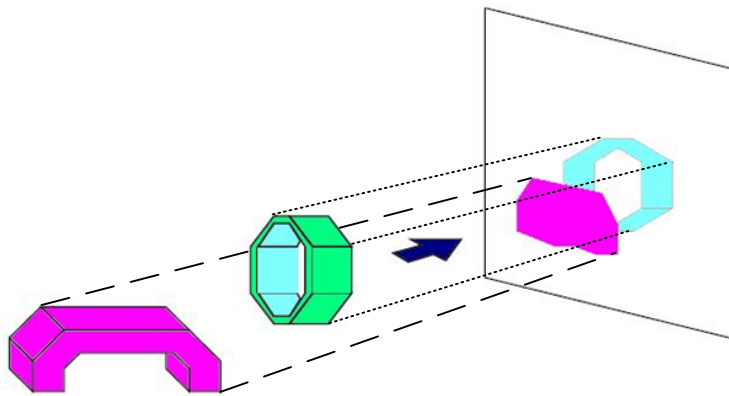


FIGURE 5.3: An example of sweeping [88].

5.4 Representations of Assembly Sequences

In an assembly sequencing system, the choice of representation for assembly sequences can be crucial. One representation is a textual statement of precedence relation, expressed as ordering constraints on liaisons, for example, a precedence relation for the product as shown in Figure 2.6 would be “ $C > B > A$ ”; the

symbol “>” means “before”. However, a product normally contains thousands of feasible sequences which could not be enumerated by this method. Attempts have been made to create more compact representations, for example, the state graphs and AND/OR graphs, which will be described separately in this section.

5.4.1 State Graphs

State graphs can be adopted easily to represent assembly sequences, in which a state is defined in terms of salient features in the assembly process, for instance, the positions of parts at the end of the operations. An assembly operation is represented by an arc in the graph from one state to another. Any path through the graph from the unassembled state to the assembled state represents an assembly sequence.

Liaison sequence diagram developed by Bourjault is an application of state graphs in the assembly sequence representation [10]. The state of an assembly is defined based on the liaisons which have been established thus far in an assembly sequence: the state with no liaisons established is the unassembled state, and the state with all liaisons established is the assembled state. An assembly operation mating two subassemblies is represented by a line from one liaison state to another. A path from the unassembled state to the assembled state represents a set of feasible sequences. The representation is applied to a simple 4-part product as shown in Figure 5.4 [10]. Arrows on the product indicate the assembly directions for part *B* relative to parts *A* and *C*, and for parts *A* and *C* relative to part *D*. The figure also shows the liaison diagram which replaces the parts with dots and the connections between parts with lines. The liaison sequence diagram for Figure 5.4 is shown in Figure 5.5. Each row contains one or more state elements containing empty or filled-in cells: empty cells indicate liaisons that have not been done, while filled-in cells indicate completed liaisons. Therefore the first row of the diagram containing empty cells represents an unassembled state with no liaisons established, and the final row containing filled-in cells represents an assembled state with all liaisons established. Each line between states is an operation, during which one or more liaisons are done. A path from the top state (no liaisons done) to the bottom state (all liaisons done) is a feasible liaison sequence. This diagram expresses two feasible sequences.

State graphs require a large amount of storage in some cases. For instance, in a liaison sequence diagram, each liaison is either established or not in any one

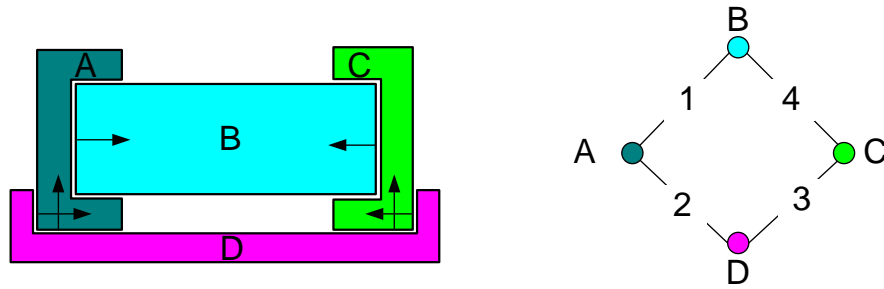


FIGURE 5.4: A simple product and its liaison diagram [10].

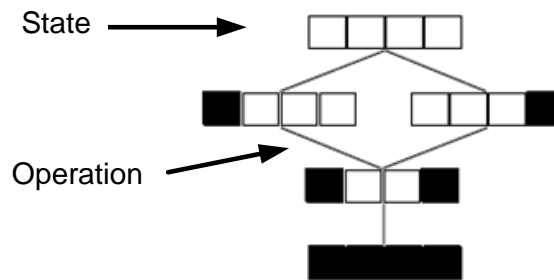


FIGURE 5.5: The liaison sequence diagram for the example product [10].

state, yielding a maximum of 2^m states for m liaisons. For representations in which assembly state features take continuous values, the state graph is obviously infinite.

5.4.2 AND/OR Graphs

To represent all feasible assembly sequences, Homen de Mello and Sanderson first introduced the AND/OR graph in assembly planning [149]. In general, an AND/OR graph is defined as a directed graph in which each node represents the product or its possible subassemblies/parts and each arc represents technically feasible disassembly operations. Here, the arcs emanating from the same node are either in an AND relation or an OR relation with each other. That is, two arcs are related by an AND relation if and only if an assembly can be disassembled by a single operation into two corresponding subassemblies, while a set of AND-arcs are related by an OR relation if and only if it is possible to disassemble an assembly into several other decompositions. Figure 5.6 shows an example of the AND/OR graph for a simple 3-part product [10].

Unlike the state graph, the AND/OR graph provides a compact representation of all feasible assembly sequences. Moreover, it is capable of

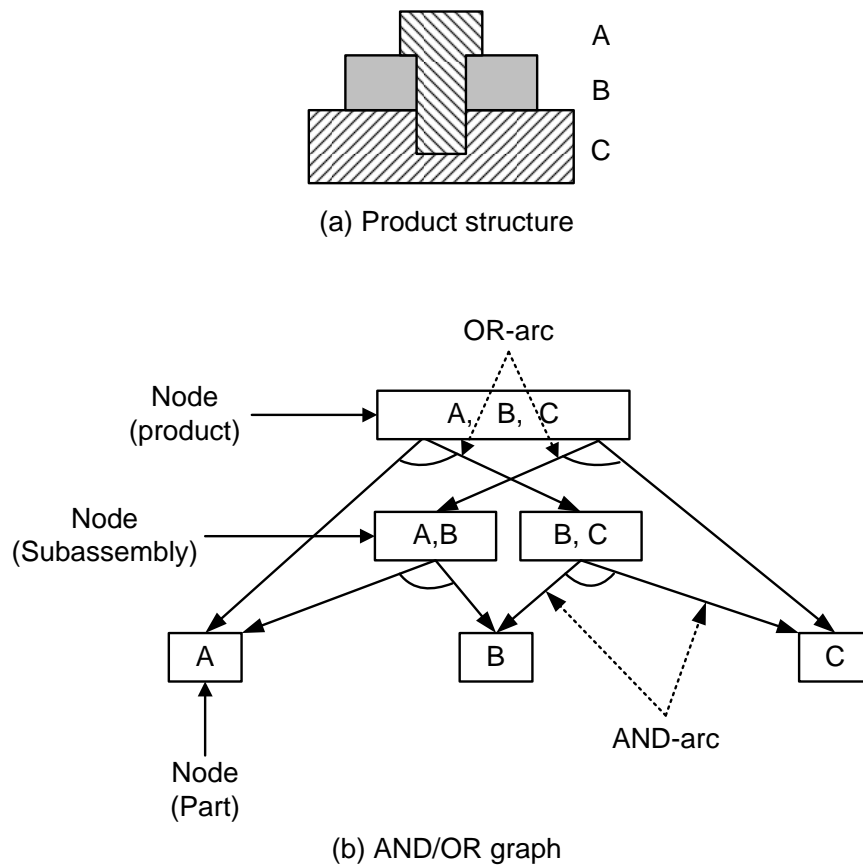


FIGURE 5.6: An example of the AND/OR graph [10].

displaying the possibility of parallel execution of assembly operations explicitly. Consequently it is adopted to represent sets of assembly sequences in Section 5.7.

5.5 Assumptions

The following assumptions hold in the chapter for a simplified assembly planning problem:

- All assembly sequences generated are binary, monotone, and linear.
- Parts are modelled as purely geometric objects: they are rigid and their positions have no tolerance. In addition, it is assumed that parts can maintain stability without any external assistance.
- Only one-step translation is considered.

5.6 Generation of all Feasible Assembly Sequences

Figure 5.7 shows a general procedure for generating assembly/disassembly sequences, starting from a completed product and working backwards through disassembly steps. Due to the assumptions of parts being rigid and non-tolerance, the disassembly sequences can then be reversed to produce the assembly sequences. The main steps in Figure 5.7 are briefly described as follows:

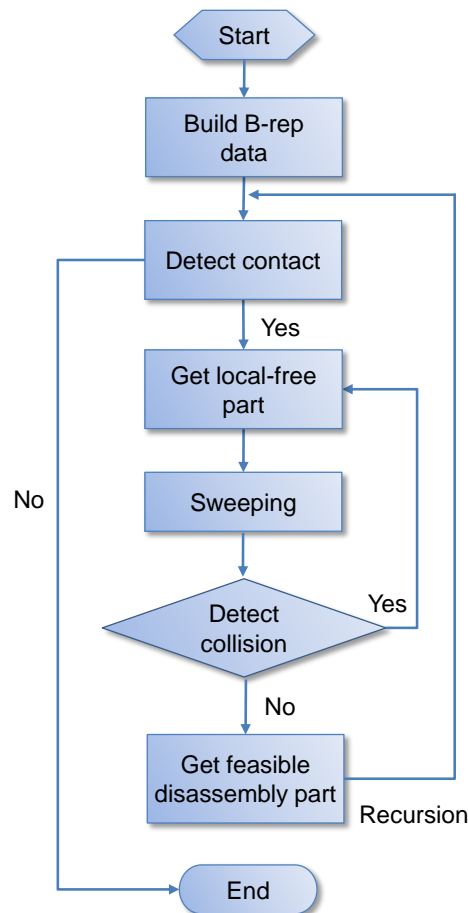


FIGURE 5.7: The procedure for generating feasible assembly/disassembly sequences.

Step 1: B-rep modelling.

Each assembly part of a product is modelled by boundary presentation method. Its geometry and topology data is stored into a file; associated with each is a homogeneous transformation matrix which specifies its final position in the world coordinate system. This is prepared for the contact detection, freedom analysis

and coordinate transformation.

Step 2: contact detection.

B-rep data of parts is taken to detect contact. Given any part p_i in product P , a function $Contacts(p_i)$ finds a set of parts in contact with p_i and returns a set of directions perpendicular to the contact surface, pointing outwards p_i .

The approach to detect contact taken from Lin and Canny is fairly simple based on part geometry descriptions: the shortest distance between each pair of parts is calculated and if it is 0.0, the pair of parts is marked as being in contact [150].

Step 3: local freedom analysis.

Local free directions of any part p_i in product P can be found after contact detection. For simplification, only 6 principal directions in Cartesian coordinate system are computed, which are defined as the set of directions $\mathbf{D} = \{\mathbf{d}_1, \mathbf{d}_2, \dots, \mathbf{d}_6\}$, where $\mathbf{d}_1, \mathbf{d}_2, \dots, \mathbf{d}_6$ represent $+X, -X, +Y, -Y, +Z$ and $-Z$ respectively. p_i is local free when satisfy Eq.(5.2):

$$\sum_{k=1}^6 \prod_{i \neq j}^n I_{p_i p_j}^{\mathbf{d}_k} \neq 0 \quad i = 1, 2, \dots, n \quad (5.2)$$

where:

$$I_{p_i p_j}^{\mathbf{d}_k} = \begin{cases} 0 & \text{if } p_i \text{ is constraint by } p_j \text{ along direction } \mathbf{d}_k \\ 1 & \text{if } p_i \text{ is not constraint by } p_j \text{ along direction } \mathbf{d}_k \end{cases} \quad (5.3)$$

And its removable directions can be returned by the set of directions $\mathbf{D}_r(p_i) = \{\mathbf{d}_k | I_{p_i p_j}^{\mathbf{d}_k} = 1\}$

Step 3: global freedom analysis.

By sweeping local free parts along their removable directions, global collision can be detected. If part p_i does not interfere with any other parts along that direction, it is included in the set of feasible disassembly parts D in the current state; otherwise, try another removable direction or another part.

Step 4: recursion.

Update product $P = P - d, d \in D$ and repeat from **Step 2** until P is empty.

Once the set of feasible disassembly parts D in each state is available, different evaluation criteria can be applied to select the optimum one out of D . This is discussed in the next section.

5.7 Criteria of Manual Assembly Sequence Evaluation

5.7.1 Visibility

In the manual assembly process, the visibility of a product and its components is determined by many factors in the assembly environment, i.e. the product's position and orientation in the workstation, the operator's anthropometric characteristics and working posture, etc. In order to quantify their influence on the visibility for the assembly process, a digital operator and workstation model is set up. The digital operator represented by DELMIA digital human model is shown in Figure 5.8 where a specific concern is given to the configuration of the main body and the head, characterised by three posture variables (α, β, γ) describing the flexibility of the joint between the main body and the head. For the comfort analysis of any adopted posture, range limits of the variables as well as the preferred ranges are provided in the model. Table 5.1 shows the anthropometric variables of a 50 percentile UK male which is defined as a standard digital operator in the assembly process. Workstation data includes the workbench height, the horizontal distance between the workbench and the operator, and the product layout (position and orientation) on the workbench.

TABLE 5.1: Anthropometric variables

Variable	Description	Mean/range	Referred value
S	Stature	1740mm	—
h	Head length	195 mm	—
h_e	Vertical distance between the eye and the top of the head	110mm	—
α	Flexion/extension	$-20^\circ/24^\circ$	$0^\circ/10^\circ$
β	Lateral left/lateral right	$-20^\circ/20^\circ$	$-5^\circ/5^\circ$
γ	Rotation right/rotation left	$-75^\circ/75^\circ$	$-38^\circ/38^\circ$

Next, a view coordinate system is set up for product rendering, which would consist of the following:



FIGURE 5.8: Properties of digital operator for the visibility evaluation.

- a viewpoint \mathbf{C} , which defines the viewer's position in world space; this can be either the origin of the view coordinate system or the centre of projection together with a view direction \mathbf{N} ;
- a view coordinate system defined with respect to the viewpoint;
- a view plane onto which the two-dimensional image of the scene is projected.

These entities are depicted in Figure 5.9.

The operator is the viewer in the assembly process and a view coordinate system is therefore established at the operator's eyes, which is determined by the anthropometric variables and the workstation data. Supposing the origin \mathbf{C} of the view coordinate system is the projection of the midpoint between two inner corners of operator eyes to the coronal plane and \mathbf{U} axis is perpendicular to the sagittal plane as shown in Figure 5.10, the viewing direction \mathbf{N} and \mathbf{V} axis is given by Eq.(5.4), where \mathbf{P} is a 'look at' point on the product.

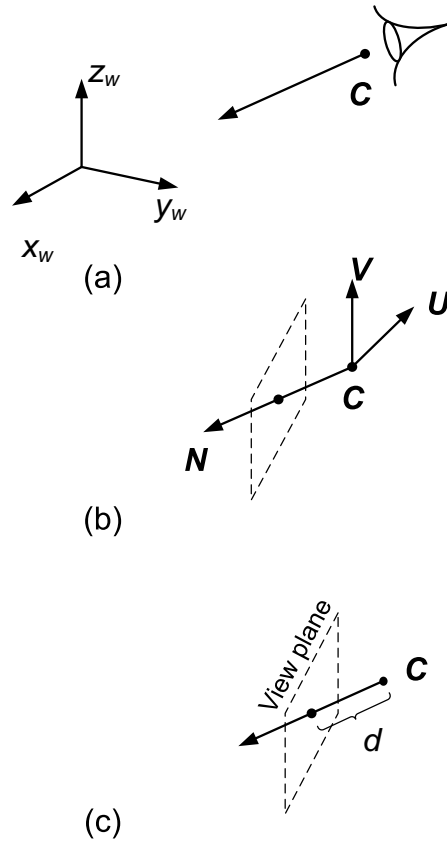


FIGURE 5.9: Minimum entities required in a viewing system.

$$\begin{aligned} N &= P - C \\ V &= N \times U \end{aligned} \tag{5.4}$$

Subsequently, any point of the product in the world coordinate system can be transformed into the view coordinate system by Eq.(5.5).

$$\begin{bmatrix} x_v \\ y_v \\ z_v \\ 1 \end{bmatrix} = T_{\text{view}} \begin{bmatrix} x_w \\ y_w \\ z_w \\ 1 \end{bmatrix} \tag{5.5}$$

where:

$$T_{\text{view}} = RT \tag{5.6}$$

and:

$$\mathbf{R} = \begin{bmatrix} U_x & U_y & U_z & 0 \\ V_x & V_y & V_z & 0 \\ N_x & N_y & N_z & 0 \\ 0 & 0 & 0 & 1 \end{bmatrix} \quad \mathbf{T} = \begin{bmatrix} 1 & 0 & 0 & C_x \\ 0 & 1 & 0 & C_y \\ 0 & 0 & 1 & C_z \\ 0 & 0 & 0 & 1 \end{bmatrix} \quad (5.7)$$

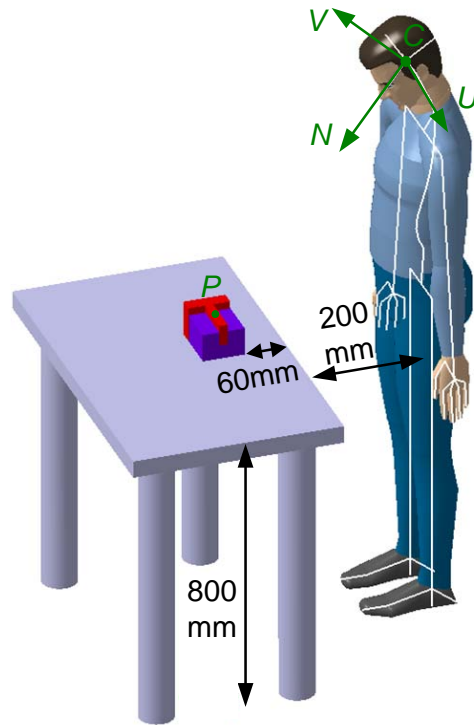


FIGURE 5.10: The determination of a view coordinate system in the assembly process.

Once the transformation of the product to the view coordinate system is finished, a planar geometric projection follows in order to render the product in a two-dimensional plane. It basically consists of parallel projection and perspective projection. Their difference is illustrated in Figure 5.11. Compared with the parallel projection, the perspective projection incorporates foreshortening: a distant line is displayed smaller than a nearer line of the same length. This enables the depth data can be perceived in the two-dimensional plane and more closely simulates the three dimensional reality through an operator's vision. Hence the perspective projection is adopted.

Figure 5.12 illustrates how a perspective projection is derived. Point $\mathbf{P}_v(x_v, y_v, z_v)$ is a three-dimensional point in the view coordinate system. This point is projected onto a view plane normal to the z_v axis and positioned at a

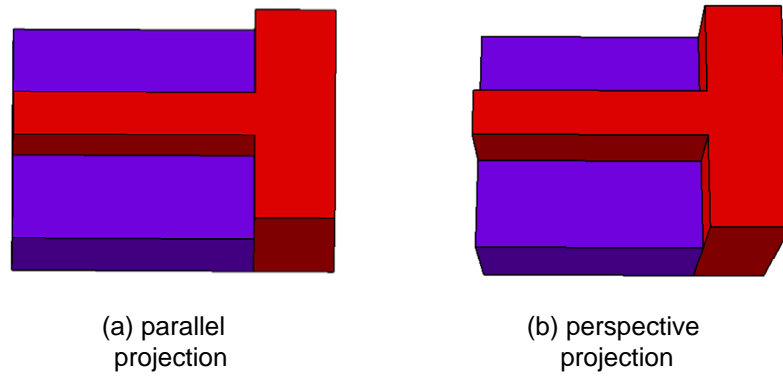


FIGURE 5.11: A comparison between the parallel projection and the perspective projection.

distance d from the origin of the system. Point \mathbf{P}'_v is the projection of \mathbf{P}_v in the view plane and has two-dimensional coordinates (x_s, y_s) in a view plane coordinate system with origin at the intersection of the z_v axis and the view plane.

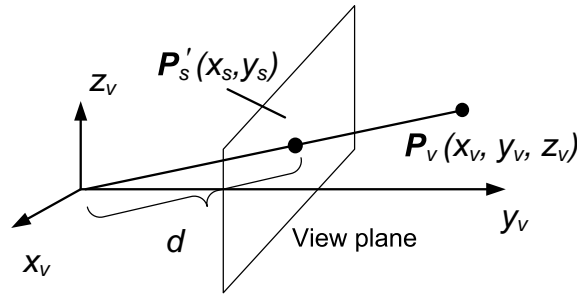


FIGURE 5.12: Deriving a perspective transformation.

x_s and y_s are given by:

$$x_s = d \frac{x_v}{z_v} \quad y_s = d \frac{y_v}{z_v} \quad (5.8)$$

It is important to note that the depth data z_v corresponding to each point \mathbf{P}'_v is stored as well which would be further used for the visible area calculation.

In this research, a new ergonomic constraint is proposed to investigate the visibility of the set of disassembly parts and potential subassemblies quantitatively. Essentially, it is concerned with two principles:

- First, disassembly parts should be visible. Empirically the percentage that is visible of a disassembly part is set to be at least 50% [96].
- Additionally, subassemblies' visibility should be improved after removal of the current part.

Given two sets of parts P and Q , a function $Area(P)$ calculates the visible area of P and another function $Area(P, Q)$ calculates the visible area of P with respect to Q . According to the description in Section 5.6, the set of feasible disassembly parts D is obtained. For any $d \in D$, its visibility percentage with respect of the subassemblies in the current state is given by Eq.(5.9):

$$Vis(d, R) = \frac{Area(d, R)}{Area(d)} \quad (5.9)$$

where: R is the set of remaining parts in the product P and $R = P - d$. With part being removed, its contribution to the visibility improvement of the subassemblies is given in Eq.(5.10):

$$Vis(R, d) = \frac{Area(R)}{Area(R, d)} \quad (5.10)$$

Therefore, a search considering each $d \in D$ is conducted in order to return the best d_v which satisfies the following conditions:

$$\begin{aligned} Vis(d_v, R) &\geq 0.5 \\ Vis(R, d_v) &\geq 1.0 \\ Score(d_v) &= \max_{d \in D} (Vis(d, R) + Vis(R, d)) \end{aligned} \quad (5.11)$$

where: $Score(d_v)$ is the total visibility score of d .

The following describes a visibility evaluation process using a simple model. As shown in Figure 5.10, the product is aligned with operator whose working posture is defined by $\{\alpha = 20^\circ, \beta = \gamma = 0^\circ\}$. Figure 5.13 (a) renders the product through the operator's eyes. Obviously, part A and part B are currently removable.

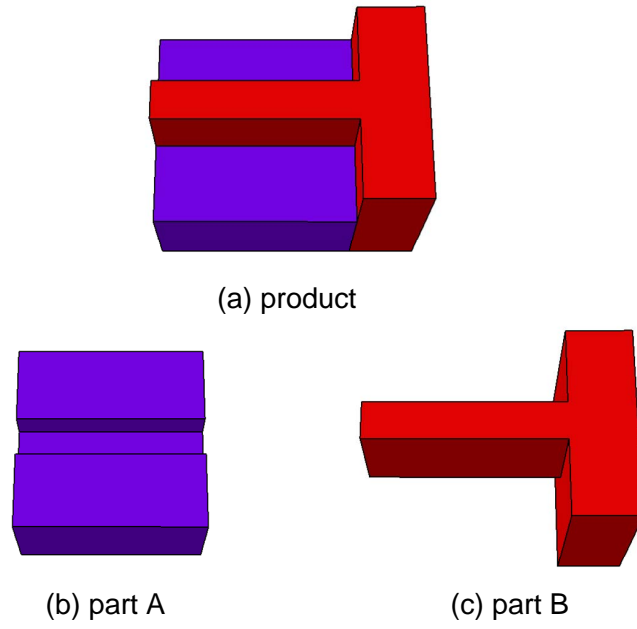


FIGURE 5.13: A product for the visibility evaluation.

Considering $d_i = A$, $R = P - d_i = P - A = B$, then calculate:

$$Vis(d_i, R) = Vis(A, B) = \frac{Area(A,B)}{Area(A)} = 0.7743 > 0.5$$

$$Vis(R, d_i) = Vis(B, A) = \frac{Area(B)}{Area(B,A)} = 1.0849 > 1.0$$

$$Score(A) = 0.7743 + 1.0849 = 1.8592$$

Considering $d_i = B$, $R = P - d_i = P - B = A$, then calculate:

$$Vis(d_i, R) = Vis(B, A) = \frac{Area(B,A)}{Area(B)} = 0.9217 > 0.5$$

$$Vis(R, d_i) = Vis(A, B) = \frac{Area(A)}{Area(A,B)} = 1.2915 > 1.0$$

$$Score(B) = 0.9217 + 1.2915 = 2.2132$$

It is obvious that based on the visibility criterion, part B is disassembled firstly.

calculations for function $Area(P)$ and function $Area(P, Q)$ refer to one of the most difficult problems in computer graphics, i.e., the hidden line/hidden surface removal problem, which results in a large number of diverse solutions [151–154].

The hidden line/hidden surface removal algorithm, which attempts to determine the lines/surfaces which are visible or invisible to a specific viewpoint in space, can be classified into the object space algorithm and the image space algorithm. The object space algorithm is implemented in the physical coordinate system in which the objects are described. Very precise results, generally to the precision of the computer, are available. The image space algorithm is implemented in the screen coordinate system in which the objects are output. Calculations are performed only to the precision of screen representation, typically 512×512 integer points. Furthermore, the computational work for an object space algorithm comparing every object in a scene with every other object in the scene grows as the number of objects squared (n^2). Similarly, the work for an image space algorithm which compares every object in the scene with every pixel location in screen grows as nN . Here, n is the number of objects in the scene, and N is the number of pixels. Theoretically, the object space algorithm requires less work than the image space algorithm for $n < N$. Due to the higher calculating precision and efficiency, the object space algorithm is chosen in this research.

As one of the object space algorithms, the Weiler-Atherton algorithm is applied whose output polygons can be used easily for hidden line as well as hidden surface elimination [153]. Generally, this algorithm involves four steps:

1. A preliminary depth sort.
2. A clip or polygon area sort based on the polygon nearest the viewpoint.
3. Removal of the polygons behind that nearest the viewpoint.
4. Recursive subdivision if required and a final depth sort to remove any ambiguities.

Firstly, an approximate depth priority list is established using a preliminary depth sort according to value of z_v , the distance of the polygon from the viewpoint. The first polygon on the list is the one with the minimum value of z_v (z_{vmin}). A copy of the first polygon on the preliminary depth-sorted list is used as the clip polygon. The remaining polygons on the list, including the first polygon, are subject polygons. Two lists are established: an inside list and an outside list. Using the Weiler-Atherton clipping algorithm, each of the subject polygons is clipped against the clip polygon. The portion of each subject polygon inside the clip polygon, if any, is placed on the inside list. The portion

outside the clip polygon, if any, is placed on the outside list. If none of the z_v coordinate values of the subject polygons on the inside list is smaller than z_{vmin} , then all the subject polygons on the inside list are hidden by the clip polygon. These polygons are eliminated and the algorithm continues with the outside list.

If the z_v coordinate value for any polygon on the inside list is less than z_{vmin} , then the subject polygon on the inside list lies at least partially in front of the clip polygon. In this case, the original preliminary depth sort is in error. The algorithm recursively subdivides the areas, using the offending polygon as the new clip polygon. The inside list is used as the subject polygons. The original clip polygon is now clipped against the new clip polygon.

The Weiler-Atherton clipping algorithm is crucial for the hidden surface removal. It is capable of clipping not only a convex polygon, but also a concave polygon with interior holes. The new boundaries created by clipping the subject polygon against the clip polygon are identical to portions of the clip polygon. No new edges are created. Hence, the number of resulting polygons is minimised.

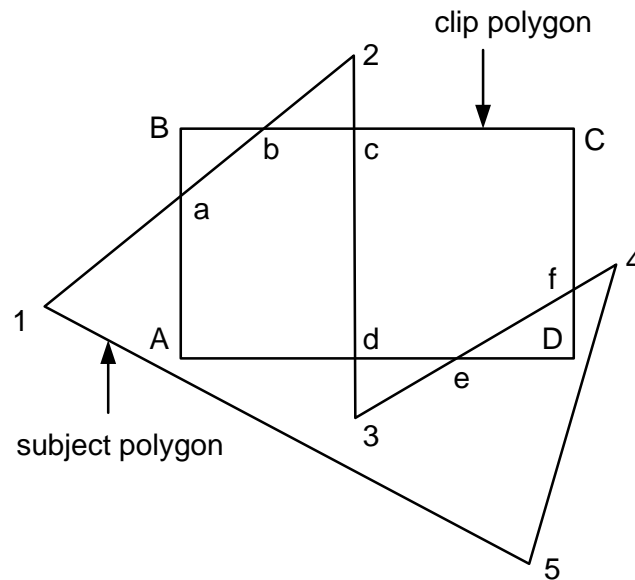
The algorithm describes both subject and clip polygons by a circular list of vertices. The exterior boundaries of the polygons are described clockwise. When traversing the vertex list, this convention ensures that the inside of the polygon is always to the right. The boundaries of the subject polygon and the clip polygon may or may not intersect. If they intersect, then the intersections occur in pairs. One of the intersections occurs when a subject polygon edge enters the inside of the clip polygon and one when it leaves. Fundamentally, the algorithm starts at an entering intersection and follows the exterior boundary of the subject polygon clockwise until an intersection with the clip polygon is found. At the intersection a right turn is made, and the exterior boundary of the clip polygon is followed clockwise until an intersection with the subject polygon is found. Again, at the intersection, a right turn is made, with the subject polygon now being followed. The process is continued until the starting point is reached.

The routine of the algorithm is described following:

S is the subject polygon vertex array; C is the clip polygon vertex array; SI is the new subject polygon vertex array with intersections; CI is the new clip polygon vertex array with intersections; the entering intersection is marked as En and the leaving intersection is marked as Lv .

1. Initialise array Q and empty it. Search the entering intersection from SI . If no entering intersection is found, the routine is determined.
2. If an entering intersection is found, put it into an array P temporarily.
3. Put the entering intersection into Q , and delete its mark.
4. Follow array SI clockwise: if no leaving intersection is found, put the vertex into Q and jump to 5; otherwise, jump to 6.
5. Follow the array CI clockwise: if no entering intersection is found, put the vertex into Q and jump to 6; otherwise, jump to 7.
6. If the vertex is not the vertex in array S , jump back to 4, continue to follow SI clockwise; otherwise, output the array Q .
7. Jump back to 1 in case of separate boundaries until no entering intersection is found.

The routine is illustrated in Figure 5.14.



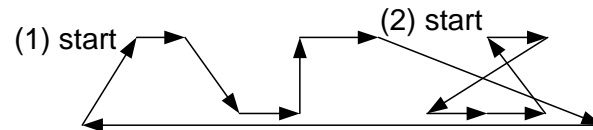
(a) subject polygon and clip polygon

S: 1 2 3 4 5

C: A B C D

		<i>En</i>	<i>Lv</i>		<i>En</i>	<i>Lv</i>		<i>En</i>	<i>Lv</i>	
--	--	-----------	-----------	--	-----------	-----------	--	-----------	-----------	--

<i>Sl</i> :	1	a	b	2	c	d	3	e	f	4	5
-------------	---	---	---	---	---	---	---	---	---	---	---



<i>Cl</i> :	A	a	B	b	c	C	f	D	e	d
		<i>En</i>		<i>Lv</i>	<i>En</i>		<i>Lv</i>		<i>En</i>	<i>Lv</i>

<i>Q</i> :	(1)	a	b	c	d	A	a
	(2)	e	f	D	e		

(b) subject polygon and clip polygon

FIGURE 5.14: Weiler-Atherton clipping.

Obviously, the hidden surface removal algorithm which deals with polygons in the view coordinate system partially or totally obscure others is complicated. In order to speed up its computation, back-face elimination is adopted. It is an operation that compares the orientation of complete polygons with the viewpoint and removes those polygons which are invisible. On average, half of the polygons in the view coordinate system are back-facing (Figure 5.15) and the advantage of the operation is distinct: a simple test can remove these polygons from the consideration of a more expensive hidden surface removal algorithm.

The test for visibility of each polygon is straightforward. The outward normal for a polygon is calculated and the dot product of the outward normal and the view direction is examined. Thus:

$$\text{visibility} = \mathbf{N}_p \bullet \mathbf{N} > 0 \quad (5.12)$$

where: \mathbf{N}_p is the polygon normal and \mathbf{N} is the view direction which has been defined by Eq. (5.4).

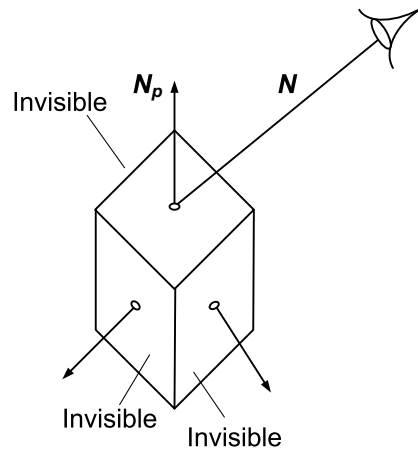


FIGURE 5.15: Back-face elimination.

Figure 5.16 shows the flowchart for visible area determination. When a visible polygon is available after clipping, its area calculation is simple which is developed by [155]. For a n -vertices polygon I , its area $Area(I)$ is:

$$Area(I) = \sum_{i=1}^n x_{s_i} (y_{s_{i+1}} - y_{s_{i-1}}) \quad (5.13)$$

For any part P , its visible area $Area(P)$ is the sum of its visible surface area:

$$Area(P) = \sum_{j=1}^k Area(I_j) \quad (5.14)$$

where k is the number of its visible surface.

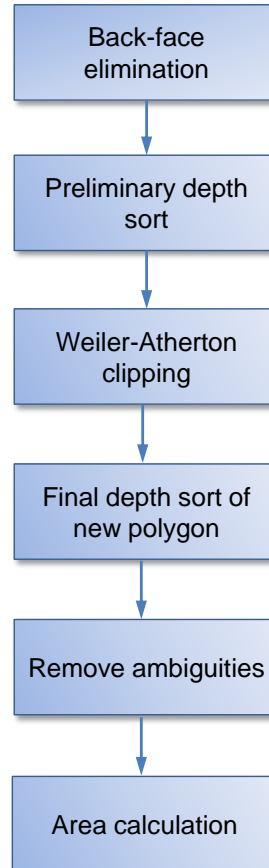


FIGURE 5.16: The flowchart for the visible area determination.

Finally, the whole procedure for assembly sequence selection based on visibility criterion is outlined in Figure 5.17.

5.7.2 Accessibility

For the hand accessibility analysis, a term **approach direction** is defined as a direction along which operator's hand can manipulate assembly parts without any obstruction. For the free approach of parts, adequate space must be given along a direction. According to anthropometric data of hands, a space of a 35 mm diameter circle in the two-dimensional plane will allow human fingers for insertion, rotation and extraction [30]. Hence, it is set as the standard circle

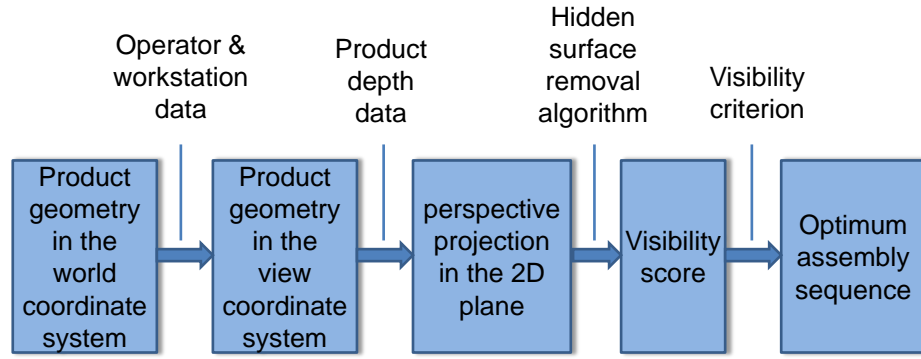


FIGURE 5.17: The procedure of assembly sequence selection based on the visibility criterion.

($Std(cir)$). Its spatial extent in a certain direction is used to determine an approach direction.

Clipping based on the Weiler-Atherton algorithm is executed to obtain the two-dimensional hand manipulation space along a specific direction. For example in Figure 5.18, parts A , B and C are three barriers to grasp part D along direction $+Z$ in the world coordinate system. The hand manipulation space of part D along direction $+Z$ is a projection polygon defined by a list of vertices p_1, p_2, \dots, p_{14} , which is a remaining portion of the red area of part D clipped by all surfaces before it. Subsequently, the determination of a clearance satisfying the ergonomic standard is transformed to determine if the final clipped polygon can encapsulate a 35 mm diameter circle.

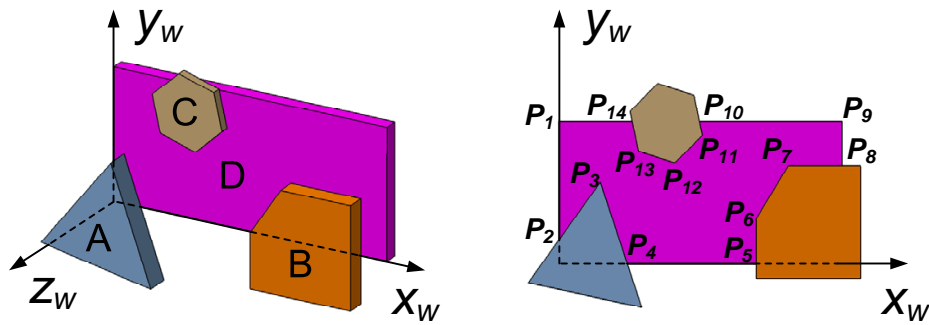


FIGURE 5.18: An example of hand manipulation space.

For simplification only 6 principal approach directions in Cartesian coordinate system are of interest. Let D_a denotes the set of approach directions as:

$$D_a = \{d_{a1}, d_{a2}, \dots, d_{a6}\} = \{d_{ak}\} \quad k = 1, 2, \dots, 6 \quad (5.15)$$

where: $\mathbf{d}_{a1}, \mathbf{d}_{a2}, \dots, \mathbf{d}_{a6}$ represent $+X, -X, +Y, -Y, +Z$ and $-Z$, respectively.

For any part p_i in product P , a mapping of the set of approach directions for p_i is defined as:

$$v(p_i) = \{v_{a1}, v_{a2}, \dots, v_{a6}\} = \{v_{ak}\} \quad k = 1, 2, \dots, 6 \quad (5.16)$$

where: $v_{a1}, v_{a2}, \dots, v_{a6}$ represent a mapping of \mathbf{d}_{ak} to determine if it is an approach direction for p_i . It is further defined as:

$$v_{ak} = \begin{cases} 1 & \text{Surface of } p_i \text{ is sorted first in direction } \mathbf{d}_{ak} \\ 1 & \text{Clipped polygon of } p_i \text{ encapsulates } Std(cir) \text{ in direction } \mathbf{d}_{ak} \\ 0 & \text{Clipped polygon of } p_i \text{ does not encapsulate } Std(cir) \text{ in direction } \mathbf{d}_{ak} \end{cases} \quad (5.17)$$

Therefore, the amount of approach directions for p_i is achieved by Eq. (5.18).

$$Num(p_i) = \sum_{k=1}^6 v_{ak}(p_i) \quad (5.18)$$

Figure 5.19 shows a flowchart to calculate the amount of approach directions. It is observed that to determine if a clipped polygon can encapsulate $Std(cir)$ in the two-dimensional plane is crucial for the approach direction calculation. A straightforward approach for the problem is to obtain the inscribed circle in the clipper polygon firstly and then to compare it with $Std(cir)$: if the diameter of the inscribed circle is greater than 35 mm (the diameter of $Std(cir)$), an approach direction is determined and vice versa. However, this approach has its limitation, i.e. it is only suitable for convex polygons [156, 157]. Due to the arbitrariness of the clipped polygons (convex or concave), a new approach is required. It is widely known that for any polygon, the centre of its inscribed circle is at the intersection of two angle bisectors. Based on this geometrical property, a powerful approach is developed to meet the requirement in this research. It is described as follows:

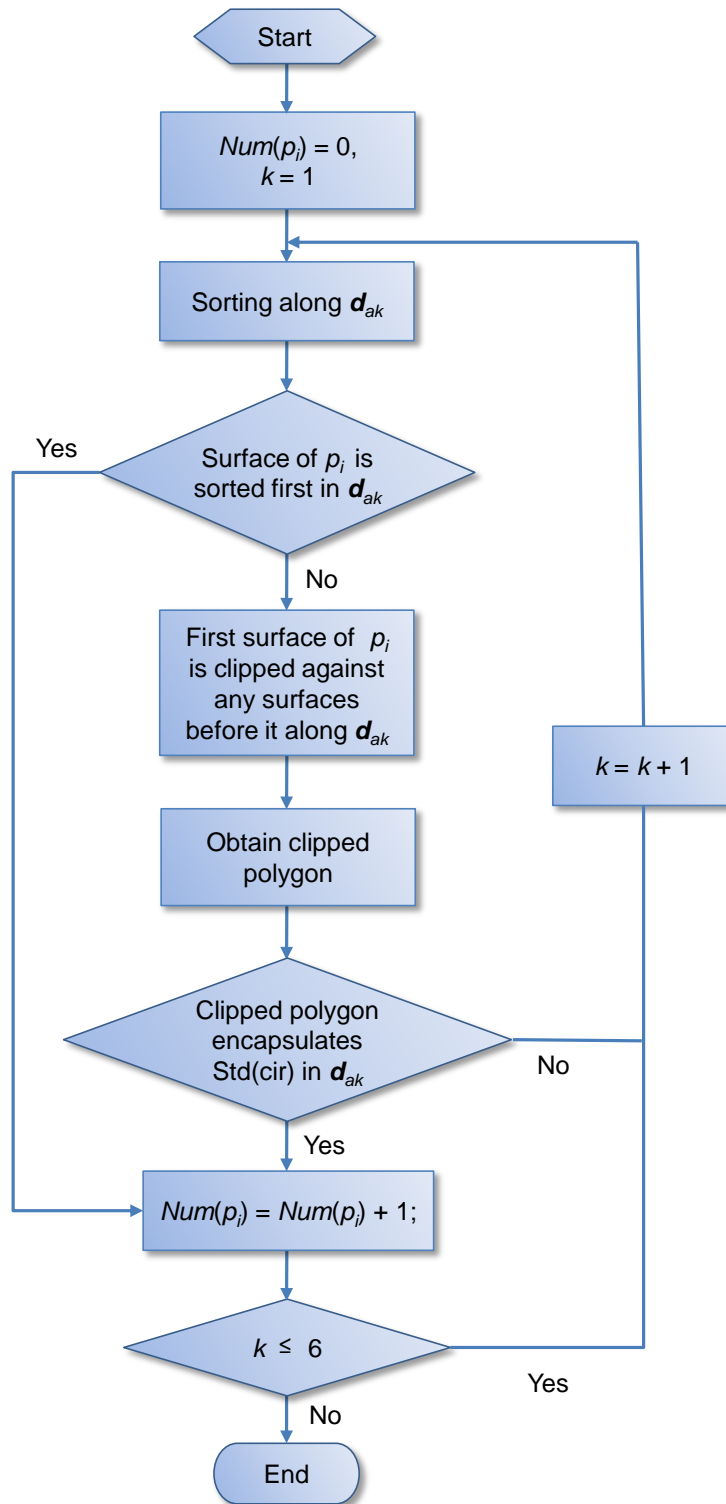


FIGURE 5.19: The flowchart to calculate the amount of approach directions.

For any n -vertices polygon, its vertex is defined as the set of points $P = \{P_1, P_2, \dots, P_n\} = \{P_i(x, y)\}$ and its edge is defined as:

$$\mathbf{E}_i(t) = \mathbf{P}_i + t\mathbf{d}_i \quad t \in [0, 1] \quad (5.19)$$

where:

$$\mathbf{d}_i = \mathbf{P}_{i+1} - \mathbf{P}_i \quad (i = 1, 2, \dots, n) \quad (5.20)$$

Therefore, any angle bisector of the polygon between the edges can be given by:

$$\mathbf{L}_i(t) = \mathbf{P}_i + t(\mathbf{d}_i + \mathbf{d}_{i+1}) \quad t \in [0, 1] \quad (5.21)$$

The intersection of the angle bisectors $(\mathbf{P}_c(x_c, y_c))$ probably be the centre of the inscribed circle is given by:

$$\begin{aligned} x_c &= \mathbf{P}_i(x) + t_c \mathbf{delt}_i(x) \\ y_c &= \mathbf{P}_i(y) + t_c \mathbf{delt}_i(y) \end{aligned} \quad (5.22)$$

where:

$$\begin{aligned} \mathbf{delt}_i &= \mathbf{d}_i + \mathbf{d}_{i+1} \\ t_c &= \frac{(\mathbf{P}_{i+1} - \mathbf{P}_i) \bullet \mathbf{delt}_i}{\mathbf{delt}_i \bullet \mathbf{delt}_{i+1}} \quad t_c \in [0, 1] \end{aligned} \quad (5.23)$$

If \mathbf{P}_c is inside the polygon, the distance (ds) from \mathbf{P}_c to every edge of the polygon is calculated. If the perpendicular from \mathbf{P}_c to the edge intersects with the edge, ds is given by:

$$ds_i = \frac{A\mathbf{P}_i(x) + B\mathbf{P}_i(y) + C}{A^2 + B^2} \quad (i = 1, 2, \dots, n) \quad (5.24)$$

where:

$$\begin{aligned} A &= -\mathbf{d}_i(y) \\ B &= -\mathbf{d}_i(x) \\ C &= \mathbf{P}_i(x)\mathbf{d}_i(y) - \mathbf{P}_i(y)\mathbf{d}_i(x) \end{aligned} \quad (5.25)$$

Else,

$$ds_i = \min \{ \|\mathbf{P}_c \mathbf{P}_i\|, \|\mathbf{P}_c \mathbf{P}_{i+1}\| \} \quad (i = 1, 2, \dots, n) \quad (5.26)$$

If $ds_i \geq 35/2$ ($i = 1, 2, \dots, n$), a circle circumscribed by the polygon whose centre is at the intersection of the angle bisectors is greater $Std(cir)$. Therefore the clipped polygon can encapsulate $Std(cir)$. However, If a circle satisfying the above inequality can not be found until all intersections of any two angle bisectors have been traversed, the polygon fails to encapsulate $Std(cir)$.

Finally, it is important to differentiate an approach direction and a disassembly direction. As shown in Figure 5.20, the operator's hand can access part A along direction $+Y$ and then exert force for manipulation and therefore, $+Y$ is an approach direction of part A. However, part A can not be disassembled along $+Y$ due to the geometrical constraint. Hence, a dissemble direction is different from an approach direction in this case.

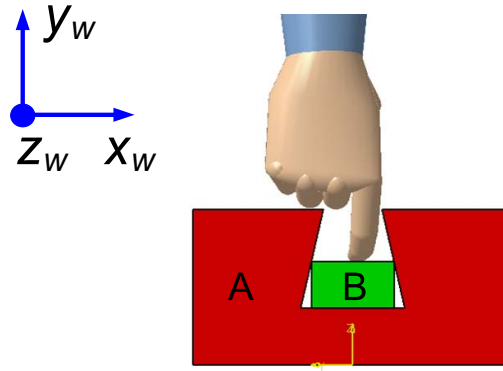


FIGURE 5.20: An illustration of the approach direction.

In this research, the accessibility criterion is proposed to evaluate disassembly sequences according to the amount of approach directions. Normally, three types of hand grasp exist as shown in Figure 5.21. It can be easily concluded that at least two surfaces/edges (planar or non-planar) of parts contact with the operator's fingers with a minimum angle θ between them for maintaining the part's balance during manual manipulation. Thus the first prerequisite for hand access is that two approach directions are demanded. Next, in order to maximise the flexibility of operator's fingers, it is preferential to remove a part with more manipulation space. For example, it is typical in a 3×3 array of blocks that the middle block is not removed first. Therefore, the accessibility criterion is formulated as Eq. 5.27 when the set of feasible disassembly parts D is available.

$$Num(d_a) \geq 2$$

$$Num(d_a) = \max_{d \in D} (Num(d)) \quad (5.27)$$

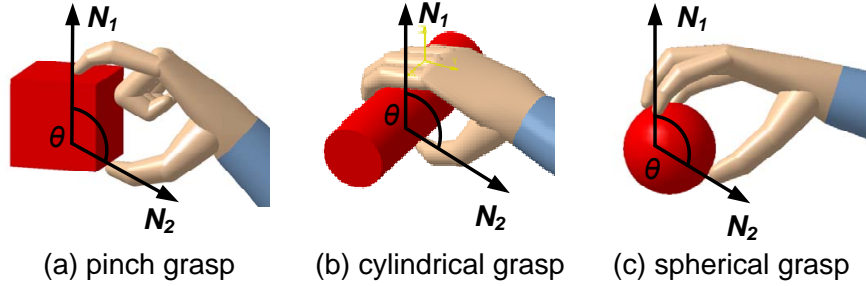


FIGURE 5.21: Three types of hand grasp.

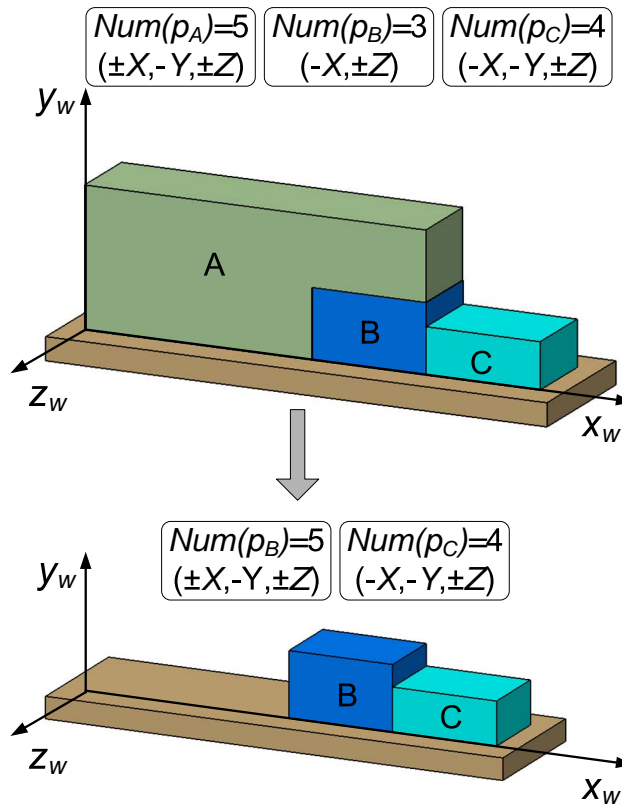


FIGURE 5.22: An example of the accessibility criterion application.

Figure 5.22 shows a simple model used to describe the accessibility criterion application in the disassembly sequence selection. Parts A , B and C are removable in the current state. The amounts of approach directions are: $Num(d_A) = 5$, $Num(d_B) = 3$, $Num(d_C) = 4$. Therefore, part A is chosen to disassemble firstly. Next, the amounts of approach directions for parts B and C

are updated in the new state and calculate as: $Num(d_B) = 5, Num(d_C) = 4$. As a result part B is disassembled. The sequence to disassemble the product based on the accessibility criterion is from left to right.

5.7.3 Combination of Visibility and Accessibility

After visibility and accessibility investigation, the rank of feasible disassembly part in every state is generated. If the value is set equal to its rank in the current state, then the final value combining visibility and accessibility is the sum of visibility rank and accessibility rank. The part with the minimum value is selected which gives the best condition with visibility and accessibility considerations.

5.8 A Manual Assembly Sequence Planning System

5.8.1 System Description

A Liverpool Assembly Sequence Planning (LASP) system has been developed to embed the high-level ergonomic consideration (i.e. visibility and accessibility) in the early stage of product design. Figure 5.23 schematically shows the framework of the system.

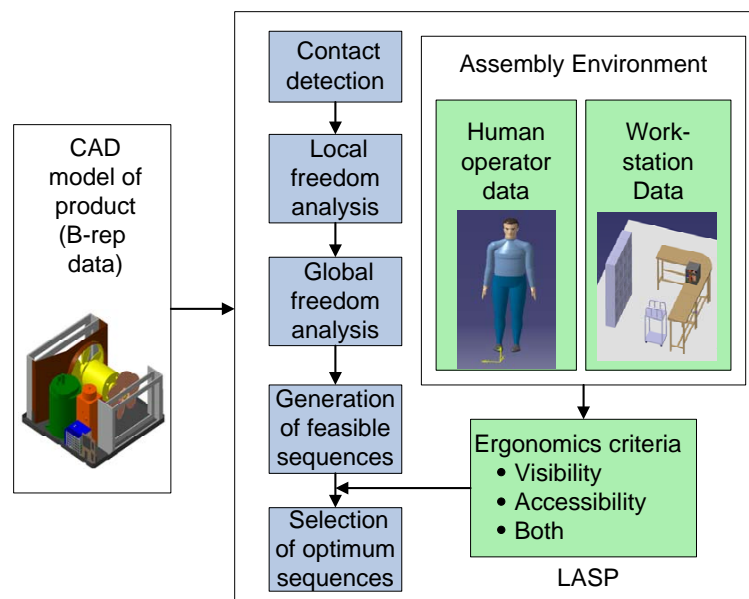


FIGURE 5.23: The framework of LASP system.

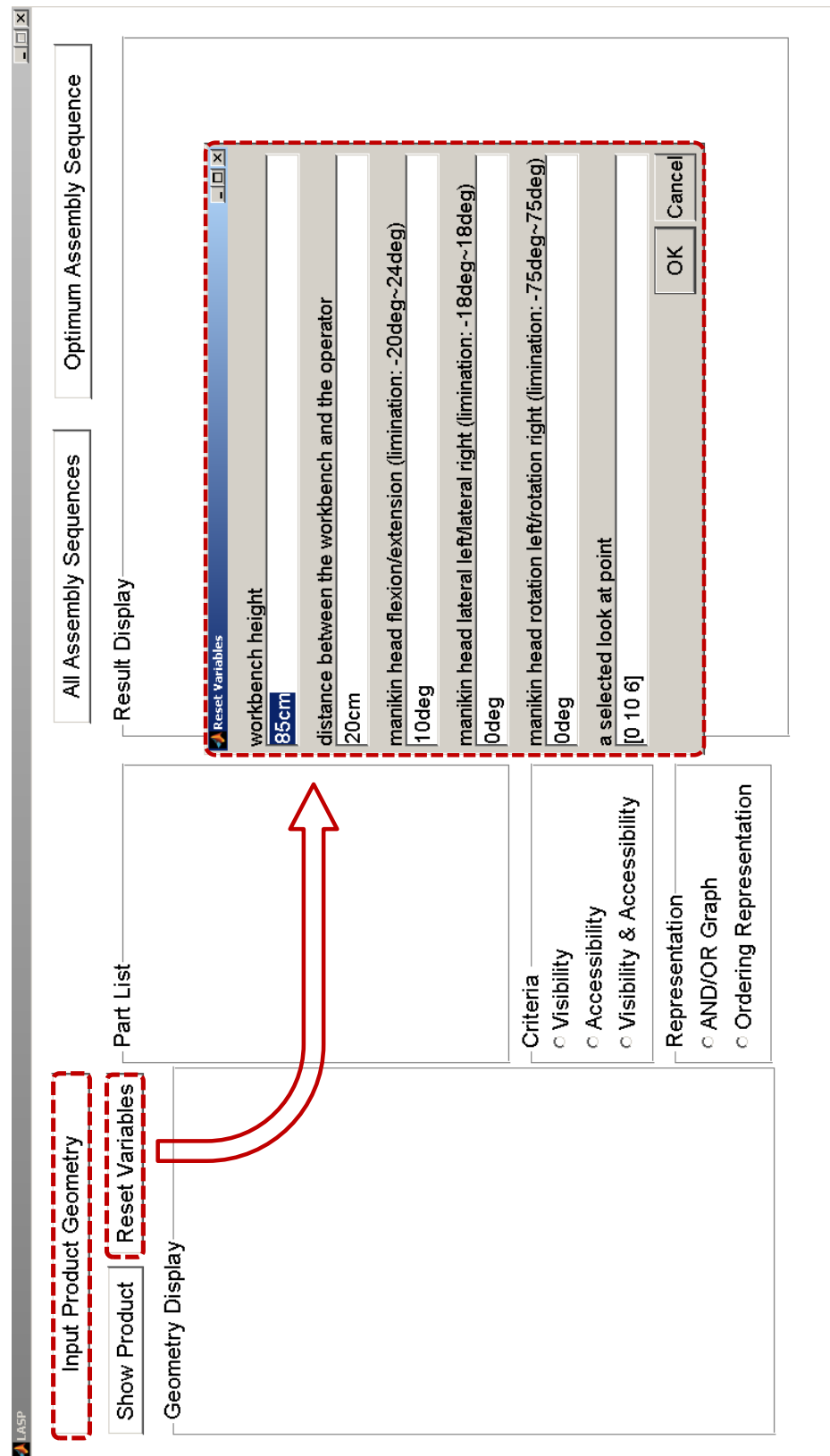


FIGURE 5.24: A typical interface of LASP.

Generally, LASP is capable of generating all assembly sequences of a product based on its geometric description and represent them in the AND/OR graph. When the human operator data and workstation data is available with appropriate user-interface facilities, LASP can further generate the optimum assembly sequences of the product by applying the visibility criterion, accessibility criterion or both. The optimum assembly sequences are represented in the AND/OR graph or ordering presentation which textually states the precedence relation of assembly operations. Figure 5.24 shows a typical system interface.

5.8.2 System Input

The input of LASP consists of:

- **Geometry data :** the geometry of each part of the product. These geometry inputs are gathered together into an assembly file which contains a list of filenames describing parts; associated with each is a 4×4 transformation matrix which specifies the position and orientation of the part in the final assembled state in the world coordinate system.
- **Operator data :** a default 50 percentile UK male operator has been constructed. His posture in the assembly process needs to be defined by three variables in the system, which are the head flexion/extension (α), lateral left/lateral right (β) and rotation left/rotation right (γ).
- **Workstation data :** used to specify the relationship between the product and the operator in the assembly environment. It includes the workbench height, the horizontal distance between the workbench and the operator, a preferred position and orientation of the product on the workbench, and a 'look at' point on the product.

The minimum input information consists of the product geometry and a 'look at' point on the product. The product position and orientation on the workbench corresponding to the world coordinate system are specified in the assembly file and input with the product geometry after "Input Product Geometry" is enabled as shown in Figure 5.24. All other information is optional, and the system can produce assembly sequences with the default values as set in "Reset Variables" dialog box in Figure 5.24. The default workbench height is 85 cm which is the optimum value of workbench height obtained from the ergonomic design of workplace in Section 3.7; the distance between the

workbench and the operator is set as 20 cm so the parts of product are located in the operator's upper extremity reach envelop; the operator stands with slightly downward head of 10° , which is in his referred joint range.

5.8.3 Case Study

LASP is implemented in MATLAB and a series of object models has been tested in the system, including a CAD model for an 11-part air conditioner as shown in Figure 5.25 [158] (the cover of the air conditioner has been removed for internal viewing). The air conditioner can be disassembled purely manually without any mechanical assistance (fixtures, assembly tools, etc). Figure 5.26 shows the disassembly environment for the air conditioner with a standard digital operator. The geometry data of the air-conditioner is a boundary representation of the polyhedral model. Faces are convex and non-convex which are ideal for the verification of algorithms developed for the system.

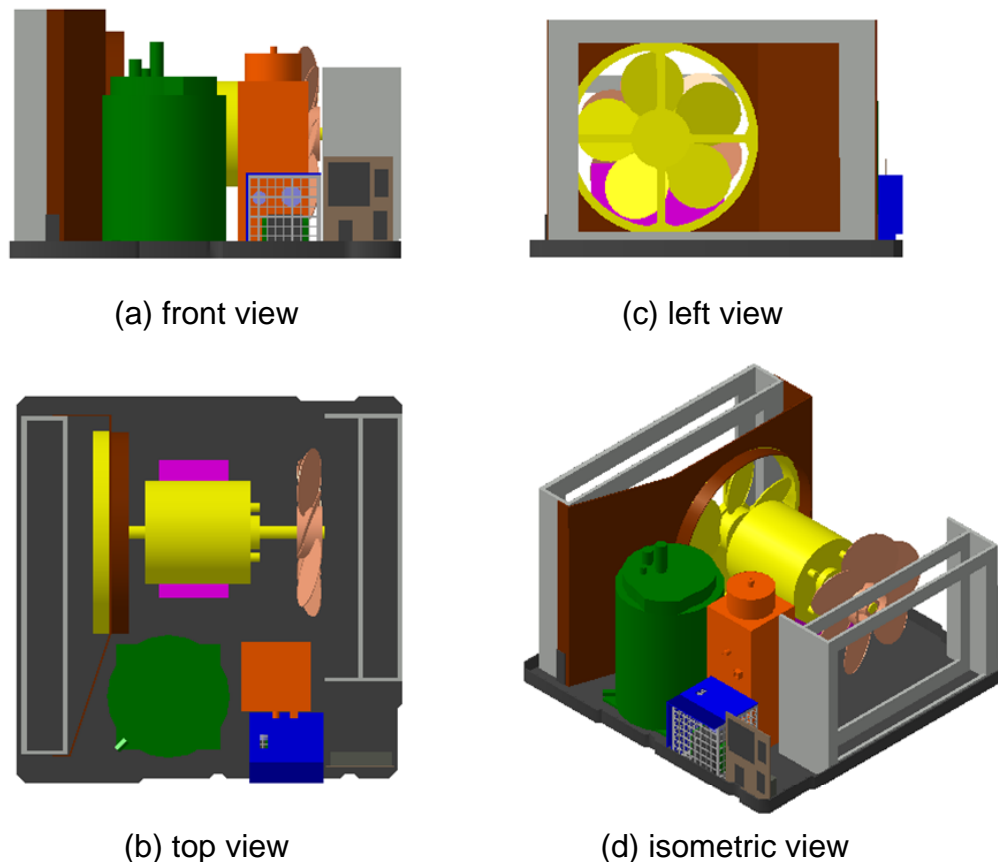


FIGURE 5.25: The CAD model of air conditioner [158].

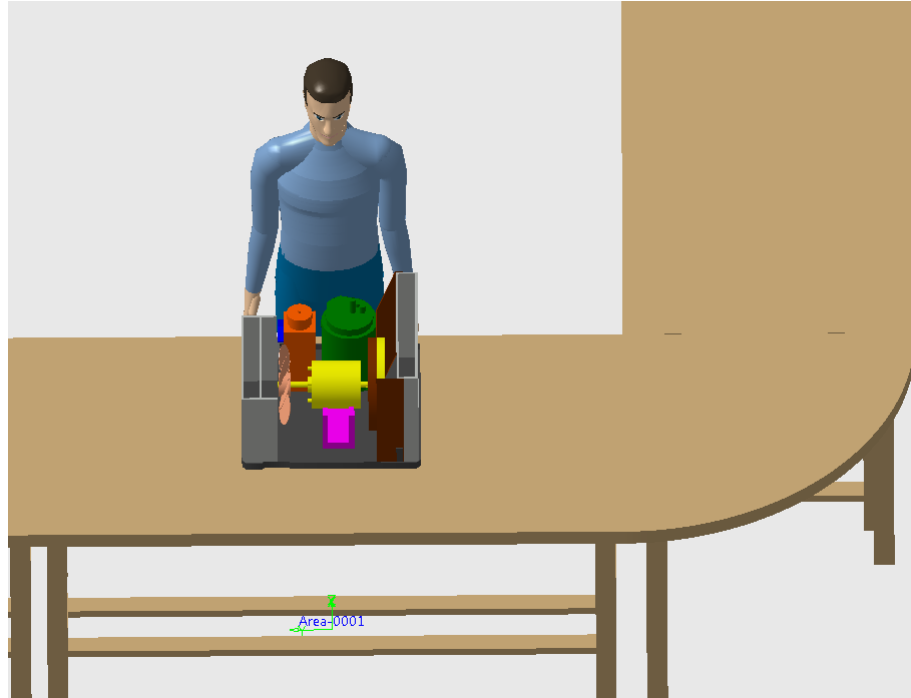


FIGURE 5.26: The disassembly environment of the air conditioner.

First of all, all feasible assembly sequences of the air conditioner are automatically generated and presented in the AND/OR graph as shown in Figure 5.27. Next, by applying different criteria, optimum sequences are selected among them. In LASP, relevant scores of feasible disassembly parts in the current state are computed and displayed beside them in the AND/OR graph, hence possible design faults with regard to restricted visibility and obstructed accessibility can be detected easily. For example as shown in Figures 5.28 and 5.29, during disassembly if a part's visibility percentage is less than 50% ($vis \leq 50\%$) or the amount of approach directions is less than 2 ($acc \leq 2$), it is reported immediately and this feedback can be provided to designers for design improvements. After that, the disassembly part with the maximum value is highlighted in red colour. Other edges in the current state which do not represent the optimum subassemblies are deleted. The deleting feature can quickly reduce the original large set of sequences to a reasonable few; permitting an efficient calculation and a distinct display of calculated results. Through the step-by-step selection, an optimum sequence considering different ergonomic constraints is generated, which can be shown in an ordering presentation as well. Figures 5.28, 5.29 and 5.30 show the AND/OR graphs of air condition assembly considering the visibility criterion, accessibility criterion and both in which chosen top-down disassembly routes are highlighted in red. Table 5.2 shows the optimum sequences in the ordering presentation.

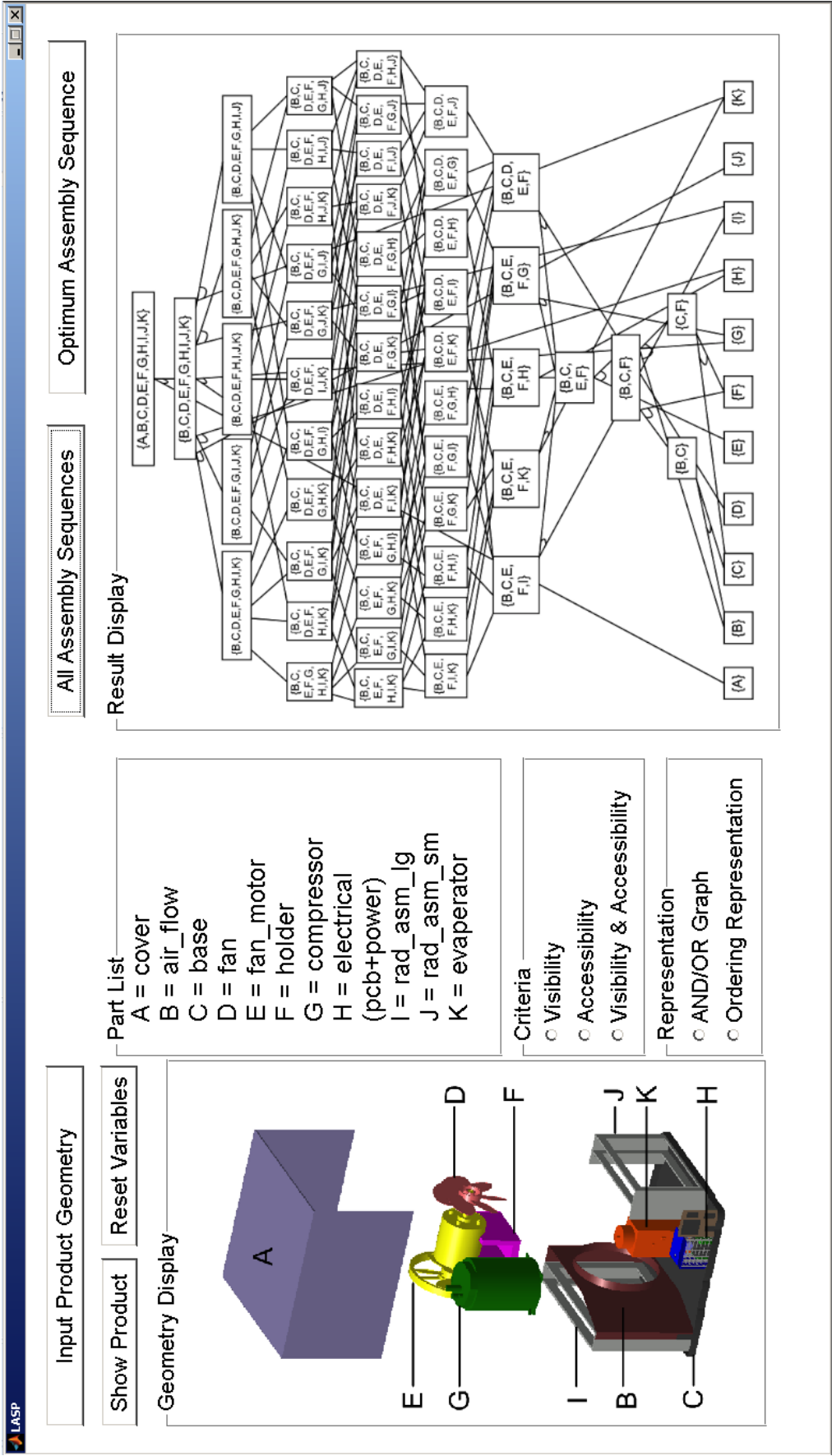


FIGURE 5.27: AND/OR graph of air conditioner assembly.

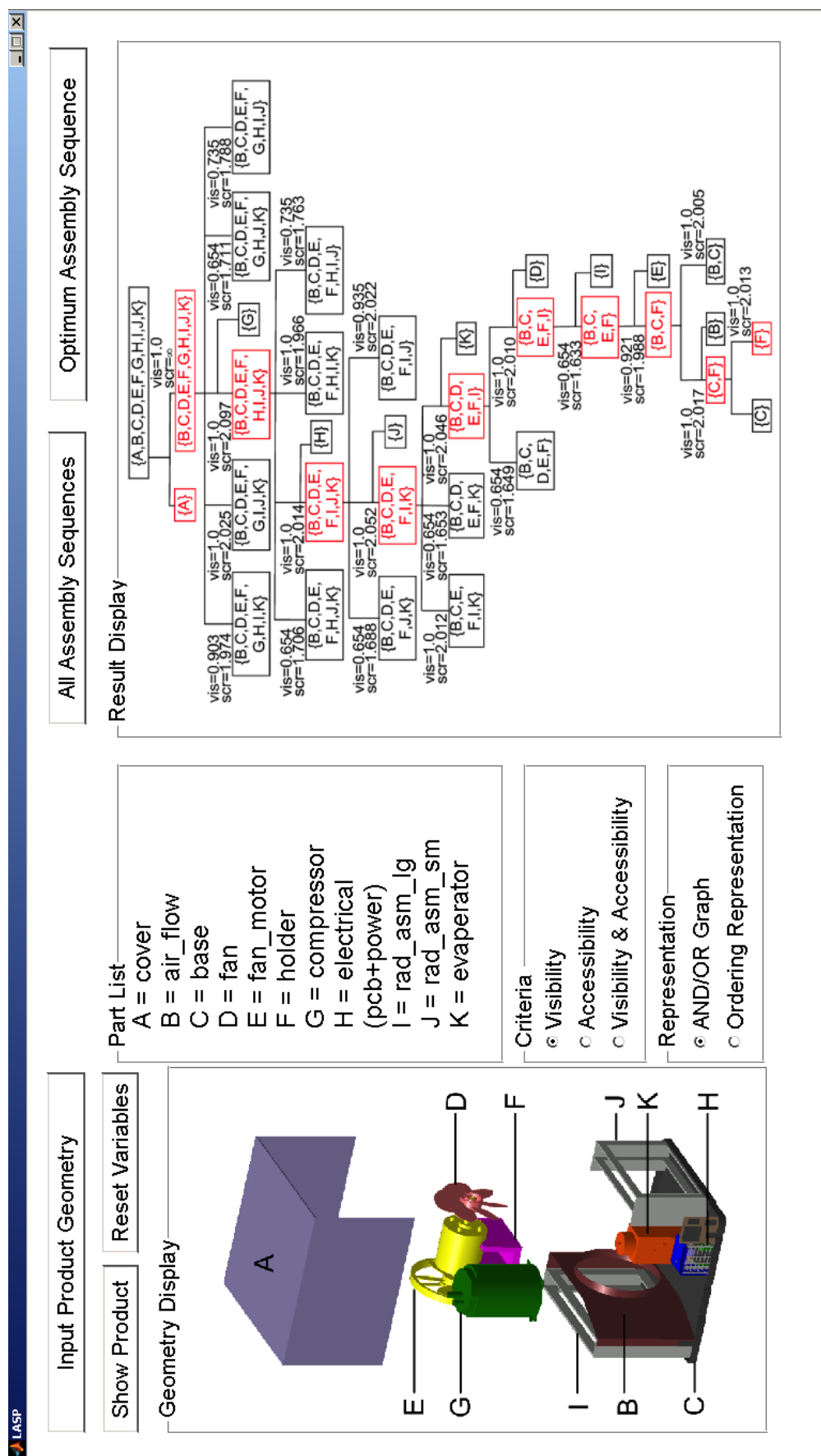


FIGURE 5.28: AND/OR graph of air condition assembly with the visibility criterion.

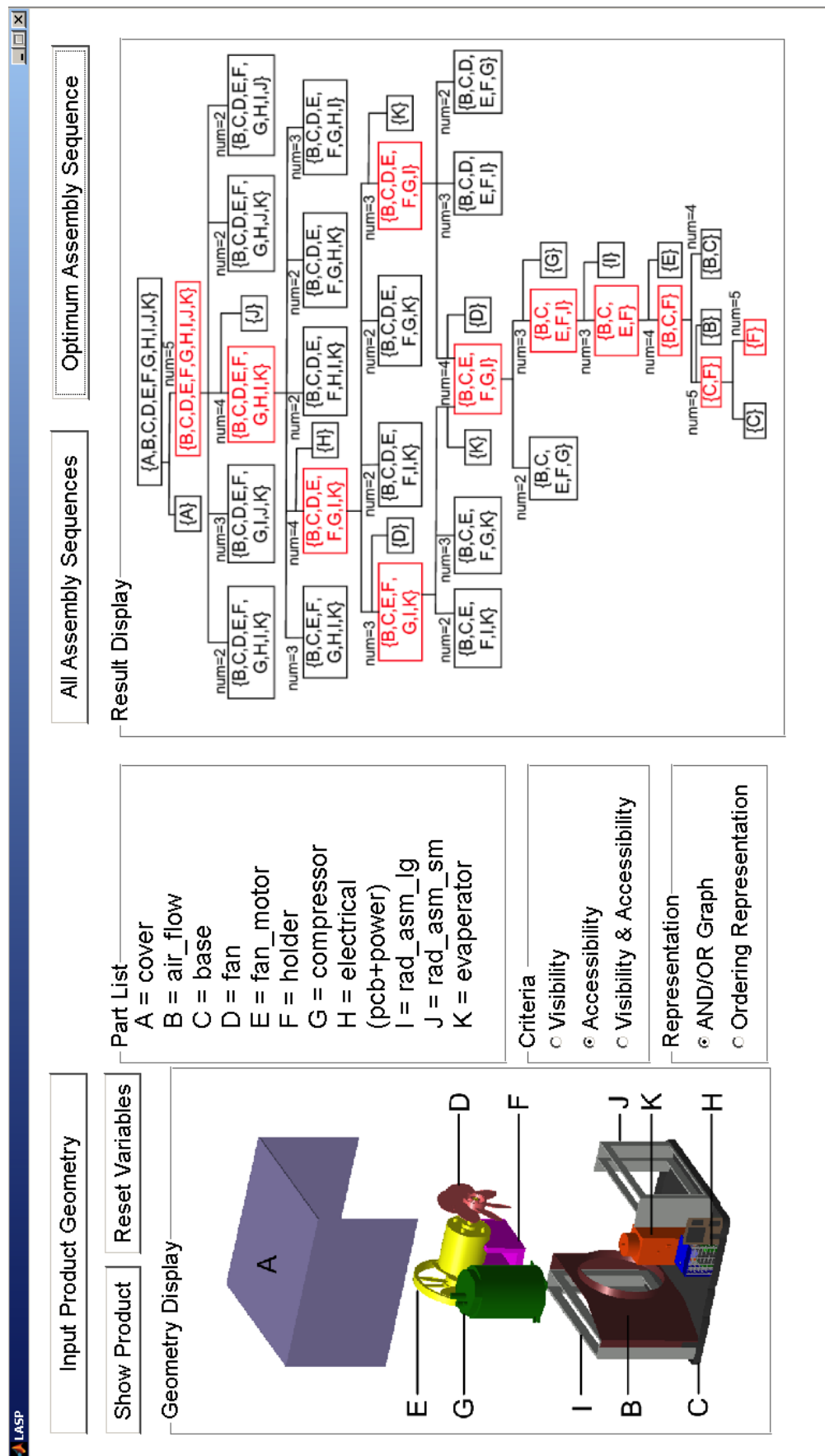


FIGURE 5.29: AND/OR graph of air condition assembly with the accessibility criterion.

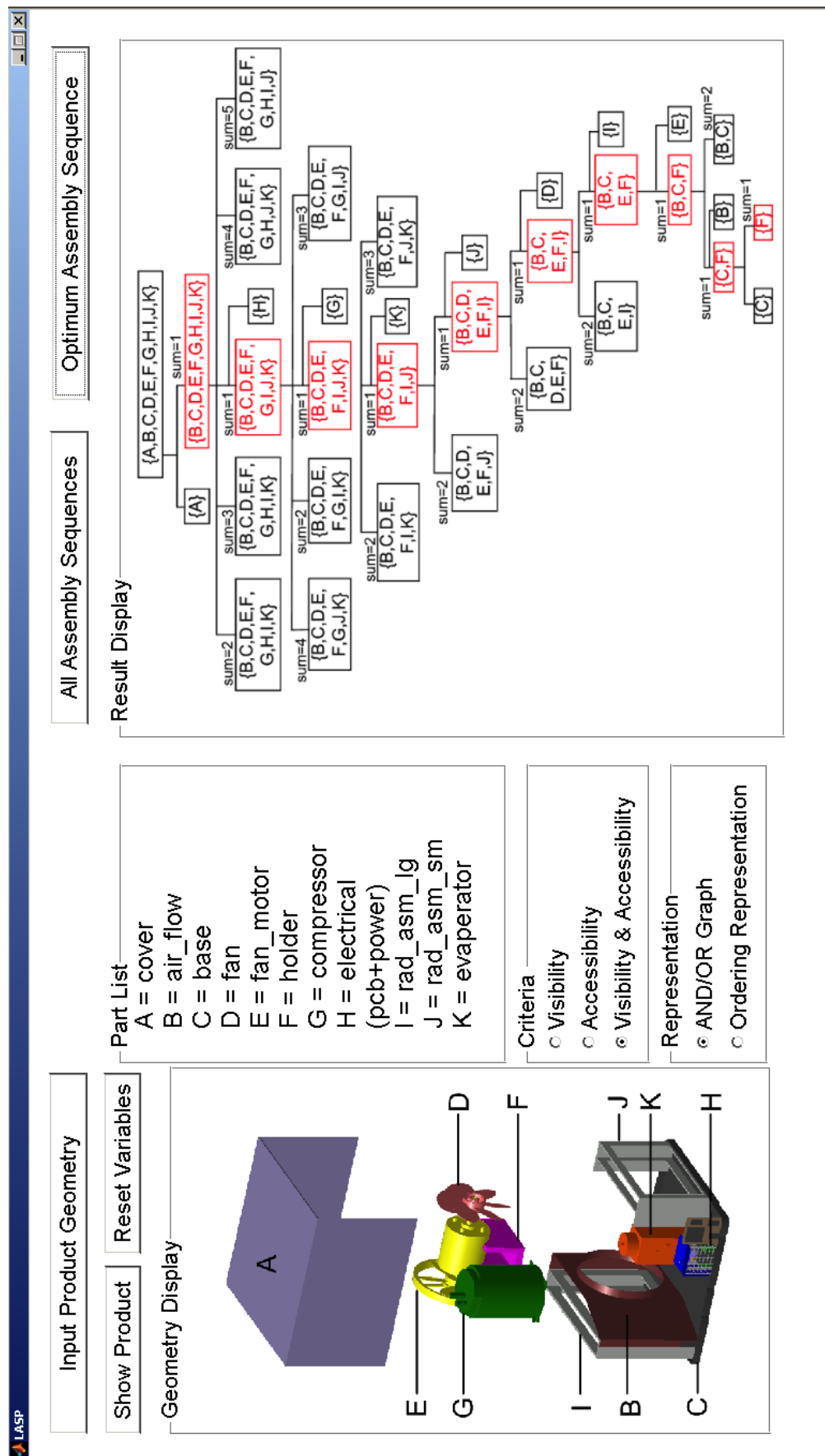


FIGURE 5.30: AND/OR graph of air condition assembly with the visibility and accessibility criteria.

It can be found from the sequences in Table 5.2 that the operation orders for parts C , F , B , E and I are identical within different assembly criteria considerations because of the geometrical constraints of the air conditioner. When they have been fixed in their final position, parts D , H , I , J , K can be assembled arbitrarily. Considering the visibility criterion, they are sequenced in a back-to-front order according to the distance from the viewpoint of the operator for maintaining good visibility of the parts added in each step. Considering the accessibility criterion, they are sequenced in a left-to-right order in order to keep access space for the hand of the operator as large as possible. These sequences selected among thousands of feasible ones are specifically easy to implement for manual assembly. Meanwhile, a clear instruction is provided in the system to operators before carrying out the assembly task.

TABLE 5.2: Optimum assembly sequences of air conditioner

Criteria	Optimum assembly sequences
Visibility	$C > F > B > E > I > D > K > J > H > G > A$
Accessability	$C > F > B > E > I > G > K > D > H > J > A$
	$C > F > B > E > I > G > D > K > H > J > A$
Both	$C > F > B > E > I > D > J > K > G > H > A$

5.8.4 Discussion

The purpose of LASP is to apply new ergonomic criteria for manual assembly sequence evaluation. The system performance is largely dominated by the geometric, visibility and accessibility computations using computer graphic algorithms. With more sophisticated algorithms developed in the field of computer graphics, the system computation efficiency could be improved, promoting the system performance in the future.

LASP is only capable of generating linear assembly sequences which require the insertion of a single part to the rest of the assembly in each step. The subassembly, for example, the electrical component (tag H in the part list) in the air conditioner including a printed circuit board (PCB) and a power was simplified as a single part so the system can handle its sequence generation and evaluation.

In LASP, only one-step translations along principal axes are considered in the local freedom analysis. Using Guibas et al.'s approach can enhance the system's capability to handle multi-step translations and rotations in all motion directions

[159]. A localised change to the module within the system can achieve this enhancement rather change to the framework of the system itself.

5.9 Conclusions

In this chapter, a Liverpool Assembly Sequence Planning (LASP) system was presented which enables a combination of ergonomic constraints in the assembly sequence generation and evolution for manual assembly tasks. Basically, it automatically generates all feasible assembly sequences of a product given only a description of the parts' geometry. Additionally, LASP can compute and select the optimum sequences applied by two new evaluation criteria, i.e. visibility, accessibility or both, in terms of the workstation description, operator's anthropometry characteristics, and working posture.

Using the visibility criterion, a digital human model and workstation data were introduced to evaluate the visibility of the product and its components in the assembly environment quantitatively. Moreover, a perspective projection which incorporates foreshortening was proposed to closely simulate the real scene of the product in the assembly environment through the operator's eyes. Finally, the visibility criterion was identified which is mainly concerned with the visibility of feasible disassembly part and its contribution to the visibility improvement of the subassemblies.

Using the accessibility criterion, an approach direction was defined and determined based on the anthropometric characteristics of the operator's hands. By generalising the feature of hand grasp, the accessibility criterion was proposed as: firstly, at least two approach directions are required for a feasible disassembly part and secondly, the more approach directions a feasible disassembly part possess, the easier for it to be manipulated by the operator.

The criteria proposed in the chapter represent a significant addition to and improvement over previous work [89–92, 96, 97]. With the high-level ergonomic consideration, designers are aware of visibility and accessibility of parts and components in every assembly state as well as the possible faults with regard to restricted visibility and obstructed accessibility. Therefore, design changes in terms of product geometry and sequencing can be considered as early as possible. Also, the optimum sequences with maximum visibility and/or accessibility score

can be provided automatically to operators for ease of manual assembly, facilitating higher assembly quality and efficiency.

Chapter 6

Conclusions and Future Research

6.1 Conclusions

Benefits of ergonomics application in the manual assembly process are first of all linked to the reduction in the occupational injury risks and to the improvement of physical workload with a drastic reduction in all costs related to absence, medical insurance and rehabilitation. In addition, ergonomics investigations improve the assembly quality and productivity. The primary objective of this research is to apply ergonomics early and thoroughly enough in the design stage of product and process, therefore achieving ergonomic benefits before the product and process prototyping.

In this research, product assemblability for manual assembly was evaluated via the assembly process simulation and ergonomics analysis in DELMIA. Ergonomic requirements in the manual assembly process including the assembly object's visibility, weight, working distance, assembly force and clearance were examined separately based on the capabilities of DELMIA. The simulation results showed that poor product design, poor assembly process planning and improper working height/distance cause awkward working postures of operators, and decrease assembly quality and efficiency. Furthermore, a good agreement was obtained between the results from simulations and those from reality. This proved that DELMIA is capable for realistic and accurate ergonomics research. However, its strong dependence upon user's manipulation, and limitations in vision analysis and hand access analysis are revealed, which require further improvements.

This research proposed an approach for the ergonomic effective design of the manual assembly workplace. Feasible design alternatives were defined by multiple design factors including work bench heights, workplace layouts and part locations. After the workplace alternatives identification, a comparison study was carried out via the manual assembly process simulation and ergonomics analysis in order to evaluate the impact of each design factor on human performance measures. The result of the approach is a complete new workplace characterised by several ergonomic improvements in terms of RULA scores, process cycle time and energy expenditure. It also concludes that work bench height should be carefully designed due to its significant influence on human performances. Assuming that the product is manipulated or held at an intermediate height, a optimum bench height could be estimated which is equal to the elbow height of the assembly operator minus half of the product height. Workplace layout is another important factor in workplace design. Process cycle time and energy expenditure could be deducted considerably in an effective workplace layout by reducing ineffective walking motion of the assembly operator.

An actual and accurate assembly posture modelling method was developed in this research. Associated with assembly features, a simplified 10-DOF human model was proposed focusing on the joint representations such as the ankle, knee, hip, trunk, shoulder, elbow and wrist. In order to assist human model manipulation and constraint construction, 4 control points placed on the foot, hip, eye and hand were defined. The anthropometric data for British male, aged 19 to 65 years was depicted in digital human modelling, leading to a consideration of human diversity for posture modelling and analysis. Multi-objective optimisation (MOO) method was applied afterward to closely simulate assembly postures. Objectives functions consisting of minimum joint discomfort and minimum metabolic energy expenditure were described, which are both important to design postures without excessive strain or fatigue. Their automatic combination was accomplished in adopting the weighted sum method. In order to examine the above models, a verification experiment was carried out by comparing the predicted postures and the postures captured in reality and the results have proved the validity and accuracy of these models.

Assembly postures were designed in terms of task constraints, human diversity and human performances in this research. Compared with manual lifting, manual assembly has higher demands on the object positions (i.e. visual demands) which were summarised and formulated. When satisfying certain

visual demands, assembly posture modelling method was employed to study optimum assembly postures (i.e., the postures with the minimum joint discomfort and minimum metabolic energy expenditure) for diverse assembly operators under different assembly conditions. A series of posture strategies was proposed. It was concluded that a squat posture was favoured in 1) taller assembly operators; 2) objects in lower positions; 3) objects which were closer to the operator; and 4) heavier objects.

New ergonomic constraints were proposed in this research regarding assembly workstation, operator's characteristics and working posture for objective evaluation of manual assembly sequences, which consist of visibility criterion, accessibility criterion and both. A digital human model and workstation data were identified to quantitatively evaluate the visibility of the product and its components in the assembly environment. The visibility criterion mainly concerned with the visibility of feasible disassembly part and its contribution to the visibility improvement of the subassemblies. For the hand accessibility evaluation, an approach direction was defined based on the anthropometry characteristics of operator's hands and the general features of hand grasp were summarised. The accessibility criterion was proposed as: at least two approach directions are required for a feasible disassembly part and the more approach directions a feasible disassembly part has, the easier it would be manipulated by the assembly operator.

This research achieved an automatic generation and optimisation of manual assembly sequencing in an assembly sequencing system known as LASP, i.e. Liverpool Assembly Sequence Planning System. New ergonomic constraints were embedded into the system to assess product geometry and sequence planning in the early design stage. Based on the minimum input, i.e. geometry data, operator data and workstation data, LASP was capable of generating all feasible assembly sequences of a product and the optimum ones among them by applying different criteria (visibility, accessibility criteria or both). The results were directly showed by AND/OR graph or precedence ordering representation. According to the results, possible design faults with regard to restricted vision and obstructed access could be detected and reported to product designers readily for design changes. Also, the optimum sequences with maximum visibility and/or accessibility score could be provided distinctly to assembly operators for ease of manual assembly. An air condition assembly sequence planning was

tested in this system to demonstrate its capability and functionality.

The following summarises and outlines the main contributions of this research project.

1. Manual assembly process simulation has been achieved in the early stage of product/process design, promoting time, energy and cost saving by means of ergonomic investigations using the commercial software tool. This also facilitates ergonomics applications in manufacture industry.
2. A new method for practical and precise assembly posture modelling is developed. Assembly postures in terms of a variety of human operators and working conditions are designed. On both accounts, considerable progress has been obtained for manual assembly task simulation and analysis.
3. The use of integrated ergonomic constraints for the objective evaluation of manual assembly sequencing is proposed. This high-level ergonomic consideration and its implementation in an assembly sequencing system have shown a significant improvement over previous research in the field of assembly process planning.

6.2 Future Research

Based on the evolutionary nature of research, the following summarises the promising directions for future work in this area.

1. A digital human model in this research is regarded as a mechanical system, which is time independent. The physical capacity of a digital operator is initialised as constant and its reduction along with time is not considered in the simulation. For example, joint maximum torque limit keeps consistent in the metabolic energy expenditure rate calculation. However, changes of physical status can be experienced by various working scheduling and working conditions. One important challenge of present DHM tools is that operators can range from the physical to the physiological [160]. A more realistic representation of variations in human performance measures should be embedded in the next generation human models and therefore the physiological mechanism of operators can be taken into account.
2. The dynamic model of the digital human should be explored in order to predict human motions in assembly tasks. It encompasses both kinematics

components (considering velocity and acceleration of body segments) and kinetic components (considering forces causing the movements of body segments). Taken these components into account, several basic assumptions in this research could be released in future research, for instance, a static loading of assembly object on the digital operator and his body maintaining in static equilibrium during the assembly task. Afterward, a more precise human performance measure (e.g. metabolic energy expenditure rate) can be applied which is essential for conducting human motion prediction and analysis. This is particular useful for determining the maximum assembly work done by the operator without excessive fatigue or risk of injury.

3. Hand model of DHM tools requires further development. Currently, it is problematic for users to simulate hand actions in DELMIA due to their complexity and variety. In the posture prediction method, movements at the joints of human fingers (including the thumb, index, middle, ring and little finger) are generally neglected for simplifications; only movements at the wrist are concern. Therefore, a convenient and effective approach to achieve the dexterity and precision of hand movements in digital human modelling is desirable, which can facilitate ergonomics applications in the design of products, tools and assembly tasks.
4. An assembly posture modelling method based on multi-objective optimisation was proposed in this research. This method was verified via an experiment with respect to 6 male subjects and 4 target objects located in the subjects' upper extremity reach envelope. Subject and object fitness is essential for ease of posture capture so the first comprehensive study on the posture modelling method can be achieved. In order to further evaluate and develop this method, experiment data from a wide range of subjects and objects are required since operators would exhibit diverse tactics with respect to different object weights, locations and dimensional features. Moreover, experiment data can benefit the investigation on human performance measures and their combination through the weighted sum method. The effect of different weights assigned to individual objective function on predicted postures can be further analysed and therefore a more realistic combination of objective functions can be obtained.
5. The assembly sequence planning system i.e. LASP accomplished in this research enables an automatic generation of optimum assembly sequences

with the user-defined input, such as the operator working posture and workplace layout. In the future, its capabilities can be enhanced to cover more practical conditions. For example, based on the assembly posture prediction method proposed in Chapter 4, an optimum reach posture with least joint discomfort and metabolic energy expenditure rate can be predicted and used for visibility and accessibility calculation. Under this circumstance, the optimum assembly sequences selected by LASP with maximum visibility score and/or approach directions are also comfortable and energy efficient for an operator to perform. Furthermore, using hand tools in the manual assembly process should be considered. The space required to apply various hand tools (e.g., the wrench, screwdriver, or hammer) to perform assembly operations should be investigated specifically. Therefore, LASP's capability in accessibility analysis can be improved.

Appendix A

Anatomical and Anthropometric Terminology

A.1 Anatomical Position

The anatomical position is standing erect, the eyes looking forward to the horizon, the arms by the sides, the palms of the hands and the toes directed forward (Figure A.1).

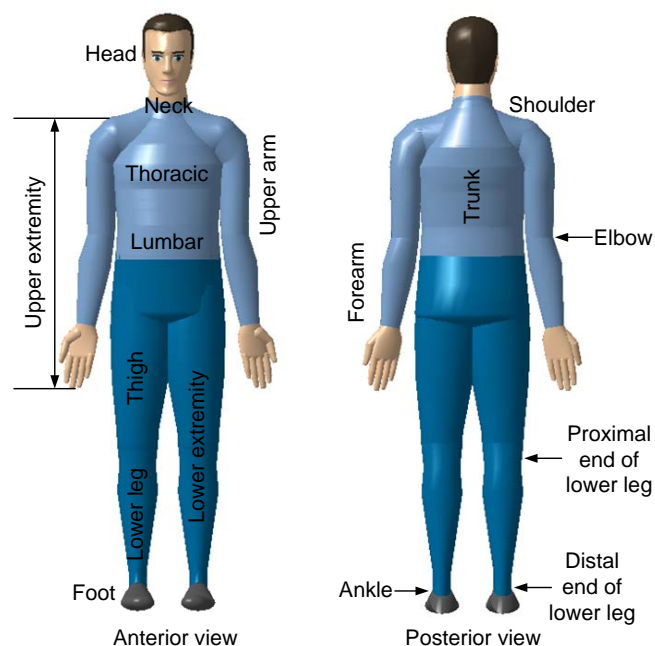


FIGURE A.1: The human body in the anatomical position.

A.2 Reference Planes

As shown in Figure A.2, there are three general reference planes: the sagittal plane (there is also a special sagittal plane, called midsagittal), coronal plane, and transverse plane.

- **Midsagittal (median) plane** is a vertical plane dividing the body into right and left halves. A **sagittal plane** refers to any vertical plane parallel to and including the Midsagittal plane which divides the body into right and left parts.
- **Coronal plane** is any vertical plane perpendicular to the midsagittal plane which divide the body into anterior and posterior portions.
- **Transverse plane** is any horizontal plane at right angles to the sagittal and coronal planes, dividing the body into superior and inferior parts.

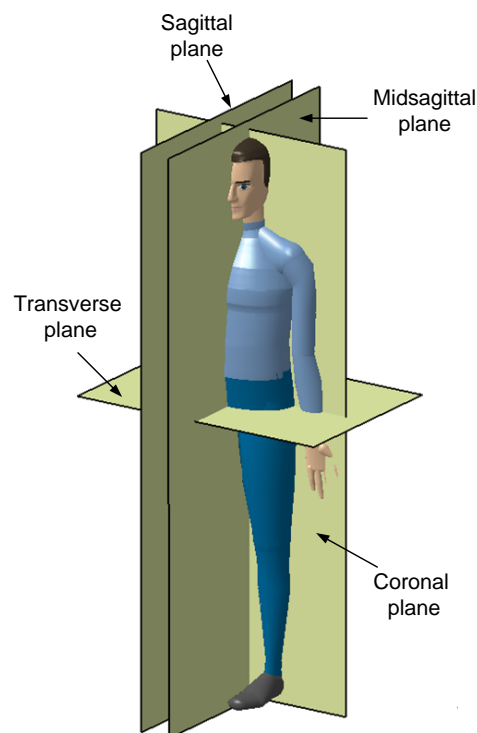


FIGURE A.2: Reference planes.

A.3 Anatomical Relationship

The terms of spatial anatomical relationships are briefly described in Table A.1 and illustrated in Figure A.3.

TABLE A.1: Terms of relationship.

Term	Meaning
Anterior	Refers to front, nearer the front surface of the body
Posterior	Refers to back, nearer the back surface of the body
Superior	Above, upper or higher part of body, or nearer the crown of the head
Inferior	Below, lower part of the body, or nearer the soles of the feet
Medial	Nearer the median plane of the body (or body part) which divides the body into right and left halves
Lateral	Farther from the median plane
Proximal	The end of a body segment nearer the body
Distal	The end of a body segment farther from the body
Palmar or volar	Anterior surface of the hand or forearm
Dorsal	Pertaining to back, nearer the back (of the foot, hand and forearm, e.g., dorsal surface the hand, opposite of palmar)
Plantar	Refers to the sole of the foot

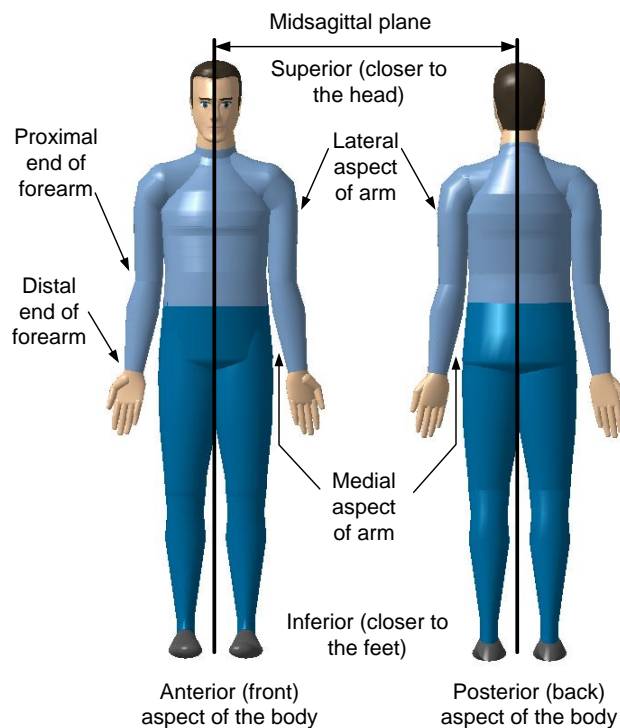


FIGURE A.3: Terms of relationship.

A.4 Joint Movements

The freely movable joints can perform one or more of the following joint movements: flexion, extension, abduction, adduction, rotation, pronation, and supination. These movements are described as follows:

- **Extension and flexion:** Flexion is a movement which decreases the angle between two bones. It is also referred to as bending or making an angle. Extension is a stretching or straightening movement which increases the angle between two bones. Figure A.4 illustrates extension and flexion movements of joints.

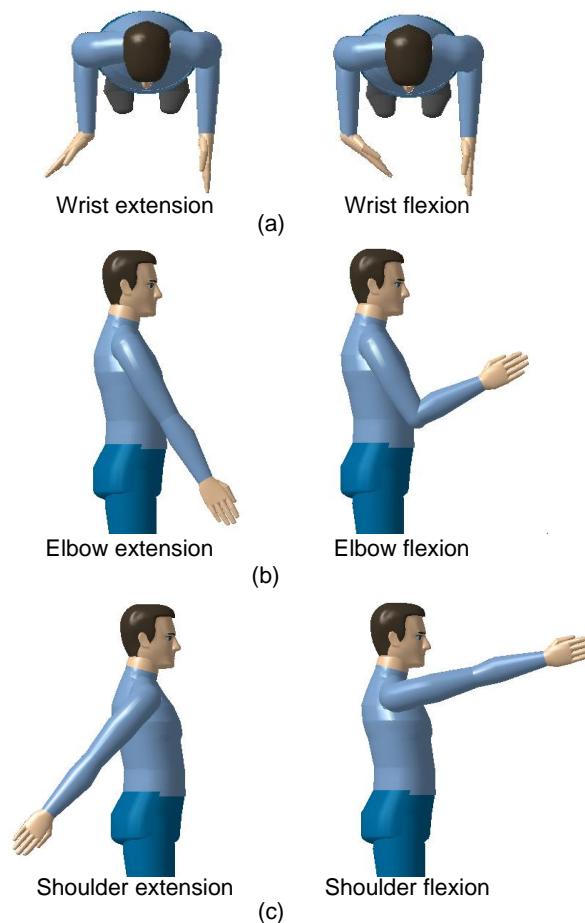


FIGURE A.4: Extension and flexion of (a) the wrist; (b) the elbow; (c) the shoulder.

- **Abduction and adduction:** Abduction means moving away laterally from the central axis of the body (e.g., the median plane). Adduction means moving toward the central axis of the body (e.g., the median plane). Figure A.5 illustrates abduction and adduction movements of joints.

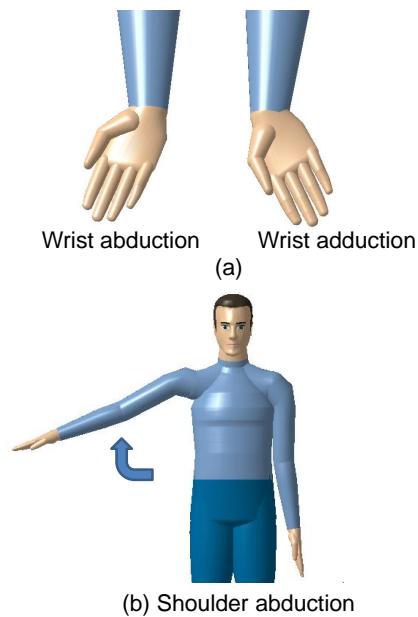


FIGURE A.5: Abduction and adduction of (a) the wrist; (b) the shoulder.

- **Rotation** is a movement of a bone around its long axis, such as the rotation of the humerus in the upper arm. Figure A.6 illustrates the rotation of the elbow in which the radius rotates around the ulna.



FIGURE A.6: The elbow rotation.

- **Pronation and supination:** Pronation is a medial rotation of a body segment. For example, medial rotation of the shoulder (Figure.A.7(a)) brings the palm of the hand downward (facing the ground). Supination is a lateral rotation of a body segment. For example, lateral rotation (Figure.A.7(b)) of the shoulder brings the palm of the hand upward (facing up).

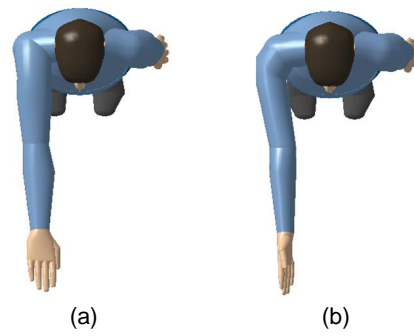


FIGURE A.7: (a) Pronation and (b) supination of the shoulder.

Appendix B

MATLAB Optimization Routines

In this appendix, a number of MATLAB codes are provided highlighting the core algorithms/methods/approaches demonstrated in Chapter 4.

B.1 Constraints

```
function [c, constraints] = DOF10_Constraint(variable)

% variable(1) = hip_height
% variable(2) = q5
% variable(3) = q6
% variable(4) = q7
% variable(5) = q8
% variable(6) = q9
% variable(7) = q10

global D;
global H;
global d;
global percentile;
global BW;

% Read anthropometry data according to percentile
dimension = GetDimensionData(percentile);

l1 = dimension(1);
l2 = dimension(2);
delt_l = dimension(3);
```

```

l3 = dimension(4);
l_se = dimension(5);
l4 = dimension(6);
l5 = dimension(7);
l6 = dimension(8);
half_w_se = dimension(10)/2;

% Joint DOF
hip = variable(1);

q2 = acos((hip^2-l2^2-l1^2)/(2*l1*l2));
q(2) = q2*180/pi;

q3 = acos(l2*sin(q2)/hip);
q(3) = q3*180/pi + q(2) - 90;

q(1) = q(2)- q(3);

[eye_x,eye_y] = EyePosition(D,H,d,hip,percentile);

a = cos(q2+q3);
b = sin(q2+q3);

q4 = acos((a*eye_y + b*(eye_x-hip))/l3);
q(4) = q4*180/pi-q(3);

for kk = 2:7
    q(kk+3) = variable(kk);
end

shoulder = [eye_x-l_se*cos(CovertToRadian(q(4)));
            -eye_y+l_se*sin(CovertToRadian(q(4)));
            half_w_se;
            1];

rad1 = q(5)*pi/180;
rad2 = -q(6)*pi/180;
rad3 = q(7)*pi/180;

```

```
rad4 = -q(8)*pi/180;
rad5 = -q(9)*pi/180;
rad6 = q(10)*pi/180;
```

```
A1 = [cos(rad1)    0    sin(rad1)    0;
      sin(rad1)    0   -cos(rad1)    0;
      0            1    0            0;
      0            0    0            1;];
```

```
A2 = [cos(rad2)    0    sin(rad2)   -14*cos(rad2);
      sin(rad2)    0   -cos(rad2)   -14*sin(rad2);
      0            1    0            0;
      0            0    0            1;];
```

```
A3 = [1            0    0            0;
      0    cos(rad3) -sin(rad3)    0;
      0    sin(rad3)  cos(rad3)    0;
      0            0    0            1;];
```

```
A4 = [cos(rad4)    0    sin(rad4)   -15*cos(rad4);
      sin(rad4)    0   -cos(rad4)   -15*sin(rad4);
      0            1    0            0;
      0            0    0            1;];
```

```
A5 = [cos(rad5)    0    sin(rad5)    0;
      sin(rad5)    0   -cos(rad5)    0;
      0            1    0            0;
      0            0    0            1;];
```

```
A6 = [cos(rad6)    0    sin(rad6)   -16*cos(rad6);
      sin(rad6)    0   -cos(rad6)   -16*sin(rad6);
      0            1    0            0;
      0            0    0            1;];
```

```
A = A1*A2*A3*A4*A5*A6;
```

```
c=[];
```

```
constraints(1) = shoulder(1) + A(1,4) - H ;
constraints(2) = shoulder(2) + A(2,4) + D ;
constraints(3) = shoulder(3) + A(3,4);

end
```

B.2 Multi-Objective

```
function out = DOF10_MultiObjective(variable)

% variable(1) = hip_height
% variable(2) = q5
% variable(3) = q6
% variable(4) = q7
% variable(5) = q8
% variable(6) = q9
% variable(7) = q10

global D;
global H;
global d;
global LH;
global percentile;
global BW;

% Read anthropometry data according to percentile
dimension = GetDimensionData(percentile);

l1 = dimension(1);
l2 = dimension(2);
delt_l = dimension(3);
l3 = dimension(4);
l_se = dimension(5);
l4 = dimension(6);
l5 = dimension(7);
l6 = dimension(8);
hip_height = variable(1);
```

```

% Joint DOF
q2 = acos((hip_height^2-l2^2-l1^2)/(2*l1*l2));
q(2) = q2*180/pi;

q3 = acos(l2*sin(q2)/hip_height);
q(3) = q3*180/pi + q(2) - 90;

q(1) = q(2) - q(3);

[eye_x,eye_y] = EyePosition(D,H,d,hip_height,percentile);

a = cos(q2+q3);
b = sin(q2+q3);

q4 = acos((a*eye_y + b*(eye_x-hip_height))/l3);
q(4) = q4*180/pi-q(3);

for kk = 2:7
    q(kk+3) = variable(kk);
end

% Calculation of Joint Discomfort
% Joint Range
q_upper = [ 38; 135; 113; 56; 170; 80; 97; 140; 80; 20;];
q_lower = [-50; 0; -18; -19; -60; -18; -20; 0; -70; -30;];
q_neutr = [ 0; 0; 0; 0; 0; 0; 0; 90; 0; 0;];

ref1 = GetRefDiscomfort;

for ii = 1:length(q)
    q_norm(ii) = (q(ii)-q_neutr(ii))/(q_upper(ii)-q_lower(ii));
    q_up_ply(ii) = ((0.5*sin(5.0*(q_upper(ii)-q(ii)))/(q_upper(ii)-q_lower(ii))+1.571)+1)^100/(4.0656*10^17);
    q_low_ply(ii) = ((0.5*sin(5.0*(q(ii)-q_lower(ii)))/(q_upper(ii)-q_lower(ii))+1.571)+1)^100/(4.0656*10^17);

```

```

    if isequal(q_lower(ii),0)
        q_dft(ii) = q_norm(ii)^2 + q_up_ply(ii);
    else
        q_dft(ii) = q_norm(ii)^2 + q_up_ply(ii) + q_low_ply(ii);
    end

    % Joint Discomfort
    out1 = out1 + ref1(ii) * q_dft(ii);
end

% Calculation of Energy Expenditure Rate
thera_6 = q(3)+90-q(2);
thera_5 = 90+q(3);
thera_4 = 90-q(4);
thera_3 = q(4)+90-q(5);
thera_2 = thea_3-q(8);
thera_1 = thea_2-q(10);

rad(6) = CovertorRadian(thera_6);
rad(5) = CovertorRadian(thera_5);
rad(4) = CovertorRadian(thera_4);
rad(3) = CovertorRadian(thera_4);
rad(2) = CovertorRadian(thera_2);
rad(1) = CovertorRadian(thera_1);

M_wrist = LH*cos(rad(1))*l6+0.006*BW*cos(rad(1))*l6*0.506;
R1 = LH+0.006*BW;
M_elbow = M_wrist+R1*cos(rad(2))*l5+0.017*BW*cos(rad(2))*l5*0.43;
R2 = R1+0.017*BW;
M_shoulder = M_elbow+R2*cos(rad(3))*l4+0.028*BW*cos(rad(3))*l4*0.436;
R3 = R2+0.028*BW;
M_waist = M_shoulder+R3*cos(rad(4))*(l3-l_se)+0.366*BW*cos(rad(4))*
(l3-l_se)*0.43;
R4 = R3+0.366*BW;
M_knee = M_waist +R4*cos(rad(5))*l2+0.234*BW*cos(rad(5))*l2*0.567;
R5 = R4+0.234*BW;
M_ankle = M_knee+R5*cos(rad(6))*l1+0.043*BW*cos(rad(6))*l1*0.567;

```

```

% Total Energy Expenditure Rate
ref2 = GetRefEnergy;
torque = ref2(1)*abs(M_ankle) + ref2(2)*abs(M_knee) +ref2(3)*
abs(M_waist) + ref2(4)*abs(M_shoulder) + ref2(5)*abs(M_elbow)
+ ref2(6)*abs(M_wrist);
BMR = (0.685*BW+29.8)/4.18/1000*60;
out2 = BMR + torque;

out = Norm(out1) + Norm(out2);

end

```

B.3 SQP Algorithm

```

%initilize
clc;
clear all;

global D;
global H;
global d;
global LH;
global percentile;

% input data:
% object data
D = 500;
H = 700;
LH = 0.1;
% visual demand
d = 500;
% anthropometry data
percentile = 50;

% Fitness function and numver of variables
fitnessFcn = @(variable)DOF10_Objective(variable);

n_design_var = 7;

```



```
% If decision variables are bounded provide a bound e.g, LB and UB.
UB = [ 920 170      80          97          140      80      20];
LB = [ 545 -60     -18         -20           0     -70    -30];

Bound = [LB;UB];
% If unbounded then Bound = []

options = optimset('LargeScale', 'off','MaxIter',1000,'TolX',1e-8, ...
                  'MaxFunEval',200000,'GradConstr','off','GradObj','off',...
                  'FinDiffType','central','DiffMinChange',1e-2,...
                  'FunValCheck','on','Display','iter','DerivativeCheck',...
                  'off','TolCon',1e-8,'Algorithm','sqp');

x0 = zeros(7,1);
x0 =[920;0;0;0;90;0;0];
[x,fval] = fmincon(fitnessFcn,x0,[],[],[],[],LB,UB,...
@DOF10_Constraint,options);

save fin_design.mat x;
```

Appendix C

Optimum Assembly Postures

Optimum assembly postures for UK male operators varying from 5th percentile to 95th percentile are graphically shown in Figures C.1-C.5, where the assembly object (i.e. a screw) weighs 0.1kg, its distance to the operator is 500mm, height from the floor is 700mm, and visual demand d is 500mm.

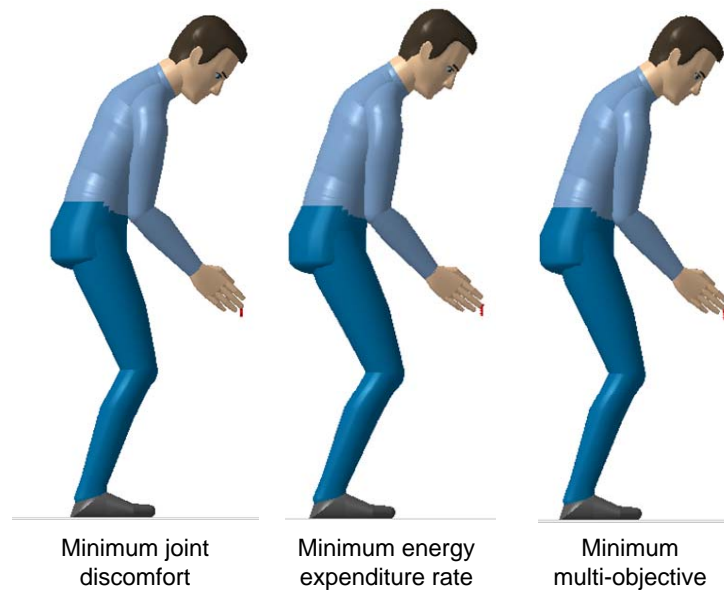


FIGURE C.1: Optimum assembly postures for 5th percentile operators.

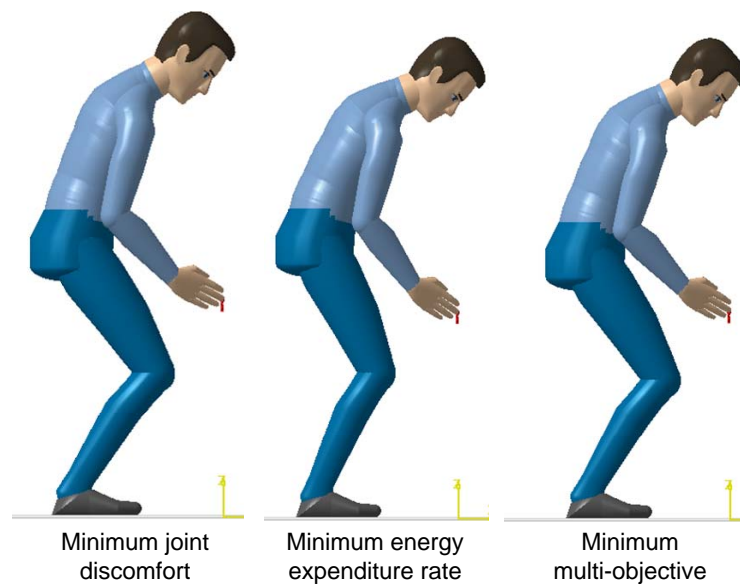


FIGURE C.2: Optimum assembly postures for 25th percentile operators.

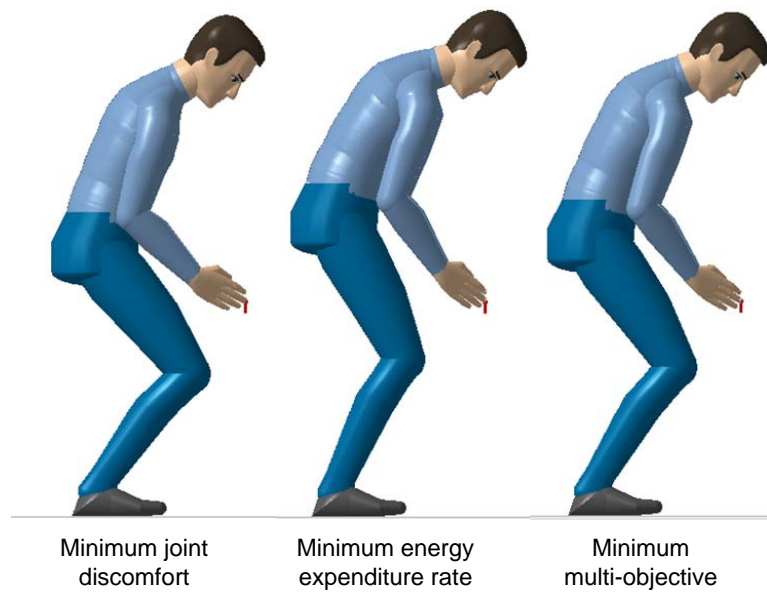


FIGURE C.3: Optimum assembly postures for 50th percentile operators.

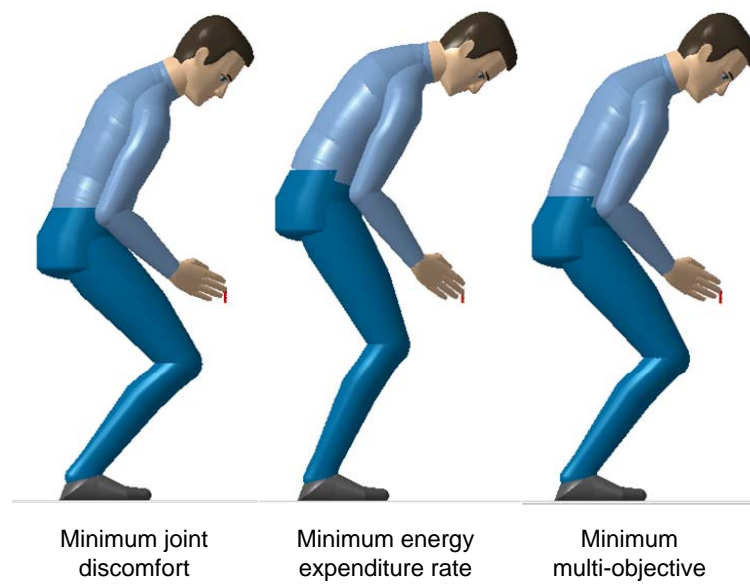


FIGURE C.4: Optimum assembly postures for 75th percentile operators.

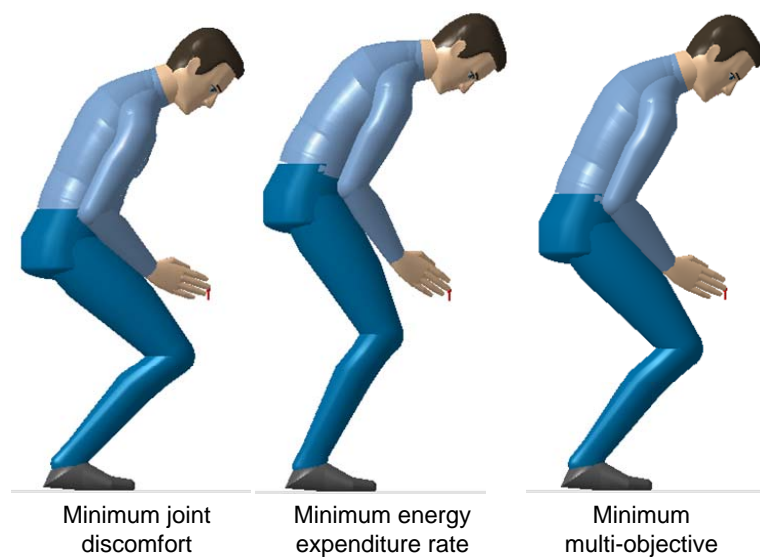


FIGURE C.5: Optimum assembly postures for 95th percentile operators.

Bibliography

- [1] H. Bley, Reinhart G., G. Seliger, M. Bernardi, and T. Korne. Appropriate human involvement in assembly and disassembly. *CIRP Annals - Manufacturing Technology*, 53(2):487–509, 2004.
- [2] Price Waterhouse in Robert L.Cattoi. *Some Economic Perspectives in Global Advanced Manufacturing*. Montreal, Canada, 2003.
- [3] H.W. Hendrick. The technology of ergonomics. *Theoretical Issues in Ergonomics Science*, 1(1):22–33, 2000.
- [4] M. Oxenburgh, P. Marlow, and A. Oxenburgh. *Increasing Productivity and Profit through Health and Safety: The Financial Returns from a Safe Working Environment*. London:Taylor and Francis, 2004.
- [5] P. Vink, E.A.P. Koningsveld, and J.F. Molenbroek. Positive outcomes of participatory ergonomics in terms of greater comfort and higher productivity. *Applied Ergonomics*, 37:537–546, 2006.
- [6] J. Eklund. Relationships between ergonomics and quality in assembly work. *Applied Ergonomics*, 26(1):15–20, 1995.
- [7] J. Eklund. Ergonomics, quality and continuous improvementconceptual and empirical relationships in an industrial context. *Ergonomics*, 40(10):982–1001, 1997.
- [8] A.C. Falck, R. Örtengren, and D. Högberg. The impact of poor assembly ergonomics on product quality: A cost-benefit analysis in car manufacturing. *Human Factors and Ergonomics In Manufacturing*, 20(1):24–41, 2010.
- [9] L. H. Steve. Ergonomic evaluation of manufacturing system designs. *Journal of Manufacturing Systems*, 20(6):429–444, 2001/2002.
- [10] D. E. Whitney. *Mechanical assemblies*. Oxford series on advanced manufacturing. New York : Oxford University Press, 2004.

- [11] M. Helander and M. Nagamachi. *Design For Manufacturability: A Systems Approach To Concurrent Engineering In Ergonomics*. Taylor and Francis, 1992.
- [12] S. J. Hu, J. Ko, L. Weyand, H. A. ElMaraghy, T.K. Lien, Y. Koren, H. Bley, G. Chrysosolouris, N. Nasr, and M. Shpitalni. Assembly system design and operations for product variety. *CIRP Annals - Manufacturing Technology*, 60(2):715–733, 2011.
- [13] T. K. Lien and F. O. Rasch. Hybrid automaitc manual assembly systems. In *CIRP General Assembly*, pages 19–25, 2001.
- [14] F. Tayyari and J. L. Smith. *Occupational ergonomics : principles and applications*. Manufacturing systems engineering series: 3. London : Chapman and Hall., 1997.
- [15] W.L. Myun. New paradigm, new market and new theatre in ergonomics. *Ergonomics*, 43:975–982, 2000.
- [16] B. Das and A.K. Sengupta. Industrial workstation design: A systematic ergonomics approach. *Applied Ergonomics*, 27(3):157–163, 1996.
- [17] R. Kadefors and M. Forsman. Ergonomic evaluation of complex work: A participative approach employing video-computer interaction, exemplified in a study of order picking. *International Journal of Industrial Ergonomics*, 25(4):435–445, 2000.
- [18] G.B. Scott and N.R. Lambe. Working practices in a perchery system, using the ovako working posture analysing system (owas). *Applied Ergonomics*, 27(4):281–284, 1996.
- [19] O. Karhu, R. Harkonen, P. Sorvali, and P. Vepsalainen. Observing working postures in industry: examples of owas application. *Applied Ergonomics*, 12(1):13–17, 1981.
- [20] J. A. Engels, J. A. Landeweerd, and Y. Kant. An owas-based analysis of nurses’ working postures. *Ergonomics*, 37(5):909–919, 1994.
- [21] R. Temple and T. Adams. Ergonomic analysis of a multi-task industrial lifting station using the niosh method. *Journal of Industrial Technology*, 16(2):2–6, 2000.
- [22] P.G. Dempsey. Usability of the revised niosh lifting equation. *Ergonomics*, 45(12):817–828, 2002.

- [23] S. Jayaram, J. Vance, R. Gadh, U. Jayaram, and H. Srinivasan. Assessment of vr technology and its applications to engineering problems. *Journal of Computing and Information Science in Engineering*, 1(1):72–83, 2001.
- [24] V.N. Rajan, K. Sivasubramanian, and J.E. Fernandez. Accessibility and ergonomic analysis of assembly product and jig designs. *International Journal of Industrial Ergonomics*, 23(5-6):473–487, 1999.
- [25] G. Chrysosolouris, D. Mavrikios, D. Fragos, and V. Karabatsou. Virtual reality-based experimentation environment for the verification of human-related factors in assembly processes. *Robotics and Computer-Integrated Manufacturing*, 16(4):267–276, 2000.
- [26] A. Sundin, M. Christmansson, and M. Larsson. A different perspective in participatory ergonomics in product development improves assembly work in the automotive industry. *International Journal of Industrial Ergonomics*, 33(1):1–14, 2004.
- [27] U. Jayaram, S. Jayaram, I. Shaikh, Y. Kim, and C. Palmer. Introducing quantitative analysis methods into virtual environments for real-time and continuous ergonomic evaluations. *Computers in Industry*, 57(3):283–296, 2006.
- [28] T. Dukic, M. Rönnäng, and M. Christmansson. Evaluation of ergonomics in a virtual manufacturing process. *Journal of Engineering Design*, 18(2):125–137, 2007.
- [29] A. Cimino, F. Longo, and G. Mirabelli. A multimeasure-based methodology for the ergonomic effective design of manufacturing system workstations. *International Journal of Industrial Ergonomics*, 39(2):447–455, 2009.
- [30] S. Pheasant and C. M. Haslegrave. *Bodyspace : anthropometry, ergonomics, and the design of work*. Boca raton, Fl. ; Taylor and Francis, 2006.
- [31] N.I. Badler, J. O’Rourke, and H. Toltzis. A spherical representation of a human body for visualizing movement. In *Proceedings of the IEEE*, volume 67, pages 1397–1403, 1979.
- [32] P. Bapu, S. Evans, P. Kikta, J. McDaniel, and DAYTON UNIV OH RESEARCH INST. *User’s Guide for COMBIMAN Programs (Computerized Biomechanical Man-Model). Version 4*. Defense Technical Information Center, 1981.

- [33] E. C. Kingsley, N. A. Schofield, and K. Case. A computer aid for man machine modelling. *SIGGRAPH Computer Graphics*, 15(3):163–169, 1981.
- [34] G.D. Frisch and L.A. D'Aulerio. Bioman - an improved occupant-crew station compliance modeling system. *Aviation Space and Environmental Medicine*, 51(2):160–167, 1980.
- [35] W. A. Fetter. A progression of human figures simulated by computer graphics. *IEEE Comput. Graph. Appl.*, 2(9):9–13, 1982.
- [36] N. I. Badler, Martha S. Palmer, and Rama Bindiganavale. Animation control for real-time virtual humans. *Commun. ACM*, 42(8):64–73, 1999.
- [37] N.I. Badler, M.S. Phillips, and Bonnie. L. W. *Simulating Humans*. Oxford University Press, 1993.
- [38] N. Thalmann and D. Thalmann. *Computer animation: theory and practice*. Springer-Verlag, 1990.
- [39] L. Emering, R. Boulic, S. Balcisoy, and D. Thalmann. Real-time interactions with virtual agents driven by human action identification. In *Proceedings of the first international conference on Autonomous agents*, AGENTS '97, pages 476–477, 1997.
- [40] H. Noser and D. Thalmann. The animation of autonomous actors based on production rules. In *Proceedings of the Computer Animation*, CA '96, pages 47–59, 1996.
- [41] X. Zhang and D.B. Chaffin. Task effects on three-dimensional dynamic postures during seated reaching movements: An investigative scheme and illustration. *Human Factors*, 39(4):659–671, 1997.
- [42] B. Das and D.N. Behara. Three-dimensional workspace for industrial workstations. *Human Factors*, 40(4):633–646, 1998.
- [43] J.J. Faraway, X. Zhang, and D.B. Chaffin. Rectifying postures reconstructed from joint angles to meet constraints. *Journal of Biomechanics*, 32(7):733–736, 1999.
- [44] J. Zhao and N. I. Badler. Inverse kinematics positioning using nonlinear programming for highly articulated figures. *ACM Transactions on Graphics*, 13(4):313–336, 1994.

- [45] V. Riffard and P. Chedmail. Optimal posture of a human operator and cad in robotics. *Proceedings - IEEE International Conference on Robotics and Automation*, 2:1199–1204, 1996.
- [46] W. Yu. *Optimal placement of serial manipulators*. PhD thesis, University of Iowa, 2001.
- [47] Z. Mi. *Task-based prediction of upper body motion*. PhD thesis, University of Iowa, 2004.
- [48] J. Zhao and S.X. Bai. Load distribution and joint trajectory planning of coordinated manipulation for two redundant robots. *Mechanism and Machine Theory*, 34(8):1155–1170, 1999.
- [49] S.F.P. Saramago and Steffen J.V. Optimization of the trajectory planning of robot manipulators taking into account the dynamics of the system. *Mechanism and Machine Theory*, 33(7):883–894, 1998.
- [50] S.F.P. Saramago and Steffen J.V. Optimal trajectory planning of robot manipulators in the presence of moving obstacles. *Mechanism and Machine Theory*, 35(8):1079–1094, 2000.
- [51] J. Yang, R.T. Marler, H. Kim, J.S. Arora, and K. Abdel-Malek. Multi-objective optimization for upper body posture prediction. *Collection of Technical Papers - 10th AIAA/ISSMO Multidisciplinary Analysis and Optimization Conference*, 4:2288–2305, 2004.
- [52] R.T. Marler, J.S. Arora, J. Yang, H.-J. Kim, and K. Abdel-Malek. Use of multi-objective optimization for digital human posture prediction. *Engineering Optimization*, 41(10):925–943, 2009.
- [53] L. Ma, W. Zhang, D. Chablat, F. Bennis, and F. Guillaume. Multi-objective optimisation method for posture prediction and analysis with consideration of fatigue effect and its application case. *Computers and Industrial Engineering*, 57(4):1235–1246, 2009.
- [54] V.J. Gawron. *Human performance measures handbook*. Lawrence Erlbaum Associates Publishers, 2000.
- [55] M. Govindaraju, A. Pennathur, and A. Mital. Quality improvement in manufacturing through human performance enhancement. *Integrated Manufacturing Systems*, 12(5):360–367, 2001.

- [56] V.Z. Priel. A numerical definition of posture. *Human Factors*, 16(6):576–584, 1974.
- [57] O. Karhu, P. Kansi, and I. Kuorinka. Correcting working postures in industry: A practical method for analysis. *Applied Ergonomics*, 8(4):199–201, 1977.
- [58] L. McAtamney and E.N. Corlett. Rula: A survey method for the investigation of work-related upper limb disorders. *Applied Ergonomics*, 24(2):91–99, 1993.
- [59] L. Hignett, S. and McAtamney. Rapid entire body assessment (reba). *Applied Ergonomics*, 31(2):201–205, 2000.
- [60] Kristina Kemmlert. A method assigned for the identification of ergonomic hazards – plibel. *Applied Ergonomics*, 26(3):199–211, 1995.
- [61] M. Keyserling, W.M. and Brouwer and B.A. Silverstein. A checklist for evaluating ergonomic risk factors resulting from awkward postures of the legs, trunk and neck. *International Journal of Industrial Ergonomics*, 9(4):283–301, 1992.
- [62] U. Aberg, K. Elgstrand, P. Magnus, and A. Lindholm. Analysts of components and prediction of energy expenditure in manual tasks. *International Journal of Production Research*, 6(3):189–196, 1967.
- [63] Ergonomics guide to assessment of metabolic and cardiac costs of physical work. *American Industrial Hygiene Association journal*, 32(8):560, 1971.
- [64] Eastman Kodak Company. *Kodak’s ergonomic design for people at work*. Hoboken, NJ : Wiley., 2004.
- [65] NIOSH. *Criteria for a recommended standard: occupational exposure to hot environment*. National Institute for Occupational Safety and Health, 1986.
- [66] A. Garg, D.B. Chaffin, and G.D. Herrin. Prediction of metabolic rates for manual materials handling jobs. *American Industrial Hygiene Association Journal*, 39(8):661–674, 1978.
- [67] C. Burford, J. Ramsey, F. Tayyari, C. Lee, and R. Stepp. A method for systematic workload estimation (swe). *Proceedings of the Human Factors and Ergonomics Society Annual Meeting*, 28(11):997, 1984.

- [68] B.R. Umberger, K.G. Gerritsen, and P.E. Martin. A model of human muscle energy expenditure. *Computer methods in biomechanics and biomedical engineering*, 6(2):99–111, 2003.
- [69] F.C. Anderson and M.G. Pandy. Static and dynamic optimization solutions for gait are practically equivalent. *Journal of Biomechanics*, 34(2):153–161, 2001.
- [70] G. Khang and F.E. Zajac. Paraplegic standing controlled by functional neuromuscular stimulation. i. computer model and control-system design. *Biomedical Engineering, IEEE Transactions on*, 36(9):873–884, 1989.
- [71] NIOSH. *A Work Practices Guide for Manual Lifting*. National Institute for Occupational Safety and Health, 1981.
- [72] M.J. Dysart and J.C. Woldstad. Posture prediction for static sagittal-plane lifting. *Journal of Biomechanics*, 29(10):1393–1397, 1996.
- [73] J.H. Kim, K. Abdel-Malek, J. Yang, T. Marler, and K. Nebel. Lifting posture analysis in material handling using virtual humans. *American Society of Mechanical Engineers, Manufacturing Engineering Division, MED*, 16-2: 1445–1453, 2005.
- [74] M.M. Ayoub and C.J. Lin. Biomechanics of manual material handling through simulation: Computational aspects. *Computers and Industrial Engineering*, 29(1-4):427–431, 1995.
- [75] M.M. Ayoub. A 2-d simulation model for lifting activities. *Computers and Industrial Engineering*, 35(3-4):619–622, 1998.
- [76] C. Huang, P.N. Sheth, and K.P. Granata. Multibody dynamics integrated with muscle models and space-time constraints for optimization of lifting movements. In *Proceedings of the ASME International Design Engineering Technical Conferences and Computers and Information in Engineering Conference - DETC2005*, volume 6A, pages 391–398, 2005.
- [77] Y.J. Xiang, J. S. Arora, and K Abdel-Maler. 3d human lifting motion prediction with different performance measures. *International Journal of Humanoid Robotics*, 9(2):1250012–1–1250012–21, 2012.
- [78] Y. Xiang, S. Rahmatalla, H. Chung, and J. Kim. Optimization-based dynamic human lifting prediction. In *Digital Human Modeling for Design and Engineering Symposium*, 2008.

- [79] H. W. Randall. *On Geometric Assembly Planning*. PhD thesis, Stanford University, 1992.
- [80] T. De Fazio and D. Whitney. Simplified generation of all mechanical assembly sequences. *Robotics and Automation, IEEE Journal of Robotics and Automation*, 3(6):640–658, 1987.
- [81] D.F. Baldwin, T. E. Abell, M. M. Lui, T. L. De Fazio, and D.E. Whitney. An integrated computer aid for generating and evaluating assembly sequences for mechanical products. *IEEE Transactions on Robotics and Automation*, 7(1):78–94, 1991.
- [82] M.N. Kolountzakis. Partitioning a planar assembly into two connected parts is np-complete. *Information Processing Letters*, 55(3):159–165, 1995.
- [83] S. Lee and Y.G. Shin. Assembly planning based on geometric reasoning. *Computers and Graphics*, 14(2):237–250, 1990.
- [84] A.K. Subramani and P. Dewhurst. Automatic generation of product disassembly sequences. *CIRP Annals - Manufacturing Technology*, 40(1):115–118, 1991.
- [85] R. Hoffman. Automated assembly planning for b-rep products. In *IEEE International Conference on Systems Engineering*, pages 391–394, 8 1990.
- [86] J. D. Wolter. On the automatic generation of assembly plans. In *IEEE International Conference on Robotics and Automation*, pages 62–68, 1989.
- [87] D. Dutta. Automatic disassembly and total ordering in three dimensions. *Journal of engineering for industry*, 113(2):207–213, 1991.
- [88] B. Romney, C. Godard, M. Goldwasser, and G. Ramkumar. An efficient system for geometric assembly sequence generation and evaluation. *ASME Database Symposium*, pages 699–712, 1995.
- [89] L. S. Homem de Mello and A. C. Sanderson. Two criteria for the selection of assembly plans: Maximizing the flexibility of sequencing the assembly tasks and minimizing the assembly time through parallel execution of assembly tasks. *IEEE Transactions on Robotics and Automation*, 7(5):626–633, 1991.
- [90] S. Kanai, H. Takahashi, and H. Makino. Aspen: Computer-aided assembly sequence planning and evaluation system based on predetermined time standard. *CIRP Annals - Manufacturing Technology*, 45(1):35–39, 1996.

- [91] A.J.D. Lambert. Optimal disassembly of complex products. *International Journal of Production Research*, 35(9):2509–2523, 1997.
- [92] M.R. Johnson and M.H. Wang. Economical evaluation of disassembly operations for recycling, remanufacturing and reuse. *International Journal of Production Research*, 36(12):3227 – 3252, 1998.
- [93] J. M. Milner, S. C. Graves, and D. E. Whitney. Using simulated annealing to select least-cost assembly sequences. *Proceedings - IEEE International Conference on Robotics and Automation*, (3):2058–2062, 1994.
- [94] G. Dini, F. Failli, B. Lazzerini, and F. Marcelloni. Generation of optimized assembly sequences using genetic algorithms. *CIRP Annals - Manufacturing Technology*, 48(1):17–20, 1999.
- [95] H.E. Tseng, W.P. Wang, and H.Y. Shih. Using memetic algorithms with guided local search to solve assembly sequence planning. *Expert Systems with Applications*, 33(2):451–467, 2007.
- [96] M. Agrawala, D. Phan, J. Heiser, J. Haymaker, J. Klingner, P. Hanrahan, and B. Tversky. Designing effective step-by-step assembly instructions. *ACM SIGGRAPH 2003 Papers, SIGGRAPH '03*, pages 828–837, 2003.
- [97] R. H. Wilson. A framework for geometric reasoning about tools in assembly. In *IEEE International Conference on Robotics and Automation*, volume 2, pages 1837–1844, 1996.
- [98] E. Fadier and J. Ciccotelli. How to integrate safety in design: Methods and models. *Human Factors and Ergonomics In Manufacturing*, 9(4):367–379, 1999.
- [99] Dassault Systemes. Delmia documentation, 2010. http://catiadoc.free.fr/online/CATIAfr_C2/hpaugCATIAfrs.htm.
- [100] H. B. Maynard, G. J. Stegemerten, and J.L. Schwab. *Methods-time measurement*. McGraw-Hill Industrial Organization and Management Series. New York, 1948.
- [101] G. Boothroyd, P. Dewhurst, and W. A. Knight. *Product design for manufacture and assembly*. Manufacturing engineering and materials processing. New York, 2002.

- [102] Dassault Systemes. Virtual ergonomics: Taking human factors into account for improved product and process, 2012. <http://www.3ds.com/fileadmin/PRODUCTS/DELMIA/OFFERS/Virtual-Ergonomics-Solutions/PDF/Virtual-Ergonomics-whitepaper.pdf>.
- [103] VCS 8003-29. *Ergonomics Requirement - Application*. Volvo Corporate Standard. Volvo Car Corporation, Sweden, 2006.
- [104] T. Fujita and G. Boothroyd. *Data Sheets and Case Study for Manual Assembly*. University of Massachusetts, 1982.
- [105] M. Ronnang, D. Lamkull, T. Dukic, and R. Ortengren. Task-related field of view parameters. In *SAE transactions*, volume 113 of *Digital human modeling for design and engineering; Digital human modeling for design and engineering*, pages 264–269, 2004.
- [106] W.N. Kama. *Volumetric Workspace Study. Part I. Optimum Workspace Configuration for Using Various Screwdrivers*. Defense Technical Information Center, 1963.
- [107] W.N. kama. *Volumetric Workspace Study. Part Ii. Optimum Workspace Configuration for Use of Wrenches*. Defense Technical Information Center, 1965.
- [108] S.K. Adams and P.J. Peterson. Maximum voluntary hand grip torque for circular electrical connectors. *Human Factors*, 30(6):733–745, 1988.
- [109] A.V. Savescu, L. Cheze, X. Wang, G. Beurier, and J.P. Verriest. A 25 degrees of freedom hand geometrical model for better hand attitude simulation. *SAE Transactions*, 113:270–275, 2004.
- [110] E. P. Pitarch, J. Yang, and K. Abdel-Malek. Santos hand: A 25 degree-of-freedom model. In *Papers - Society of Automotive Engineers New York*, Digital human modeling for design and engineering 2005, page 2727, 2005.
- [111] D.B. Chaffin. *Digital Human Modeling for Vehicle and Workplace Design*. Society of Automotive Engineers, 2001.
- [112] D. B. Chaffin. Human motion simulation for vehicle and workplace design. *Human Factors and Ergonomics in Manufacturing*, 17(5):475–484, 2007.
- [113] W.E. Woodson and D.W. Conover. *Human engineering guide for equipment designers*. Berkeley: University of California Press., 1964.

- [114] T. Zecher. *Pro Engineer Wildfire Tutorial*. SDC Publication, ISBC., 2008.
- [115] M.M. Ayoub. Workplace design guidelines. In *Proceedings of International Symposium on Ergonomics*, 1994.
- [116] G. Taguchi, S. Konishi, and S. Konishi. *Orthogonal Arrays and Linear Graphs: Tools for Quality Engineering*. American Supplier Institute, 1987.
- [117] M. S. Phadke. *Quality Engineering Using Robust Design*. Prentice Hall PTR, 1995.
- [118] E Grandjean. *Fitting the task to the man*. London: Taylor and Francis, 1981.
- [119] E. N. Corlett. *Analysis and evaluation of working posture*. London: Butterworths, 1983.
- [120] M. L. Magnusson, A. Aleksiev, D. G. Wilder, M. H. Pope, K. Spratt, S. H. Lee, V. K. Goel, and J. N. Weinstein. Unexpected load and asymmetric posture as etiologic factors in low back pain. *European Spine Journal*, 5: 23–35, 1996.
- [121] S. T. Pheasant. *Ergonomics, work and health*. London: Macmillan., 1991.
- [122] J. Denavit and R. S. Hartenberg. A kinematic notation for lower-pair mechanisms based on matrices. *ASME Journal of Applied Mechanics*, 23: 215–221, 1955.
- [123] A.M. Karim, Y. Jingzhou, M. Timothy, B. Steven, M. Anith, Z. Xianlian, P. Amos, and A. Jasbir. Towards a new generation of virtual humans. *Int.J. Human Factors Modelling and Simulation*, 1(1):2–37, 2006.
- [124] L. Ma, D. Chablat, F. Bennis, W. Zhang, B. Hu, and F. Guillaume. Fatigue evaluation in maintenance and assembly operations by digital human simulation in virtual environment. *Virtual Reality*, 15(1):55–68, 2011.
- [125] J. Yang, T. Sinokrot, and M. K. Abdel. A general analytic approach for santosa upper extremity workspace. *Computers and Industrial Engineering*, 54(2):242–258, 2008.
- [126] OPCS. *Adult Heights and Weights Survey*. London: Office of Population Census and Surveys, 1981.

- [127] I. Knight and J. Eldridge. *The heights and weights of adults in Great Britain*. London: H.M.S.O, 1984.
- [128] W. T. Dempster. *Space Requirements of the Seated Operator*. Aerospace Medical Research Laboratories, Ohio, 1955.
- [129] D.A. Winter. *Biomechanics and motor control of human movement*. New York: Wiley-Interscience, 1990.
- [130] NASA. *Anthropometric source book*. NASA reference publication: 1024. Washington: National Aeronautics and Space Administration, Scientific and Technical Information Office, 1978.
- [131] R. T. Marler, S. Rahmatalla, M. Shanahan, and K. Abdel-Malek. A new discomfort function for optimization-based posture prediction. In *SAE Human Modeling for Design and Engineering Conference*, Digital human modeling for design and engineering, page 2680. Society of Automotive Engineers, June 2005.
- [132] Q.L. Zou, Q.H. Zhang, J.Z. Yang, and J. Gragg. An inverse optimization approach for determining weights of joint displacement objective function for upper body kinematic posture prediction. *Robotica*, 30(03):389–404, 2012.
- [133] E. Homsher and C.J. Kean. Skeletal muscle energetics and metabolism. *Annual Review of Physiology*, 40:93–131, 1978.
- [134] R.C. Woledge, N. A. Curtin, and E. Homsher. *Energetic aspects of muscle contraction*. Monographs of the Physiological Society: 41. London: Academic Press, 1985.
- [135] H. Hatze and J.D. Buys. Energy-optimal controls in the mammalian neuromuscular system. *Biological Cybernetics*, 27:9–20, 1977.
- [136] K. Hase and N. Yamazaki. Development of three-dimensional whole-body musculoskeletal model for various motion analyses. *JSME International Journal, Series C: Dynamics, Control, Robotics, Design and Manufacturing*, 40(1):25–32, 1997.
- [137] E.N. Horn. Optimization-based dynamic human motion prediction, 2005.
- [138] L.J. Bhargava, M.G. Pandy, and F.C. Anderson. A phenomenological model for estimating metabolic energy consumption in muscle contraction. *Journal of Biomechanics*, 37(1):81–88, 2004.

- [139] D.B. Chaffin and G.B.J. Andersson. *Occupational Biomechanics*. Wiley-interscience publications. New York: Wiley, 1991.
- [140] R.T. Marler and J.S. Arora. Survey of multi-objective optimization methods for engineering. *Structural and Multidisciplinary Optimization*, 26(6):369–395, 2004.
- [141] H. P. Geering. *Optimal control with engineering applications*. Berlin : Springer, 2007.
- [142] K. P. Yoon and C.L. Hwang. *Multiple attribute decision making: an introduction*. Quantitative applications in the social sciences: 104. Sage, Thousand Oaks (Calif.), 1995.
- [143] A. Garg and G. D. Herrin. Stoop or squat: A biomechanical and metabolic evaluation. *A I I E Transactions*, 11(4):293–302, 1979.
- [144] K. S. Park and D. B. Chaffin. A biomechanical evaluation of two methods of manual load lifting. *A I I E Transactions*, 6(2):105–113, 1974.
- [145] X. Zhang, M.A. Nussbaum, and D.B. Chaffin. Back lift versus leg lift: An index and visualization of dynamic lifting strategies. *Journal of Biomechanics*, 33(6):777–782, 2000.
- [146] H.M. Toussaint, C.E. Van Baar, P.P. Van Langen, M.P. De Looze, and J.H. Van Dieen. Coordination of the leg muscles in backlift and leglift. *Journal of Biomechanics*, 25(11):1279–1289, 1992.
- [147] L. R. Burgess and B. Abernethy. Toward a quantitative definition of manual lifting postures. *Human Factors*, 39(1):141–148, 1997.
- [148] J. D. Wolter. *On the Automatic Generation of Plans for Mechanical Assembly*. PhD thesis, Stanford University, 1988.
- [149] L.S. Homem de Mello and A.C. Sanderson. And/or graph representation of assembly plans. *IEEE Transactions on Robotics and Automation*, 6(2):188–199, 4 1990.
- [150] M.C. Lin and J.F. Canny. A fast algorithm for incremental distance calculation. In *International Conference on Robotics and Automation*, volume 2, pages 1008–1014, 4 1991.
- [151] M. E. Newell, R. G. Newell, and T. L. Sancha. A new approach to the shaded picture problem. In *Proc. ACM National Conference*, pages 443–450, 1972.

- [152] I. E. Sutherland, R. F. Sproull, and R. A. Schumacker. A characterization of ten hidden-surface algorithms. *Computing Surveys*, 6(1):1–55, 1974.
- [153] K. Weiler and P. Atherton. Hidden surface removal using polygon area sorting. In *Computer Graphics*, pages 214–222, 1977.
- [154] E. Catmull. Computer display of curved surfaces. In *Proc. IEEE Conf. on Computer Graphics, pattern recognition and Data Structures*, pages 11–17, 1975.
- [155] D. Sunday. Area of triangles and polygons, 2012. http://geomalgorithms.com/a01-_area.html.
- [156] T. Lozano-Perez. Spatial planning: A configuration space approach. *IEEE Transactions on Computers*, C-32(2):108–120, 2 1983.
- [157] P.J. Schneider and D.H. Eberly. *Geometric tools for computer graphics*. Amsterdam, Boston, 2003.
- [158] *DELMIA - Digital Manufacturing and Production DPM Assembly*. DASSAULT SYSTEMES, 2010.
- [159] L.J. Guibas, D. Halperin, H. Hirukawa, J. C. Latombe, and R.H. Wilson. A simple and efficient procedure for polyhedral assembly partitioning under infinitesimal motions. In *IEEE International Conference on Robotics and Automation*, volume 3, pages 2553–2560, 1995.
- [160] M. Shahrokhi and A. Bernard. A framework to develop an analysis agent for evaluating human performance in manufacturing systems. *CIRP Journal of Manufacturing Science and Technology*, 2(1):55–60, 2009.